AN INVESTIGATION INTO THE PHYSICOCHEMICAL PROPERTIES AND TOXICITY OF BIOMASS COMBUSTION EMISSIONS

by

Khairallah Atwi

(Under the Direction of Rawad Saleh)

ABSTRACT

Brown carbon (BrC) particles, emitted from incomplete combustion, are characterized by a large uncertainty in their light-absorption properties (defined as the imaginary component of the index of refraction, *k)*. In this work, we present a method to isolate different classes of BrC, capitalizing on the correlation between BrC's light absorption properties and their solubility in organic solvents such as methanol. Therein, we divided BrC produced from biomass combustion into a methanol-soluble (MSBrC) and a methanol-insoluble (MISBrC) fraction and estimated the average light-absorption properties of each. We found that, although the MSBrC fraction dominated the BrC by mass (~90%), a major fraction of light absorption (~70% at 532 nm) was contributed by the MIBrC. Further, *k* values for the MIBrC were typically 2 orders of magnitude larger than those of the MSBrC at 532 nm.

The physicochemical properties of BrC are associated with the combustion conditions under which they were produced. This variability in physicochemical properties could cause different toxicity outcomes. To evaluate the importance of combustion conditions, we used a highly controlled combustion setup, simulating smoldering and flaming combustion, to produce BrC

from the combustion of toluene. We then exposed cells *in vitro* to the produced BrC at different exposures and assessed the cell viability (using WST-8) after 24 hours. We found that the BrC produced at the lower temperatures (smoldering) was significantly more toxic than the BrC produced at the higher temperature (flaming), with cell viabilities of 25% and 65%, respectively, at the highest exposure.

After they are emitted, biomass combustion emissions evolve in the atmosphere, undergoing myriad processes, such as oxidation and evaporation, that lead to fundamentally different particle compositions over time. Inside an environmental chamber, we burnt biomass fuels and initiated photooxidation reactions to simulate such atmospheric evolution. We collected fresh and aged particles and evaluated their toxicity to cells using the WST-8 cell viability assay. We found that the fresh particles were significantly more toxic to cells than the aged ones.

INDEX WORDS: Biomass combustion, Brown carbon, light-absorption properties, toxicity, combustion conditions, photooxidation, atmospheric aging.

AN INVESTIGATION INTO THE PHYSICOCHEMICAL PROPERTIES AND TOXICITY OF BIOMASS COMBUSTION EMISSIONS

by

Khairallah Atwi

B.E., American University of Beirut, Lebanon, 2011

M.E., American University of Beirut, Lebanon, 2017

A Dissertation Submitted to the Graduate Faculty of The University of Georgia in Partial Fulfillment of the Requirements for the Degree

DOCTOR OF PHILOSOPHY

ATHENS, GEORGIA

2021

AN INVESTIGATION INTO THE PHYSICOCHEMICAL PROPERTIES AND TOXICITY OF BIOMASS COMBUSTION EMISSIONS

by

KHAIRALLAH ATWI

Major Professor:	Rawad Saleh
Committee:	Amanda Frossard
	Brandon Rotavera
	Hitesh Handa

Electronic Version Approved:

Ron Walcott
Vice Provost for Graduate Education and Dean of the Graduate School
The University of Georgia
August 2021

ACKNOWLEDGEMENTS

I would first like to thank my major professor, Dr. Rawad Saleh, for giving me the opportunity to pursue my PhD in his lab. I also thank him for being tirelessly engaged in my research and its advancement, finding the right balance between helping me become an independent researcher and providing the needed guidance along the way to make that possible. Further, I thank him for infusing his spirit and motivation into this research to make sure we came through when things were tough. Finally, I also thank him for being an available and approachable mentor throughout, all of which greatly enhanced my experience during this period.

I thank my committee members, Dr. Amanda Frossard, Dr. Brandon Rotavera, and Dr. Hitesh Handa for their constructive feedback through all the steps of this PhD. I also thank them for being available for questions regarding research and for the collaborative work we did together.

I would like to thank the lab members in Dr. Frossard's, Dr. Rotavera's, and Dr. Handa's labs who worked with me on multiple projects and were excellent colleagues to work with.

I thank my lab mates, Jay, Omar, Charles, Chase, and all the undergraduate assistants who were available to assist in experimental work and take over whenever needed. I thank Soroush, the modeler, for being great company at the lab and for helping me improve my serve ball.

I would like to thank my friends, whom I will not enumerate, for their immeasurable support. My girlfriend, Payton, for all the support and love she gave me throughout. And finally, my family for their endless love and support and for never being far away despite being on different continents. This dissertation would not have been possible without all of you.

TABLE OF CONTENTS

Page

ACKNOWLEDGEMENTSS iv

LIST OF TABLES vii

LIST OF FIGURES viii

CHAPTER

1 INTRODUCTION 1

1.1 Introduction 1

1.2 The light absorption properties of BrC 3

1.3 The toxicity of combustion particulate matter 5

1.4 Specific aims and summary of chapters 8

1.5 Summary 12

References 13

2 A DOMINANT CONTRIBUTION TO LIGHT ABSORPTION BY METHANOL-INSOLUBLE BROWN CARBON PRODUCED IN THE COMBUSTION OF BIOMASS FUELS 22

2.1 Introduction 24

2.2 Methods 27

2.3 Results 33

2.4 Conclusions 41

References 43

3 PHYSICOCHEMICAL PROPERTIES AND CYTOTOXICITY OF BROWN CARBON PRODUCED UNDER DIFFERENT COMBUSTION CONDITIONS 50

3.1 Introduction 53

3.2 Methods 59

3.3 Results and Discussion 67

3.4 Conclusions 76

References 77

4 CHEMICAL COMPOSITION AND CYTOTOXICITY OF FRESH AND PHOTOCHEMICALLY AGED BIOMASS BURNING ORGANIC AEROSOLS 87

4.1 Introduction 90

4.2 Methods 93

4.3 Results and Discussion 99

4.4 Conclusions 109

References 110

5 Conclusion 122

Appendix 1 125

Appendix 2 132

Appendix 3 138

LIST OF TABLES

Page

Table 4.1: Metal concentration in fresh BBOA samples..... 106

Table A2.1: Estimates of unextracted BrC using the OCEC analyzer..... 136

LIST OF FIGURES

Page

Figure 2.1: Procedure for particle apportionment into MSBrC, MIBrC, and EC 30

Figure 2.2: Procedure of apportionment of light absorption 32

Figure 2.3: The light absorption properties of BrC aerosols 36

Figure 2.4: *k* values for the MSBrC and MIBrC using UV-Vis and optical closure 37

Figure 2.5: Light absorption properties of BrC aerosol, MSBrC, and MIBrC 39

Figure 2.6: Mass fractions and fractions of absorption of MSBrC, MIBrC, and EC 41

Figure 3.1: Schematic of experimental setup 60

Figure 3.2: Particle size statistics over the filter collection period 69

Figure 3.3: The light absorption properties of the two BrC samples 70

Figure 3.4: LDI mass spectra of the two BrC samples 72

Figure 3.5: Viability of cells upon exposure to increasing doses of BrC 74

Figure 4.1: Evolution of C_{OA} inside the chamber 100

Figure 4.2: Mass spectra of fresh and aged BBOA retrieved using ESI-MS 102

Figure 4.3: Mass fraction of species with different elemental compositions 103

Figure 4.4: Changes in OC:OM and N:C vs O:C upon photochemical aging 105

Figure 4.5: Cell viability upon exposure to increasing concentrations of fresh and aged BBOA 107

Figure A1.1: Effect of spherical particle assumption on k_{MIBrC} 129

Figure A2.1: *k* vs λ retrieved from UV-Vis measurements..... 134

Figure A3.1: OA enhancement after photochemical aging for pine and oak BBOA..... 139

CHAPTER 1

INTRODUCTION

1.1 Introduction

Incomplete combustion produces high concentrations of light absorbing particles which have a direct impact on air quality and the earth's radiative balance. Those particles are divided according to their light absorption properties into the absorbing black carbon (BC) and the moderately to weakly absorbing brown carbon (BrC). The warming potential attributed to BC is one of the most important contributors to climate change, along with carbon dioxide and methane (Pachauri et al., 2014). However, a large uncertainty remains associated with the warming by BC, partly due to the unaccounted-for warming contribution of BrC. The more recent understanding of BrC estimates that, though a weaker light absorber than BC, BrC contributes up to 50% of the light absorption at short wavelengths and is responsible for about 25% of the radiative forcing caused by light absorbing aerosols (Zhang et al., 2017;Wang et al., 2014;Feng et al., 2013a).

BrC is largely emitted in the fuel rich combustion occurring in wildland fires. However, BrC can also be formed via secondary process in the atmosphere (Moise et al., 2015;Lin et al., 2015;Li et al., 2019) or undergo chemical reactions that change its chemical composition and light absorption properties (Forrister et al., 2015;Wong et al., 2017;Cheng et al., 2020). Unlike BC, the chemical makeup and properties of which are relatively well defined, BrC comprises myriad species of different molecular sizes, volatility, solubility, and light absorption properties (Laskin

et al., 2015;Feng et al., 2013b;Andreae and Gelencsér, 2006). While there have been suggestions that the light absorption properties of BrC are determined by the nature of the fuel or the type of combustion (e.g. pyrolysis of wood vs flaming), we have shown, in work separate from this dissertation, that those instead depend on the combustion conditions in a continuous fashion, with less fuel-rich conditions producing progressively darker products (Saleh et al., 2014;Saleh et al., 2018b). In other words, fuel-rich combustion at lower temperatures produces particles with weak light absorption that has a high wavelength dependence, whereas progressively higher air-fuel ratios and higher combustion temperatures produce organics with stronger light absorption and weaker wavelength dependence, approaching the light absorption properties of BC. Following this line of thought, we have proposed the hypothesis that BrC is emitted as the arrested-in-formation BC, such that the production of BC proceeds through the formation of the BrC intermediaries. Extending this framework to the molecular realm, combustion-emitted BrC would then represent the precursor organics necessary for the formation of BC and would thus fill the space of species (and molecular sizes) between the parent fuels and the large carbonaceous structures in BC. Those findings are not foreign to the combustion literature. The dependence of the molecular sizes and optical properties of particulate emissions on flame conditions has been previously reported with a similar pattern to that suggested above (Simonsson et al., 2015;Leschowski et al., 2015;López-Yglesias et al., 2014;Minutolo et al., 1996).

Here, we will focus on BrC produced in incomplete combustion. To understand the chemical composition of combustion-derived BrC, it is essential to describe the formation of pollutant species in incomplete combustion. Combustion begins at elevated temperatures with the decomposition of a fuel, a hydrocarbon (HC), into radicals or other stable hydrocarbons

(Frenklach, 2002;McEnally et al., 2006;Wang, 2011). When combustion is incomplete, those radicals react to form stable species, such as aromatics, which constitute the backbone for further molecular growth into the polycyclic aromatic hydrocarbons that make up the various gaseous and particulate emissions. This molecular growth proceeds by producing species that extend from incipient soot (i.e., the first condensable emissions of combustion, with the smallest molecular sizes) to BC (representing the final product of combustion, with very large molecular sizes). The space between the first produced, or nascent, soot and BC is occupied by various intermediate organic species (Frenklach, 2002;Wang, 2011). Because of their light absorption properties and brown appearance, the intermediate organics are known as BrC. The properties of BrC produced in combustion vary significantly, largely due to variations in combustion conditions such as temperature and air-to-fuel ratio (Cheng et al., 2019;Saleh et al., 2018b). Those conditions dictate the extent of the molecular growth of BrC (Saleh et al., 2018a) and the associated physicochemical properties which influence the climate and health impacts of BrC (Saleh, 2020;Kim et al., 2018;Leskinen et al., 2014;Bølling et al., 2009). One of the aims of this dissertation is to develop an understanding of the different properties of BrC in order to facilitate their representation in climate models. Further, we leverage our understanding of the physicochemical properties of combustion products to investigate their effects on toxicological endpoints.

1.2 The light absorption properties of BrC

The light-absorption properties of BrC, described by the imaginary component of the index of refraction, k, can vary greatly (Saleh, 2020). Values of k at mid-visible wavelengths for different species of BrC have been reported between 10^{-4} and 10^{-1}, spanning several orders of magnitude

(McClure et al., 2020;Saleh et al., 2018;Lambe et al., 2013;Updyke et al., 2012;Cheng et al., 2020;Corbin et al., 2019). At the same time, the wavelength dependence of BrC absorption is also highly variable, with larger wavelength dependence exhibited by the less absorbing BrC (Saleh et al., 2014;Kumar et al., 2018;Xie et al., 2018;Saleh et al., 2018;Cheng et al., 2019;McClure et al., 2020). While BrC was originally thought to be solely produced by low-temperature, smoldering biomass combustion, more recent work has identified BrC species emitted from both the combustion of liquid fuels (Cheng et al., 2019;Corbin et al., 2019;Bai et al., 2020) and the higher temperature combustion of biomass fuels (Saleh et al., 2014;Kumar et al., 2018;McClure et al., 2020;Xie et al., 2018). In addition, the operational definitions of BrC have expanded to include strongly absorbing, nonvolatile, and refractory species (Saleh, 2020;Shetty et al., 2021;Saleh et al., 2018;Corbin et al., 2019).

Thus, the umbrella term BrC covers a range of organic species with widely varying light-absorption and physicochemical properties. This broad range of properties causes a large uncertainty associated with the contribution of BrC to the radiative balance in the atmosphere. In particular, the majority of climate models that represent BrC absorption use a singular set of parameters (i.e., k values) to represent the various light-absorbing organic species due to the difficulty of including a more complex representation. This can underestimate the direct radiative effect of BrC by skewing towards the less-absorbing species, partly due to a dated understanding of BrC that excludes absorption at longer wavelengths. An effective representation of BrC in climate models must thus reduce the complexity associated with representing thousands of species while, at the same time, effectively capture the relevant light-absorption and physicochemical properties.

1.3 The toxicity of combustion particulate matter

Primary combustion particulate matter (PM), emitted from various combustion sources, is associated with increased morbidity through cardiovascular and cardiopulmonary diseases (Pope III and Dockery, 2006;Donaldson et al., 2005). Primary combustion PM is ubiquitous, contributing one to two thirds of all carbonaceous PM over the continental United States (Park et al., 2003;Yu et al., 2004;Bond et al., 2004). There are numerous sources of combustion PM, including the combustion of fossil fuels and biofuels (transportation, power generation, industrial applications) and the combustion of solid biomass in domestic heating and cooking as well as agricultural burning and forest fires. Despite the prevalence of combustion PM, there are lingering gaps in our understanding of its health effects (Black et al., 2017). The composition of combustion PM is highly complex, with varying fractions of organic carbon (OC) and elemental carbon (EC), inorganics, metals, ions, and ash (Hays et al., 2005;Fine et al., 2002;Liu et al., 2017). While all of those species have been associated with toxicological and health impacts, their relative importance is unclear (Dilger et al., 2016;Kasurinen et al., 2017;Reisen et al., 2015). Importantly, the composition of combustion PM is dependent not only on the source, but also on combustion conditions (Saleh, 2020;McClure et al., 2020). Therefore, even for the same fuel, differences in combustion conditions have been found to induce differences in toxicity of the emitted PM (Kim et al., 2019;Bølling et al., 2012;Tapanainen et al., 2011;Leskinen et al., 2014).

1.3.1 The influence of combustion conditions on toxicity

Several studies have compared the impacts of combustion conditions on the toxicological effects of particulate matter by using setups such as biomass burners, residential heating equipment, stoves, and pellet boilers (Leskinen et al., 2014;Bølling et al., 2012;Kocbach et al., 2008;Kim et al.,

2018;Kim et al., 2019;Happo et al., 2013). The results emerging from the different studies, however, point in different directions.

Bølling et al. (2012) found that particulate matter (PM) emitted from the combustion of wood in a cast-iron wood stove at low temperatures (500-800 °C) caused a higher cytotoxic response than PM emitted at higher temperatures (700-1000 °C). Similar results were reported by Kocbach et al. (2008) for PM emitted from the combustion of wood in a conventional stove burning birch wood at 700-1000 °C. As discussed earlier, lower combustion temperatures typically imply less efficient combustion conditions. Thus, the above the findings also agree with reports of higher PM toxicity from the inefficient operation of masonry heaters (Jalava et al., 2010;Tapanainen et al., 2011).

On the other hand, other studies reported that the PM from higher temperature combustion conditions were more toxic. Happo et al. (2013) found that particulate emissions from newer biomass heating appliances, which are typically more efficient and achieve higher combustion temperatures than older technologies, induced higher inflammatory, cytotoxic, and genotoxic responses. Uski et al. (2014) compared the toxicity of PM from smoldering and efficient combustion in heating appliances and found that, while the PM emitted under smoldering conditions caused greater DNA damage and cell death, those emitted from more efficient combustion were more effective in decreasing metabolic activity and causing oxidative stress. Kim et al. (2018) compared the toxicity induced in mice respiratory systems by PM from the combustion of different biomass fuels under smoldering and flaming conditions. They found that the latter had higher toxic and mutagenic potencies per unit mass of emitted PM. In a follow-up study in which the mice directly inhaled the biomass combustion emissions, they found that lung

inflammation caused by peat and eucalyptus smoke under both flaming and smoldering conditions was not reproduced with oak smoke (Kim et al., 2019).

Clearly, the results from different studies have not converged to determine which combustion regime generates the more toxic PM. A possible explanation of this discrepancy is the difficulty in controlling conditions, particularly in the case of biomass combustion. To conduct a systematic comparison of the toxicity of PM from different combustion conditions, it is essential to ensure that the combustion conditions are spatially uniform and stable for the duration of the experiment.

1.3.2 Atmospheric aging of combustion emissions and its effect on toxicity

Immediately after they are emitted, organic combustion emissions undergo processes that change their chemical identity and alter their phase state (Garofalo et al., 2019;Cappa et al., 2020;Hodshire et al., 2019). Downstream of the combustion source, primary organic aerosols (POA), i.e., those that are emitted in the particle phase at the source, react with atmospheric oxidants such as ozone and hydroxyl radicals, becoming more oxidized, with higher O:C ratios (Cappa et al., 2020;Hodshire et al., 2019). Primary particles could also undergo further changes due to photolytic aging (Wong et al., 2017). In addition, species emitted in the vapor phase can undergo photooxidation reactions, decreasing their volatility and leading to their condensation into the particle phase, thus forming secondary organic aerosols (SOA) (Ahern et al., 2019;Akherati et al., 2020). In a competing mechanism, the dilution of combustion plumes as they move away from the source leads to the evaporation of the more volatile components of the particles. These processes lead to fundamentally different particle compositions as combustion emissions evolve in the atmosphere and reach human populations, with possible

implications for their effect on human health. While there have been numerous studies documenting the effects of biomass combustion emissions on health (Holm et al., 2021;Naeher et al., 2007), there are no studies that we are aware of that have looked systematically at the impact of atmospheric aging on the *in vitro* or *in vivo* toxicity of biomass combustion emissions. We have found two studies that compared the oxidative potential (OP) of fresh and aged BBOA using the dithiothreitol (DTT) chemical assay (Wong et al., 2019;Jiang and Jang, 2018). Wong et al. (2019) used field and laboratory data to compare the effect of atmospheric transport time (field) and different aging mechanisms (laboratory) on the BBOA's OP. They reported a 50% increase in the OP of field BBOA after only a few hours of atmospheric transport, with relatively stable OP after that. In their laboratory experiments, however, they found that the aging of BBOA by photolysis increased their OP initially only to cause a decline after some time, while aqueous OH oxidation rapidly led to a significant decline in OP. They also examined the effects of dilution and found that the reduction of water-soluble organic content, as the more volatile species evaporated, led to a large increase in OP. Jiang and Jang (2018) measured the DTT activity of wood smoke particles over a period of several hours of photooxidation. They found that the photochemical aging of the particles led to a significant decrease in their OP, which they attributed to the decomposition of oxidizers. In all, those studies showed that atmospheric processes can have a significant effect on the OP of BBOA.

1.4 Specific aims and summary of chapters

The objectives of this dissertation can be divided into three parts. In the first, we investigate the relation between the physicochemical properties of biomass combustion BrC, specifically their solubility, and their light absorption properties. In the second, we conduct controlled

experiments simulating smoldering and flaming combustion to determine the effect of combustion conditions on the toxicity of BrC. Finally, we examine the effects of photolytic aging on the toxicity of biomass combustion emissions. In what follows, I include a summary of the aims and findings of each chapter.

1.4.1 Chapter 2 – "A dominant contribution to light absorption by methanol-insoluble brown carbon produced in the combustion of biomass fuels"

The light-absorption properties of brown carbon (BrC) are often estimated using offline, solvent-extraction methods. However, recent studies have found evidence of insoluble species of BrC which are unaccounted for in solvent-extraction. In this chapter, we produced carbonaceous aerosol particles from the combustion of three biomass fuels (dead pine needles, hickory twigs, and dead oak foliage). We utilized a combination of online and offline measurements and optical calculations to estimate the mass fractions and contribution to light absorption by methanol-soluble BrC (MSBrC), methanol-insoluble BrC (MIBrC), and elemental carbon (EC). Averaged over all experiments, the majority of the carbonaceous aerosol species were attributed to MSBrC (90% ± 5%), while MIBrC and EC constituted 9% ± 5% and 1% ± 0.5%, respectively. The BrC produced in all experiments was moderately absorbing, with an imaginary component of the refractive index (k) at 532 nm ranging between 0.01 and 0.05. However, the k values at 532 nm of the MSBrC (0.004 ± 0.002) and MIBrC (0.211 ± 0.113) fractions were separated by orders of magnitude, with MSBrC categorized as weakly absorbing BrC and MIBrC as strongly absorbing BrC. Consequently, even though MSBrC constituted the majority of the aerosol mass, MIBrC had a dominant contribution to light absorption at 532 nm (72% ± 11%). Those findings provide support for previous reports of the existence of strongly absorbing, insoluble BrC species and

indicate that relying on methanol extraction to characterize BrC in biomass-burning emissions would severely underestimate its absorption.

1.4.2 Chapter 3 – "Physicochemical properties and cytotoxicity of brown carbon produced under different combustion conditions"

In this chapter, we investigate the effect of combustion conditions on the molecular sizes of BrC, their light-absorption properties, and their cytotoxicity. We used toluene in a combustion reactor with highly controlled conditions to produce two different types of BrC under two conditions corresponding to smoldering and near-flaming combustion, with temperatures of 670 °C and 1035 °C, respectively. We performed online measurements of the size distributions and light-absorption properties of the BrC. The BrC produced at 1035 °C was more light absorbing, with an imaginary component of the refractive index at 532 nm (k532) an order of magnitude larger than that of the BrC produced at 670 °C. We also collected samples for offline chemical characterization using laser desorption ionization (LDI) mass spectrometry. The LDI mass spectra showed that the BrC produced at 1035 °C was composed of species with significantly larger molecular sizes than the BrC produced at 670 °C. Using human lung epithelial cells, we conducted in vitro cytotoxicity analysis on the two types of BrC with doses ranging from 3.5 to 136.0 μg of BrC/ml. After 24-h exposure, the viability of the cells was assessed using a WST-8 assay. The cytotoxicity analysis showed that, for both BrC samples, the cells exhibited a clear dose-dependent response with significant BrC cytotoxicity that plateaued at the higher doses. However, while the viability of cells exposed to the BrC produced at 1035 °C reached a minimum of around 65% at the highest dose, the BrC produced at 670 °C proved to be significantly more toxic, with the viability dropping asymptotically to 25%. The results presented here suggest that

organic PM of smaller molecular sizes produced under lower temperature, smoldering combustion could be significantly more toxic than those of larger molecular sizes produced under higher temperature, flaming conditions. The use of a single-molecule fuel in a highly controlled combustion setup distinguishes this work from experiments that rely on real-life sources and combustion setups, where different combustion conditions could be occurring simultaneously and clouding the conclusions.

1.4.3 Chapter 4 – "The Cytotoxicity and Chemical Properties of Laboratory-Produced Fresh and Aged Biomass Burning Organic Aerosols"

In this chapter, we conducted laboratory experiments producing biomass burning organic aerosols (BBOA) from the combustion of different biomass fuels: dead oak foliage, hickory twigs, and pine needles. We used UV radiation to initiate the photooxidation of BBOA, leading to a significant production of secondary organic particle mass. We collected fresh and aged BBOA (before and after the UV lights were turned on, respectively) and compared their toxicity *in vitro* to human lung epithelial cells using a cell viability (WST-8) assay. Using ultra-high resolution electrospray ionization mass spectrometry (ESI-MS), we found that the aging of the BBOA samples led to significant changes in their chemical makeup and to increases in their O:C and OC:OM ratios. Using induction-coupled plasma mass spectrometry (ICP-MS), we detected trace concentrations of known toxic metals such as arsenic, selenium, manganese, and others. In the cell viability assays, we found that the fresh hickory BBOA was the most toxic, followed by the pine and oak BBOA. For all fuels, the fresh BBOA particles was slightly more toxic than the aged BBOA at the highest exposure doses. However, at intermediate doses, there was a marked difference in the onset of toxicity, with the fresh BBOA more toxic at lower doses. The differences

in toxicity are likely caused by a combination of factors, including the availability and concentrations of toxic metals in the different samples as well as chemical changes following oxidation. In general, our findings indicate that both fresh and aged BBOA are significantly toxic to cells. However, we detected differences in toxicity at intermediate doses that warrant further investigation.

1.5 Summary

Particulate emissions from biomass combustion have multifaceted impacts on climate and health. The work presented in this dissertation explores the relation between the fundamentals of particle formation in combustion and the physicochemical properties of the particles, first presenting a new framework for the understanding and representation of BrC. Further, the dissertation leverages our understanding of particle formation in combustion to examine the effect of combustion conditions on the toxicity of BrC. Finally, we examined the yet unidentified impact of atmospheric processing on the toxicity of biomass combustion emissions.

References

Ahern, A., Robinson, E., Tkacik, D., Saleh, R., Hatch, L., Barsanti, K., Stockwell, C., Yokelson, R., Presto, A., and Robinson, A.: Production of secondary organic aerosol during aging of biomass burning smoke from fresh fuels and its relationship to VOC precursors, Journal of Geophysical Research: Atmospheres, 124, 3583-3606, 2019.

Akherati, A., He, Y., Coggon, M. M., Koss, A. R., Hodshire, A. L., Sekimoto, K., Warneke, C., de Gouw, J., Yee, L., and Seinfeld, J. H.: Oxygenated aromatic compounds are important precursors of secondary organic aerosol in biomass-burning emissions, Environmental Science & Technology, 54, 8568-8579, 2020.

Andreae, M., and Gelencsér, A.: Black carbon or brown carbon? The nature of light-absorbing carbonaceous aerosols, Atmospheric Chemistry and Physics, 6, 3131-3148, 2006.

Black, C., Tesfaigzi, Y., Bassein, J. A., and Miller, L. A.: Wildfire smoke exposure and human health: Significant gaps in research for a growing public health issue, Environmental toxicology and pharmacology, 55, 186-195, 2017.

Bølling, A. K., Pagels, J., Yttri, K. E., Barregard, L., Sallsten, G., Schwarze, P. E., and Boman, C.: Health effects of residential wood smoke particles: the importance of combustion conditions and physicochemical particle properties, Particle and fibre toxicology, 6, 29, 2009.

Bølling, A. K., Totlandsdal, A. I., Sallsten, G., Braun, A., Westerholm, R., Bergvall, C., Boman, J., Dahlman, H. J., Sehlstedt, M., and Cassee, F.: Wood smoke particles from different combustion phases induce similar pro-inflammatory effects in a co-culture of monocyte and pneumocyte cell lines, Particle and fibre toxicology, 9, 45, 2012.

Bond, T. C., Streets, D. G., Yarber, K. F., Nelson, S. M., Woo, J. H., and Klimont, Z.: A technology-based global inventory of black and organic carbon emissions from combustion, Journal of Geophysical Research: Atmospheres, 109, 2004.

Cappa, C. D., Lim, C. Y., Hagan, D. H., Coggon, M., Koss, A., Sekimoto, K., Gouw, J. d., Onasch, T. B., Warneke, C., and Kroll, J. H.: Biomass-burning-derived particles from a wide variety of fuels–part 2: effects of photochemical aging on particle optical and chemical properties, Atmospheric Chemistry and Physics, 20, 8511-8532, 2020.

Cheng, Z., Atwi, K. M., Yu, Z., Avery, A., Fortner, E. C., Williams, L., Majluf, F., Krechmer, J. E., Lambe, A. T., and Saleh, R.: Evolution of the light-absorption properties of combustion brown carbon aerosols following reaction with nitrate radicals, Aerosol Science and Technology, 1-15, 2020.

Cheng, Z. Z., Atwi, K., Onyima, T., and Saleh, R.: Investigating the dependence of light-absorption properties of combustion carbonaceous aerosols on combustion conditions, Aerosol Science and Technology, 53, 419-434, 10.1080/02786826.2019.1566593, 2019.

Dilger, M., Orasche, J., Zimmermann, R., Paur, H.-R., Diabaté, S., and Weiss, C.: Toxicity of wood smoke particles in human A549 lung epithelial cells: the role of PAHs, soot and zinc, Archives of toxicology, 90, 3029-3044, 2016.

Donaldson, K., Tran, L., Jimenez, L. A., Duffin, R., Newby, D. E., Mills, N., MacNee, W., and Stone, V.: Combustion-derived nanoparticles: a review of their toxicology following inhalation exposure, Particle and fibre toxicology, 2, 10, 2005.

Feng, Y., Ramanathan, V., and Kotamarthi, V. R.: Brown carbon: a significant atmospheric absorber of solar radiation?, Atmos. Chem. Phys., 13, 8607-8621, 10.5194/acp-13-8607-2013, 2013a.

Feng, Y., Ramanathan, V., and Kotamarthi, V. R.: Brown carbon: a significant atmospheric absorber of solar radiation?, Atmospheric Chemistry and Physics, 13, 8607-8621, 10.5194/acp-13-8607-2013, 2013b.

Fine, P. M., Cass, G. R., and Simoneit, B. R.: Chemical characterization of fine particle emissions from the fireplace combustion of woods grown in the southern United States, Environmental Science & Technology, 36, 1442-1451, 2002.

Forrister, H., Liu, J., Scheuer, E., Dibb, J., Ziemba, L., Thornhill, K. L., Anderson, B., Diskin, G., Perring, A. E., and Schwarz, J. P.: Evolution of brown carbon in wildfire plumes, Geophysical Research Letters, 42, 4623-4630, 2015.

Frenklach, M.: Reaction mechanism of soot formation in flames, Physical chemistry chemical Physics, 4, 2028-2037, 2002.

Garofalo, L. A., Pothier, M. A., Levin, E. J., Campos, T., Kreidenweis, S. M., and Farmer, D. K.: Emission and evolution of submicron organic aerosol in smoke from wildfires in the western United States, ACS Earth and Space Chemistry, 3, 1237-1247, 2019.

Happo, M. S., Uski, O., Jalava, P. I., Kelz, J., Brunner, T., Hakulinen, P., Mäki-Paakkanen, J., Kosma, V.-M., Jokiniemi, J., and Obernberger, I.: Pulmonary inflammation and tissue damage in the mouse lung after exposure to PM samples from biomass heating appliances of old and modern technologies, Science of the total environment, 443, 256-266, 2013.

Hays, M. D., Fine, P. M., Geron, C. D., Kleeman, M. J., and Gullett, B. K.: Open burning of agricultural biomass: physical and chemical properties of particle-phase emissions, Atmospheric environment, 39, 6747-6764, 2005.

Hodshire, A. L., Akherati, A., Alvarado, M. J., Brown-Steiner, B., Jathar, S. H., Jimenez, J. L., Kreidenweis, S. M., Lonsdale, C. R., Onasch, T. B., and Ortega, A. M.: Aging effects on biomass burning aerosol mass and composition: A critical review of field and laboratory studies, Environmental science & technology, 53, 10007-10022, 2019.

Holm, S. M., Miller, M. D., and Balmes, J. R.: Health effects of wildfire smoke in children and public health tools: a narrative review, Journal of exposure science & environmental epidemiology, 31, 1-20, 2021.

Jalava, P. I., Salonen, R. O., Nuutinen, K., Pennanen, A. S., Happo, M. S., Tissari, J., Frey, A., Hillamo, R., Jokiniemi, J., and Hirvonen, M.-R.: Effect of combustion condition on cytotoxic and inflammatory activity of residential wood combustion particles, Atmospheric Environment, 44, 1691-1698, 2010.

Jiang, H., and Jang, M.: Dynamic oxidative potential of atmospheric organic aerosol under ambient sunlight, Environmental science & technology, 52, 7496-7504, 2018.

Kasurinen, S., Jalava, P. I., Happo, M. S., Sippula, O., Uski, O., Koponen, H., Orasche, J., Zimmermann, R., Jokiniemi, J., and Hirvonen, M. R.: Particulate emissions from the combustion of birch, beech, and spruce logs cause different cytotoxic responses in A549 cells, Environmental toxicology, 32, 1487-1499, 2017.

Kim, Y. H., Warren, S. H., Krantz, Q. T., King, C., Jaskot, R., Preston, W. T., George, B. J., Hays, M. D., Landis, M. S., and Higuchi, M.: Mutagenicity and lung toxicity of smoldering vs.

flaming emissions from various biomass fuels: implications for health effects from wildland fires, Environmental health perspectives, 126, 017011, 2018.

Kim, Y. H., King, C., Krantz, T., Hargrove, M. M., George, I. J., McGee, J., Copeland, L., Hays, M. D., Landis, M. S., and Higuchi, M.: The role of fuel type and combustion phase on the toxicity of biomass smoke following inhalation exposure in mice, Archives of toxicology, 1-13, 2019.

Kocbach, A., Herseth, J. I., Låg, M., Refsnes, M., and Schwarze, P. E.: Particles from wood smoke and traffic induce differential pro-inflammatory response patterns in co-cultures, Toxicology and applied pharmacology, 232, 317-326, 2008.

Laskin, A., Laskin, J., and Nizkorodov, S. A.: Chemistry of atmospheric brown carbon, Chemical reviews, 115, 4335-4382, 2015.

Leschowski, M., Thomson, K., Snelling, D., Schulz, C., and Smallwood, G.: Combination of LII and extinction measurements for determination of soot volume fraction and estimation of soot maturity in non-premixed laminar flames, Applied Physics B, 119, 685-696, 2015.

Leskinen, J., Tissari, J., Uski, O., Virén, A., Torvela, T., Kaivosoja, T., Lamberg, H., Nuutinen, I., Kettunen, T., and Joutsensaari, J.: Fine particle emissions in three different combustion conditions of a wood chip-fired appliance–Particulate physico-chemical properties and induced cell death, Atmospheric environment, 86, 129-139, 2014.

Li, C., He, Q., Hettiyadura, A. P. S., Käfer, U., Shmul, G., Meidan, D., Zimmermann, R., Brown, S. S., George, C., and Laskin, A.: Formation of Secondary Brown Carbon in Biomass Burning Aerosol Proxies through NO3 Radical Reactions, Environmental science & technology, 2019.

Lin, P., Liu, J., Shilling, J. E., Kathmann, S. M., Laskin, J., and Laskin, A.: Molecular characterization of brown carbon (BrC) chromophores in secondary organic aerosol generated from photo-oxidation of toluene, Physical Chemistry Chemical Physics, 17, 23312-23325, 2015.

Liu, L., Kong, S., Zhang, Y., Wang, Y., Xu, L., Yan, Q., Lingaswamy, A., Shi, Z., Lv, S., and Niu, H.: Morphology, composition, and mixing state of primary particles from combustion sources—crop residue, wood, and solid waste, Scientific reports, 7, 1-15, 2017.

López-Yglesias, X., Schrader, P. E., and Michelsen, H. A.: Soot maturity and absorption cross sections, Journal of Aerosol Science, 75, 43-64, 2014.

McClure, C. D., Lim, C. Y., Hagan, D. H., Kroll, J. H., and Cappa, C. D.: Biomass-burning-derived particles from a wide variety of fuels–Part 1: Properties of primary particles, Atmospheric Chemistry & Physics, 20, 2020.

McEnally, C. S., Pfefferle, L. D., Atakan, B., and Kohse-Höinghaus, K.: Studies of aromatic hydrocarbon formation mechanisms in flames: Progress towards closing the fuel gap, Progress in Energy and Combustion Science, 32, 247-294, 2006.

Minutolo, P., Gambi, G., and D'alessio, A.: The optical band gap model in the interpretation of the UV-visible absorption spectra of rich premixed flames, Symposium (International) on Combustion, 1996, 951-957,

Moise, T., Flores, J. M., and Rudich, Y.: Optical properties of secondary organic aerosols and their changes by chemical processes, Chemical reviews, 115, 4400-4439, 2015.

Naeher, L. P., Brauer, M., Lipsett, M., Zelikoff, J. T., Simpson, C. D., Koenig, J. Q., and Smith, K. R.: Woodsmoke health effects: a review, Inhalation toxicology, 19, 67-106, 2007.

Pachauri, R. K., Allen, M. R., Barros, V. R., Broome, J., Cramer, W., Christ, R., Church, J. A., Clarke, L., Dahe, Q., and Dasgupta, P.: Climate change 2014: synthesis report. Contribution of Working Groups I, II and III to the fifth assessment report of the Intergovernmental Panel on Climate Change, Ipcc, 2014.

Park, R. J., Jacob, D. J., Chin, M., and Martin, R. V.: Sources of carbonaceous aerosols over the United States and implications for natural visibility, Journal of Geophysical Research: Atmospheres, 108, 2003.

Pope III, C. A., and Dockery, D. W.: Health effects of fine particulate air pollution: lines that connect, Journal of the air & waste management association, 56, 709-742, 2006.

Reisen, F., Duran, S. M., Flannigan, M., Elliott, C., and Rideout, K.: Wildfire smoke and public health risk, International Journal of Wildland Fire, 24, 1029-1044, 2015.

Saleh, R., Robinson, E. S., Tkacik, D. S., Ahern, A. T., Liu, S., Aiken, A. C., Sullivan, R. C., Presto, A. A., Dubey, M. K., and Yokelson, R. J.: Brownness of organics in aerosols from biomass burning linked to their black carbon content, Nature Geoscience, 7, 647, 2014.

Saleh, R., Cheng, Z., and Atwi, K.: The brown–black continuum of light-absorbing combustion aerosols, Environmental Science & Technology Letters, 5, 508-513, 2018a.

Saleh, R., Cheng, Z., and Atwi, K.: The Brown–Black Continuum of Light-Absorbing Combustion Aerosols, Environmental Science & Technology Letters, 2018b.

Saleh, R.: From Measurements to Models: Toward Accurate Representation of Brown Carbon in Climate Calculations, Current Pollution Reports, 1-15, 2020.

Simonsson, J., Olofsson, N.-E., Török, S., Bengtsson, P.-E., and Bladh, H.: Wavelength dependence of extinction in sooting flat premixed flames in the visible and near-infrared regimes, Applied Physics B, 119, 657-667, 2015.

Tapanainen, M., Jalava, P. I., Mäki-Paakkanen, J., Hakulinen, P., Happo, M. S., Lamberg, H., Ruusunen, J., Tissari, J., Nuutinen, K., and Yli-Pirilä, P.: In vitro immunotoxic and genotoxic activities of particles emitted from two different small-scale wood combustion appliances, Atmospheric Environment, 45, 7546-7554, 2011.

Uski, O., Jalava, P., Happo, M., Leskinen, J., Sippula, O., Tissari, J., Mäki-Paakkanen, J., Jokiniemi, J., and Hirvonen, M.-R.: Different toxic mechanisms are activated by emission PM depending on combustion efficiency, Atmospheric Environment, 89, 623-632, 2014.

Wang, H.: Formation of nascent soot and other condensed-phase materials in flames, Proceedings of the Combustion Institute, 33, 41-67, 2011.

Wang, X., Heald, C., Ridley, D., Schwarz, J., Spackman, J., Perring, A., Coe, H., Liu, D., and Clarke, A.: Exploiting simultaneous observational constraints on mass and absorption to estimate the global direct radiative forcing of black carbon and brown carbon, 2014.

Wong, J. P., Nenes, A., and Weber, R. J.: Changes in light absorptivity of molecular weight separated brown carbon due to photolytic aging, Environmental science & technology, 51, 8414-8421, 2017.

Wong, J. P., Tsagkaraki, M., Tsiodra, I., Mihalopoulos, N., Violaki, K., Kanakidou, M., Sciare, J., Nenes, A., and Weber, R. J.: Effects of atmospheric processing on the oxidative potential of biomass burning organic aerosols, Environmental science & technology, 53, 6747-6756, 2019.

Yu, S., Dennis, R. L., Bhave, P. V., and Eder, B. K.: Primary and secondary organic aerosols over the United States: estimates on the basis of observed organic carbon (OC) and elemental carbon (EC), and air quality modeled primary OC/EC ratios, Atmospheric Environment, 38, 5257-5268, 2004.

Zhang, Y., Forrister, H., Liu, J., Dibb, J., Anderson, B., Schwarz, J. P., Perring, A. E., Jimenez, J. L., Campuzano-Jost, P., and Wang, Y.: Top-of-atmosphere radiative forcing affected by brown carbon in the upper troposphere, Nature Geoscience, 10, 486-489, 2017.

CHAPTER 2

A DOMINANT CONTRIBUTION TO LIGHT ABSORPTION BY METHANOL-INSOLUBLE BROWN CARBON PRODUCED IN THE COMBUSTION OF BIOMASS FUELS[1]

[1] Atwi, K., Cheng, Z., El Hajj, O., Perri, C., Saleh, R. To be submitted to *Environmental Science and Technology*, August 1, 2021

Abstract

The light-absorption properties of brown carbon (BrC) are often estimated using offline, solvent-extraction methods. However, recent studies have found evidence of insoluble species of BrC which are unaccounted for in solvent-extraction. In this work, we produced carbonaceous aerosol particles from the combustion of three biomass fuels (dead pine needles, hickory twigs, and dead oak foliage). We utilized a combination of online and offline measurements and optical calculations to estimate the mass fractions and contribution to light absorption by methanol-soluble BrC (MSBrC), methanol-insoluble BrC (MIBrC), and elemental carbon (EC). Averaged over all experiments, the majority of the carbonaceous aerosol species were attributed to MSBrC (90% ± 5%), while MIBrC and EC constituted 9% ± 5% and 1% ± 0.5%, respectively. The BrC produced in all experiments was moderately absorbing, with an imaginary component of the refractive index (*k*) at 532 nm ranging between 0.01 and 0.05. However, the *k* values at 532 nm of the MSBrC (0.004 ± 0.002) and MIBrC (0.211 ± 0.113) fractions were separated by orders of magnitude, with MSBrC categorized as weakly absorbing BrC and MIBrC as strongly absorbing BrC. Consequently, even though MSBrC constituted the majority of the aerosol mass, MIBrC had a dominant contribution to light absorption at 532 nm (72% ± 11%). The findings presented in this paper provide support for previous reports of the existence of strongly absorbing, insoluble BrC species and indicate that relying on methanol extraction to characterize BrC in biomass-burning emissions would severely underestimate its absorption.

2.1 Introduction

Combustion sources can produce different species of light-absorbing particles that contribute to the radiative balance at the top of the atmosphere. Black carbon (BC), the most absorbing of those species, is one of the three most potent contributors to radiative forcing, along with carbon dioxide and methane (Pachauri et al., 2014). Other light-absorbing particles, known as brown carbon (BrC), absorb light less efficiently than BC, yet exert significant radiative forcing (Zhang et al., 2017;Wang et al., 2014;Feng et al., 2013;Brown et al., 2018).

The light-absorption properties of BrC, described by the imaginary component of the index of refraction, *k*, can vary greatly (Saleh, 2020). Values of *k* at mid-visible wavelengths for different species of BrC have been reported between 10^{-4} and 10^{-1}, spanning several orders of magnitude (McClure et al., 2020;Saleh et al., 2018;Lambe et al., 2013;Updyke et al., 2012;Cheng et al., 2020;Corbin et al., 2019). At the same time, the wavelength dependence of BrC absorption is also highly variable, with larger wavelength dependence exhibited by the less absorbing BrC (Saleh et al., 2014;Kumar et al., 2018;Xie et al., 2018;Saleh et al., 2018;Cheng et al., 2019;McClure et al., 2020). While BrC was originally thought to be solely produced by low-temperature, smoldering biomass combustion, more recent work has identified BrC species emitted from both the combustion of liquid fuels (Cheng et al., 2019;Corbin et al., 2019;Bai et al., 2020) and the higher temperature combustion of biomass fuels (Saleh et al., 2014;Kumar et al., 2018;McClure et al., 2020;Xie et al., 2018). In addition, the operational definitions of BrC have expanded to include strongly absorbing, nonvolatile, and refractory species (Saleh, 2020;Shetty et al., 2021;Saleh et al., 2018;Corbin et al., 2019).

Thus, the umbrella term BrC covers a range of organic species with widely varying light-absorption and physicochemical properties. This broad range of properties causes a large uncertainty associated with the contribution of BrC to the radiative balance in the atmosphere. In particular, the majority of climate models that represent BrC absorption use a singular set of parameters (i.e., *k* values) to represent the various light-absorbing organic species due to the difficulty of including a more complex representation. This can underestimate the direct radiative effect of BrC by skewing towards the less-absorbing species, partly due to a dated understanding of BrC that excludes absorption at longer wavelengths. An effective representation of BrC in climate models must thus reduce the complexity associated with representing thousands of species while, at the same time, effectively capture the relevant light-absorption and physicochemical properties.

In recent years, parameterizations and categorizations have been introduced to facilitate this outcome. Saleh et al. (2014) showed that light absorption properties of BrC emitted from biomass burning can be parameterized as a function of the emissions' relative BC and OA content. Those parameterizations have already been used in some models, yielding a better agreement between model predictions and observations (Brown et al., 2018). More recent classifications of BrC have also been proposed based on their physicochemical properties. Corbin et al. (2019) divided BrC into soluble BrC and tar BrC, defined by their solubility or insolubility, respectively, in any of the commonly used solvents such as water, methanol, and acetone. Corbin et al.'s categorizations of BrC further include physicochemical properties characteristic of each category, such as light-absorption properties, volatility, and molecular sizes. Saleh (2020) presented a classification based on light-absorption properties, dividing BrC into 4 bins spanning the 4 orders of magnitude

covered by reported *k* values of BrC in the literature. Saleh's light absorption-based BrC classification also highlights that more absorbing BrC species tend to be less volatile, less soluble, and to consist of larger molecular sizes.

The distinction drawn by Corbin et al. (2019) between soluble and insoluble BrC can be further extended to distinguish soluble species of BrC. Indeed, numerous studies have found that water soluble BrC is less absorbing than methanol-soluble BrC (Huang et al., 2020;Satish and Rastogi, 2019;Chen and Bond, 2010). Further, Cheng et al. (2020) showed that some BrC that is insoluble in methanol is soluble in dichloromethane (DCM), with DCM-soluble species being more light absorbing than the methanol-soluble species. Cheng et al. (2020) also found that a significant fraction of some BrC samples could be insoluble in both. Those insoluble BrC species create a disagreement between the light-absorption properties retrieved via solvent-extraction methods and those retrieved in online measurements. In fact, Shetty et al. (2019) found that the absorption properties of biomass-burning particles retrieved using solvent-extraction methods and those retrieved from online measurements could differ by up to a factor of 10, with the discrepancy increasing with increasing elemental carbon (EC) content. As shown by previous studies of biomass-burning BrC, higher EC content is correlated with stronger light absorption by BrC (McClure et al., 2020;Saleh et al., 2014).

In this paper, we present further evidence of insoluble BrC produced from the combustion of biomass fuels. We use a combination of online and offline measurements to divide the biomass-burning BrC into methanol-soluble and methanol-insoluble fractions and retrieve the light-absorption properties of each fraction. Doing so, we show that even though the majority of the BrC was methanol-soluble, the light-absorption was dominated by the methanol-insoluble BrC.

2.2 Methods

2.2.1 Experimental procedure

We burnt dead pine needles, hickory twigs, and dead oak foliage inside a 7.5 m^3 environmental chamber. These fuels are commonly consumed in wildfires and prescribed burns in the Southeastern United States (Zheng et al., 2002;Fine et al., 2002). The fuels were collected from the University of Georgia campus or purchased from a supply store. They were then dried inside an oven at 60 °C for 24 hours to reduce their moisture content. 25-50 g of each fuel were mounded on sheets of aluminum foil, ignited using a handheld butane lighter inside a fume hood, and then transferred into the environmental chamber. In general, the fuels were allowed to burn inside the chamber for tens of seconds up to a minute. Afterwards, the chamber was sealed. We then performed online measurements and collected filter samples for offline measurements over a period of several hours.

A scanning mobility particle sizer (SMPS, TSI 3882) continuously measured the particle size distribution in the range of 10-500 nm. We used a photoacoustic spectrometer (Multi-PAS III) to measure the absorption coefficient (b_{abs} , Mm^{-1}) of the aerosol at 3 wavelengths: 422 nm, 532 nm, and 782 nm. As described in Section 2.2.3, these online measurements were used to retrieve the aerosol light-absorption properties.

We collected particles on two filter trains at a flow rate of 5 SLPM for offline analysis. One consisted of a sole 47 mm Quartz (Q) filter (Pall Inc., Tissuquartz 2500), the other of a 47 mm Teflon (PTFE) filter (0.2 microns, Sterlitech Corporation, PTU024750) followed by a Quartz behind Teflon filter (QBT). We targeted a total particle mass loading of 300 µg on the Quartz and Teflon filters, estimated from the sampling flowrate and total particle mass concentration obtained

from SMPS measurements. Depending on the particle concentration in the environmental chamber, we collected the filter samples for several hours until the target loading was approximately reached. The Quartz and QBT filters were used to determine the fractions of methanol-soluble BrC (MSBrC), methanol-insoluble BrC (MIBrC), and EC (Section 2.2.2) and the Teflon filter was used to determine the light-absorption properties of MSBrC (Section 2.2.4).

2.2.2 Mass apportionment

The procedure to apportion the particle mass into fractions of MSBrC, MIBrC, and EC is illustrated in Figure 2.1. We immersed a 1.5 cm^2 punch of the Quartz filter in 3 ml of methanol for 24 hours in a process of passive extraction, i.e., without sonication. This process minimizes the physical extraction of methanol-insoluble species from the Quartz filter, while also preserving the integrity of the filter for the subsequent analysis (Shetty et al., 2019;Phillips and Smith, 2017). After 24 hours, the Quartz punch was removed, washed with more methanol, and dried using a stream of clean, dry air. We then used an organic carbon – elemental carbon (OCEC) analyzer (Sunset Laboratory Inc, Portland, OR, USA, Model 5 L) running the NIOSH-870 protocol to determine the remaining total carbon (TC) mass on the extracted filter punch ($TC_{Q,extracted}$). As further elaborated below, $TC_{Q,extracted}$ corresponds to TC of the insoluble species, including both MIBrC and EC:

$$TC_{Q,extracted} = OC_{MIBrC} + EC \quad (1)$$

Here, OC_{MIBrC} and EC were obtained from the OCEC analyzer measurements of the extracted Quartz punch. The OCEC analyzer divides the analyte into OC and EC depending on the temperature and conditions at which they evaporate during the analysis protocol. It also identifies pyrolyzed OC, which corresponds to organic species that become pyrolyzed during the

initial heating phase, resisting volatilization in the oxygen-deficient phase and appearing instead with the EC (Wu et al., 2016;Khan et al., 2012). In Equation (1), OC_{MIBrC} includes both the non-pyrolyzed and the pyrolyzed OC reported by the OCEC analyzer. An implicit assumption in Equation (1) is that all the carbon in MIBrC is detected as OC in the OCEC analyzer. In reality, it is possible that some strongly absorbing, refractory BrC is mistakenly classified as EC by thermal-optical measurements(Corbin et al., 2019;Corbin and Gysel-Beer, 2019;Cheng et al., 2019). Thus, OC_{MIBrC} could be underestimated and EC overestimated in the analysis.

In order to determine the methanol-soluble OC (OC_{MSBrC}) fraction, we ran the same OCEC analyzer protocol to determine the TC mass on an unextracted Quartz filter punch ($TC_{Q,unextracted}$) and on a QBT filter punch (TC_{QBT}). Since the QBT filter only collected adsorbed vapor species, the difference between TC_Q and TC_{QBT} corresponds to the total TC mass of particles collected (Subramanian et al., 2004), including MSBrC, MIBrC, and EC:

$$TC_{Q,unextracted} - TC_{QBT} = OC_{MSBrC} + OC_{MIBrC} + EC \quad (2)$$

Then, OC_{MSBrC} can be obtained from Equation (1) and Equation (2) as:

$$OC_{MSBrC} = (TC_{Q,unextracted} - TC_{QBT}) - TC_{extracted} \quad (3)$$

We converted OC_{MSBrC} and OC_{MIBrC} to organic-mass basis (OM_{MSBrC} and OM_{MIBrC}) assuming OM/OC of 1.8, which is typical for biomass-combustion emissions (El-Zanan et al., 2005;Aiken et al., 2008;Yao et al., 2016).

The fractions of MSBrC, MIBrC, and EC in the particles were then obtained as:

$$f_{MSBrC} = \frac{OM_{MSBrC}}{TM}; f_{MIBrC} = \frac{OM_{MIBrC}}{TM}; f_{EC} = \frac{EC}{TM} \quad (4)$$

Where TM is the total mass of carbonaceous species:

$$TM = OM_{MSBrC} + OM_{MIBrC} + EC \quad (5)$$

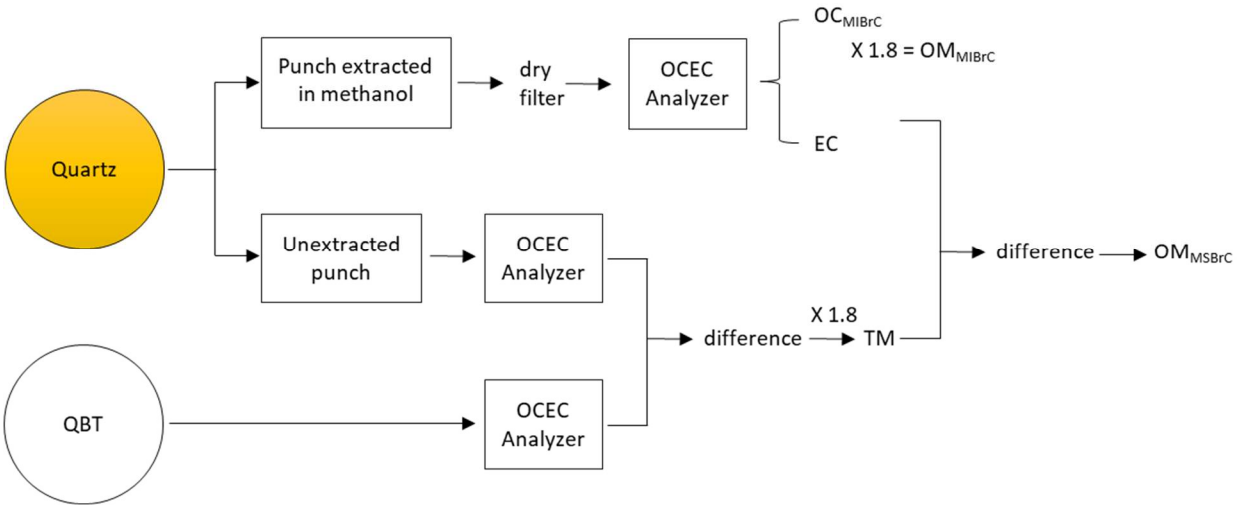

Figure 2.1. Flowchart summarizing the procedure for apportioning the carbonaceous particle mass into methanol-soluble BrC (MSBrC), methanol-insoluble BrC (MIBrC), and EC.

2.2.3 Retrieving aerosol light-absorption properties

We retrieved the imaginary component of the refractive index of the BrC aerosol ($k_{BrC,aerosol}$) at 422 nm and 532 nm using optical closure (Saleh et al., 2014;McClure et al., 2020;Chakrabarty et al., 2010;Lack et al., 2012). In brief, we used Mie calculations to constrain the $k_{BrC,aerosol}$ that, coupled with measured particle size distributions, best reproduced the measured b_{abs} at that wavelength. We calculated the wavelength dependence, $w_{BrC,aerosol}$, assuming that $k_{BrC,aerosol}$ exhibits a power-law dependence on wavelength:

$$w_{BrC,aerosol} = \frac{\log(k_{422,BrC,aerosol}/k_{532,BrC,aerosol})}{\log(532/422)} \quad (6)$$

The Mie calculations assumed a BrC real component of the refractive index equal to 1.6. To account for absorption by EC, we applied several simplifying assumptions. First, we assumed that EC and BrC were externally mixed. We also assumed that the EC particles were spherical (which is inherent in Mie calculations) and that their size distribution had the same shape as that of BrC. Therefore, the size distributions measured by the SMPS were split between EC and BrC based on

the EC/OM values obtained from the OCEC analyzer measurements. Finally, we used an EC complex refractive index of 1.85 + 0.71*i* (Bond and Bergstrom, 2006). We note that because the EC fraction was small in these experiments (EC/OC < 0.05), these simplifying assumptions had a small effect on the retrieved $k_{BrC,aerosol}$ as discussed in Appendix A.

2.2.4 Light-absorption apportionment

As summarized in Figure 2.2, we employed a combination of online and offline measurements and Mie calculations to retrieve the imaginary component of the refractive indices of methanol-soluble BrC (MSBrC) and methanol-insoluble BrC (MIBrC). First, we used the particles collected on the PTFE filters to determine the light-absorption properties of MSBrC following the procedure of (Cheng et al., 2020). For the extraction of the PTFE filters, we immersed each filter in 5 ml of methanol inside a glass vial and sonicated for 15 minutes. Unlike with the passive extraction used with the Quartz filters, sonication can physically extract a large amount of methanol-insoluble species. To remove the methanol-insoluble particles from the methanol solution, we filtered the methanol extracts through 13 mm PTFE (0.2 microns, Sterlitech Corporation, PTU021350) using a glass vial with a metal luer lock tip.

We measured the concentration of BrC in the solutions using the OCEC analyzer. To do so, we pipetted 200-300 µl (in steps of 50 µl) onto 1.5 cm^2 punches of prebaked Quartz filters and dried the filters using a stream of clean, dry air. Because methanol is relatively volatile, it evaporates rapidly under the stream of air, leaving behind the less volatile BrC. We then retrieved the total carbon mass on the punch running the NIOSH-870 protocol on the OCEC analyzer. We used the measured mass to estimate the BrC concentration in the solutions, C_{MSBrC}. As before, we assumed OM/OC = 1.8.

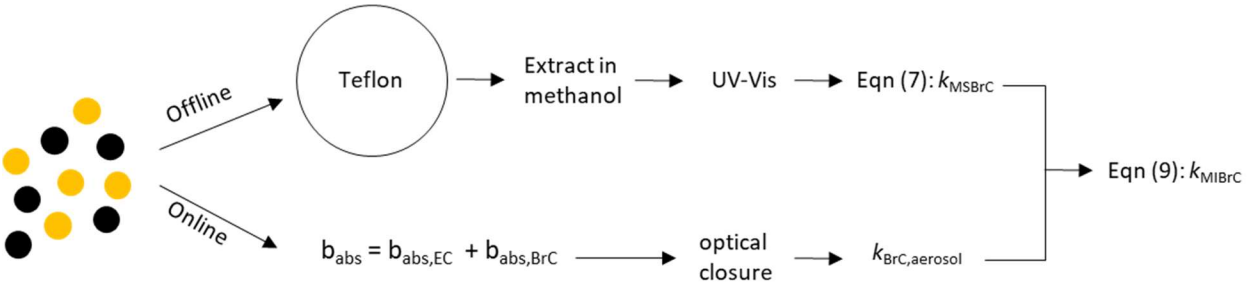

Figure 2.2 Flowchart showing the light-absorption apportionment procedure.

We used a UV-vis Spectrophotometer (Agilent, Cary 60) to measure the UV-vis absorbance of the extracts in the 200-800 nm range at a 1 nm resolution. We then converted the measured absorbance to light-absorption properties using the relation between the imaginary component of the refractive index of the MSBrC (k_{MSBrC}) and the absorption coefficient (α, cm^{-1}):

$$k_{MSBrC,\ \lambda} = \frac{\lambda}{4\pi}\alpha(\lambda) \tag{7}$$

Here, α is calculated from the UV-vis measurements using

$$\alpha(\lambda) = \ln 10 \frac{A(\lambda)\rho}{C_{MSBrC} \times L} \tag{8}$$

Where A is the measured absorbance, ρ is the density of the extracts (assumed to be 1.2 g/cm^3), L (1 cm) is the optical path length, and C_{MSBrC} is the concentration of the BrC in the solution. Although the absorption coefficients α and b_{abs} have similar units ($length^{-1}$), they express different physical quantities. b_{abs} represents the total absorption cross section of the aerosol per unit volume of air and thus depends on the aerosol concentration and size distribution, whereas α is a material property that is directly related to k (Equation 7).

We retrieved k of the methanol-insoluble BrC (k_{MIBrC}) based on the assumption that MIBrC and MSBrC were well-mixed in the BrC aerosol and that $k_{BrC,aerosol}$ (Section 2.2.3) is a volume-weighted average of k_{MSBrC} and k_{MIBrC}. Therefore:

$$k_{MIBrC} = \left(k_{BrC,aerosol} - k_{MSBrC}\frac{f_{MSBrC}}{f_{MSBrC}+f_{MIBrC}}\right)\frac{f_{MSBrC}+f_{MIBrC}}{f_{MIBrC}} \quad (9)$$

Where, k_{MSBrC} is obtained from the UV-vis measurements as described above, $k_{BrC,aerosol}$ is obtained from optical closure (Section 2.2.3), and the fractions (f_{MSBrC} and f_{MIBrC}) are obtained from the mass apportionment analysis (Section 2.2.2 and Equation 4).

We also quantified the fractional contribution to light absorption by MSBrC, MIBrC, and EC. The fractional contribution by EC was calculated as:

$$X_{abs,EC} = \frac{b_{abs,EC}}{b_{abs}} \quad (10)$$

Where $b_{abs,EC}$ is the absorption coefficient of the EC particles, obtained using Mie calculations as described in Section 2.2.2 and b_{abs} is the total aerosol absorption coefficient measured using the multi-PAS III. The contributions to absorption by MSBrC and MIBrC were then calculated as:

$$X_{abs,\,MSBrC,\,\lambda} = \left(1\text{-}X_{abs,\,EC,\,\lambda}\right)\frac{\left(k_{MSBrC,\,\lambda}\times f_{MSBrC}/f_{BrC}\right)}{k_{BrC,\,\lambda}} \quad (11)$$

$$X_{abs,\,MIBrC,\,\lambda} = \left(1\text{-}X_{abs,\,EC,\,\lambda}\right)\frac{\left(k_{MIBrC,\,\lambda}\times f_{MIBrC}/f_{BrC}\right)}{k_{BrC,\,\lambda}} \quad (12)$$

2.3 Results

2.3.1 Aerosol light-absorption properties

Figure 2.3 shows the light-absorption properties (k_{550} and w) of the BrC aerosol plotted against the EC/OM ratios retrieved from the OCEC analyzer. We note that here we use the term 'BrC aerosol' to refer to the whole BrC and to indicate that its light-absorption properties were obtained from online measurements in the aerosol phase (Section 22.3). The individual data points shown correspond to the combustion experiments we conducted with each of the three fuels. On the same figures, we show the parameterizations of k_{550} and w vs EC/OM (or, equivalently, BC/OA) presented by Saleh et al. (2014), assuming both internally mixed and

externally mixed BrC. For both k_{550} and w, our data agree with the trends of correlation between the light-absorption properties and EC/OM, with k_{550} increasing and w decreasing with increasing EC content. The inverse relation between k and w has also been repeatedly established previously for BrC (McClure et al., 2020;Sengupta et al., 2018;Xie et al., 2018). Notably, the data points from the different combustion experiments follow a similar trend, with no apparent dependence on fuel type. This indicates that the difference in the light-absorption properties of BrC produced in different combustion scenarios is primarily caused by the different combustion conditions rather than fuel type (Saleh et al., 2018).

Both k_{550} and w values obtained in this study are generally larger than the values predicted by the Saleh et al. (2014) parameterizations at the same EC/OM. This could be due to true variability, but is also likely due to discrepancies between aerosol light-absorption measurements. BrC parameterizations derived from biomass-burning measurements usually involve significant spread in the data points (Saleh et al., 2014;McClure et al., 2020;Lu et al., 2015), and while they usually exhibit similar trends, there are large differences between them (Saleh, 2020). Because of the relatively small number of data points and limited range of EC/OM in this study, we elect not to report a mathematical fit.

2.3.2 Light-absorption properties of the methanol-soluble and methanol-insoluble brown carbon

Figure 2.4 shows the imaginary component of the refractive indices of the MSBrC and MIBrC fractions (k_{MSBrC} and k_{MIBrC}) at 422 nm and 532 nm, plotted against $k_{BrC,aerosol}$. k_{MSBrC} and k_{MIBrC} were estimated from UV-Vis measurements and optical closure calculations, as described in Section 2.2.4. The figure shows that k_{MSBrC} and k_{MIBrC} are clustered in different ranges. $k_{MSBrC,422}$ and

$k_{MSBrC,532}$ had average values of 0.015 ± 0.003 and 0.004 ± 0.002, respectively, while $k_{MIBrC,422}$ and $k_{MIBrC,532}$ had average values of 0.308 ± 0.161 and 0.211 ± 0.113, respectively. At both wavelengths, the MSBrC fraction had a smaller *k* than the BrC aerosol as a whole, while the MIBrC fraction had a larger *k*. In-line with previous reports (Corbin et al., 2019;Bai et al., 2020;Cheng et al., 2020;Shetty et al., 2019), an important implication of these findings is that relying on methanol extraction can severely underestimate BrC absorption. Furthermore, as $k_{BrC,aerosol}$ increases, k_{MSBrC} is relatively capped, which further indicates that methanol extraction becomes less effective in capturing the light-absorption properties of the BrC particles as a whole as those become more absorbing (Cheng et al., 2020).

In general, the fractions' k_{MSBrC} at 422 and 532 nm were weakly dependent on the aerosols' $k_{BrC,aerosol}$ ($\log_{10}(k_{MSBrC,422}) = 0.45\times\log_{10}(k_{BrC,aerosol,422}) - 1.20$, $r^2 = 0.43$; $\log_{10}(k_{MSBrC,532}) = 0.54\times\log_{10}(k_{BrC,aerosol,532}) - 1.56$, $r^2 = 0.30$). The fractions' k_{MIBrC}, in contrast, were more correlated with $k_{BrC,aerosol}$ ($\log_{10}(k_{MIBrC,422}) = 1.33\times\log_{10}(k_{BrC,aerosol,422}) + 1.01$, $r^2 = 0.61$; $\log_{10}(k_{MIBrC,532}) = 0.84\times\log_{10}(k_{BrC,aerosol,532}) + 0.65$, $r^2 = 0.55$).

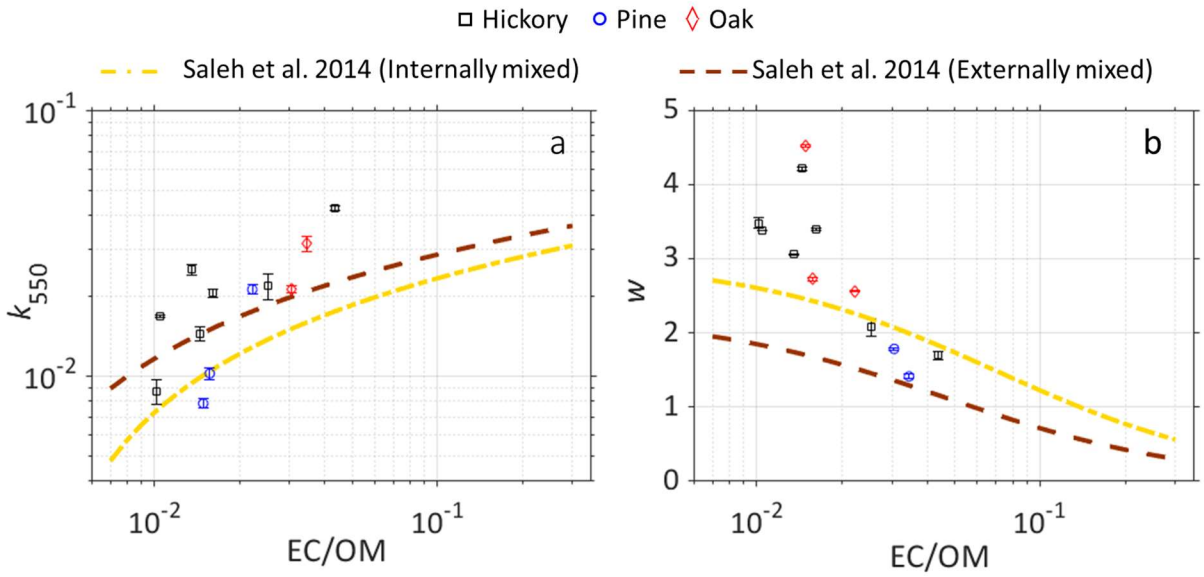

Figure 2.3. The light-absorption properties of the BrC aerosol, retrieved using optical closure, as a function of the EC/OM ratio, retrieved from the OCEC analyzer assuming OM = 1.8 x OC. (a) The imaginary component of the refractive index at 550 nm (k_{550}) versus EC/OM. (b) The wavelength dependence of the imaginary component of the refractive index (w) versus EC/OM. Also shown are the parameterizations of Saleh et al. (2014) with the assumption of internally mixed and externally mixed BC.

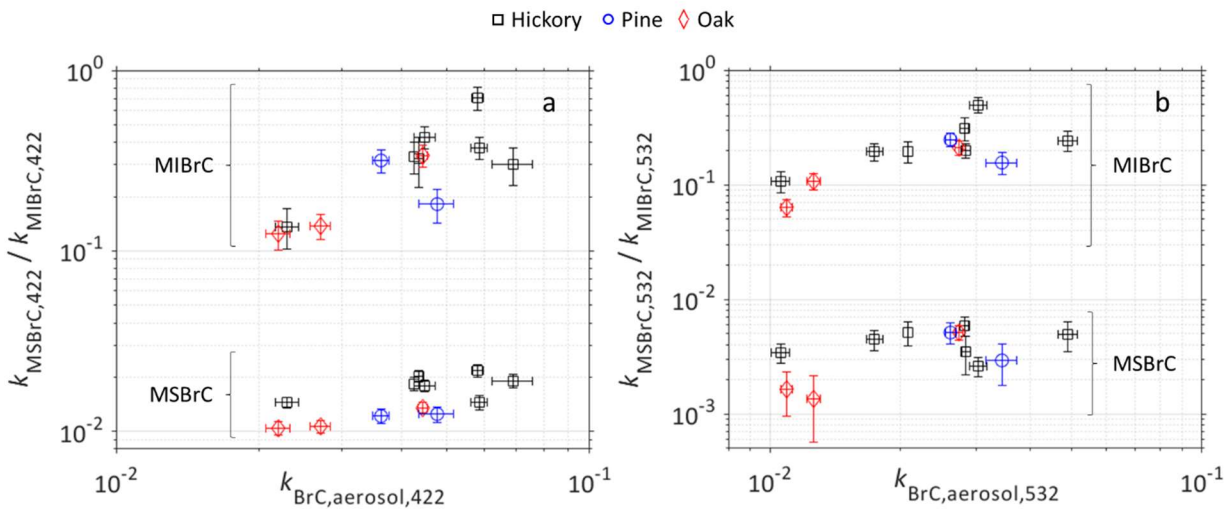

Figure 2.4 The imaginary component of the refractive index for the methanol-soluble BrC (MSBrC) and the methanol-insoluble BrC (MIBrC), retrieved from UV-Vis measurements and optical closure, respectively, plotted against *k* of the BrC aerosol at (a) λ = 422 nm and (b) λ = 532 nm.

In Figure 2.5, we show the light-absorption properties (k_{550} vs w) of the BrC aerosol and the MSBrC and MIBrC fractions retrieved in this study. In the backdrop, we show the BrC categories proposed by Saleh (2020) along with literature values of biomass-burning BrC k_{550} vs w retrieved based on methanol extraction (i.e., equivalent to MSBrC). The BrC aerosol produced in this study falls within the moderately absorbing BrC category (M-BrC). However, the fractions that compose it, namely MSBrC and MIBrC, are divided between the weakly absorbing BrC category (W-BrC) and the strongly absorbing category (S-BrC), respectively. The mean MIBrC k_{550} from all experiments is 2 orders of magnitude larger than MSBrC k_{550} ($k_{MIBrC,550}$ = 0.211 ± 0.113; $k_{MSBrC,550}$ = 0.004 ± 0.002), while MSBrC exhibited a much stronger wavelength dependence (w_{MIBrC} = 1.7 ± 1.1; w_{MSBrC} = 6.3 ± 1.7). The light-absorption properties of MSBrC obtained from our experiments are consistent with those reported for biomass-burning BrC in other works that relied on

methanol extraction (Chen and Bond, 2010;Li et al., 2016;Cheng et al., 2016;Cheng et al., 2017;Lei et al., 2018;Xie et al., 2018), all of which fall within W-BrC. As shown in Figure 2.5, there is a strongly absorbing fraction of BrC, which is insoluble in methanol, that pushes the light-absorption properties of the BrC aerosol well beyond those of its methanol-soluble fraction. The stronger light absorption of MIBrC compared to MSBrC reported here and in other works (e.g., Corbin et al. (2019), Bai et al. (2020), Cheng et al. (2020)) confirms that MSBrC cannot be used to represent the light-absorption properties of BrC aerosols as a whole. The insoluble fraction must be accounted for in order to arrive at an accurate representation of absorption by BrC. The light-absorption properties of the MIBrC in our experiments span a similar range to that suggested by Corbin et al. (2019) for marine-engine exhaust, as well as other reports of strongly absorbing BrC that have been referred to using different terminologies, including refractory BrC(Saleh et al., 2018), intermediate absorber (between BrC and BC) (Adler et al., 2019), BrC associated with extremely low volatility organic compounds (ELVOCs) (Saleh et al., 2014), and brown carbon spheres (Alexander et al., 2008).

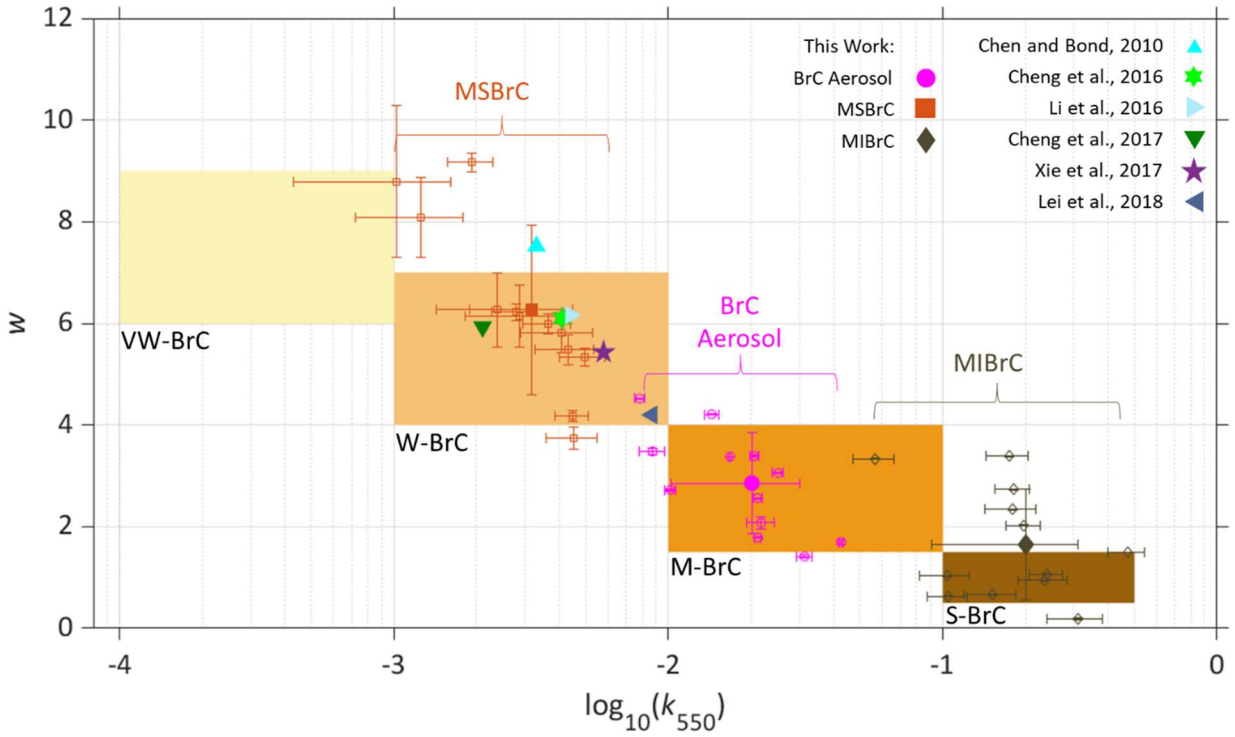

Figure 2.5 The light-absorption properties of the BrC aerosol and the MSBrC and MIBrC fractions produced in this work, shown in $\log_{10}(k_{550})$ – w space. The shaded rectangles represent the BrC categories suggested by Saleh (2020). Open circles, squares, and rhombi represent individual data points from this work, while those filled markers represent the average values retrieved for the categories of BrC aerosol, MSBrC, and MIBrC, respectively. To avoid cluttering, we did not include different markers for each fuel type in this figure. The figure also includes the average values of biomass-burning k_{550} vs w reported in or calculated from previous studies that utilized methanol extraction.

2.3.3 Mass fractions and contribution to absorption

Figure 2.6a shows the mass fractions of MSBrC (f_{MSBrC}), MIBrC (f_{MIBrC}), and EC (f_{EC}) in the carbonaceous aerosol, averaged over all the combustion experiments. MSBrC constituted by far the largest fraction (90% ± 5%), while MIBrC and EC constituted 9% ± 5% and 1% ± 0.5%,

respectively. This is consistent with previous studies that have reported methanol extraction efficiencies of >90% (Li et al., 2016;Chen and Bond, 2010). Indeed, these high extraction efficiencies by methanol have led some studies to assume that methanol effectively extracts all the organics in biomass-burning emissions (Li et al., 2016). While this assumption is justified when the purpose is to study the chemical composition of the OA (e.g., to investigate OA formation pathways in biomass burning), it is not when the purpose is to quantify BrC light absorption.

In Figure 2.6b, we show the estimated contributions to absorption by each of the MSBrC, MIBrC, and EC fractions, averaged over all experiments. Despite constituting the majority of the particles by mass, the MSBrC contributed 35% ± 11% and 16% ± 7% of the total absorption at 422 nm and 532 nm, respectively. In contrast, the MIBrC contributed 60% ± 11% and 72% ± 10% at 422 nm and 532 nm, respectively, and the EC fraction contributed 5% ± 3% and 12% ± 5% at 422 nm and 532 nm, respectively. It is worth noting that the relative differences between the contributions to absorption at 422 nm and 532 nm between MSBrC, MIBrC, and EC, is a reflection of the differences in the wavelength dependence of their absorption. As shown in Figure 2.5, w_{MSBrC} and w_{MIBrC} were 6.3 ± 1.7 and 1.7 ± 1.1, respectively, while w_{EC} was assumed to be zero.

Importantly, even though MIBrC constitutes an order-of-magnitude smaller fraction of the carbonaceous aerosol than MSBrC, it contributes a dominant fraction of the total absorption. These findings are consistent with previous reports of a dominant contribution to absorption by insoluble BrC produced from heavy fuel oil combustion (Bai et al., 2020;Corbin et al., 2019) and indicate that methanol-extraction techniques are inadequate at quantifying light absorption by biomass-burning BrC. In addition to its association with differences in light-absorption properties, solubility in methanol is also expected to be associated with differences in other physicochemical

properties, including volatility and molecular size (Saleh et al., 2018;Corbin et al., 2019). Furthermore, larger molecular size BrC species have been shown to be more resistant to decay in absorption due to photobleaching upon aging in the atmosphere (Stevens and Dastoor, 2019). Consequently, in addition to MIBrC being more light-absorbing than MSBrC, it is also expected to be less volatile, possibly less susceptible to photobleaching, and therefore have a longer lifetime in the atmosphere.

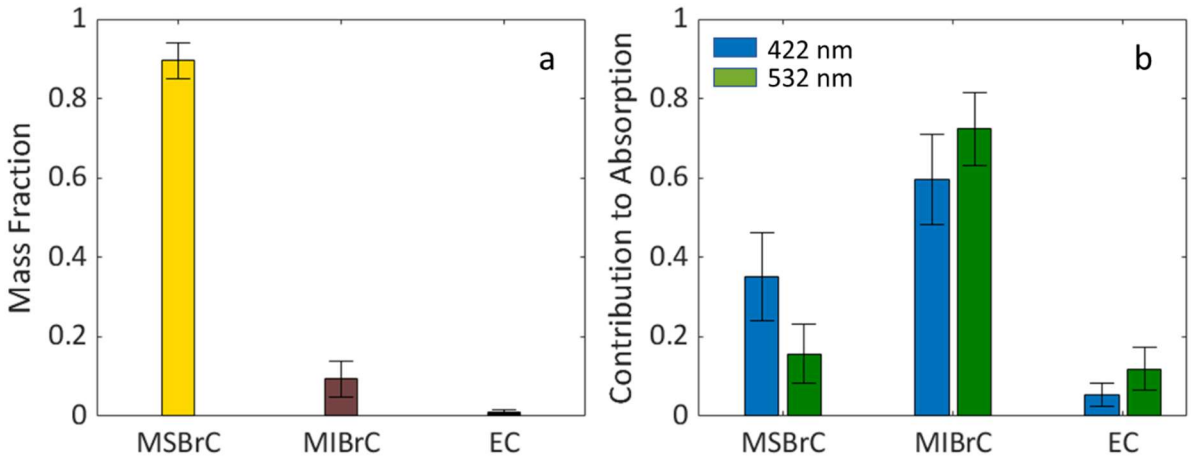

Figure 2.6 (a) Mass fractions of MSBrC, MIBrC, and EC averaged over all combustion experiments. (b) The corresponding contribution to total absorption aerosol absorption at 422 nm and 532 nm by MSBrC, MIBrC, and EC.

2.4 Conclusions

In this work, we report the existence of a methanol-insoluble BrC (MIBrC) fraction produced in biomass combustion that is significantly more light-absorbing than the methanol soluble BrC (MSBrC) fraction. These findings contribute to the growing body of literature on the association between solubility and its light-absorption properties of BrC produced in biomass combustion(Shetty et al., 2019), as well as controlled combustion of single-molecule fuels (Cheng

et al., 2020) and marine engines (Corbin et al., 2019;Bai et al., 2020). In concordance with previous studies (Li et al., 2016;Chen and Bond, 2010), methanol was efficient at extracting the organic matter produced in our biomass-burning experiment, where MSBrC constituted 90% ± 5% of the total carbonaceous species. However, using this high methanol extraction efficiency as an indication that MSBrC is representative of the overall BrC is highly misleading. Our results show that relying on methanol extraction to constrain the light-absorption properties of biomass-burning BrC results in a severe misrepresentation of these properties, leading to an order-of-magnitude underestimation of BrC light absorption at mid-visible wavelengths.

References

Adler, G., Wagner, N. L., Lamb, K. D., Manfred, K. M., Schwarz, J. P., Franchin, A., Middlebrook, A. M., Washenfelder, R. A., Womack, C. C., and Yokelson, R. J.: Evidence in biomass burning smoke for a light-absorbing aerosol with properties intermediate between brown and black carbon, Aerosol Science and Technology, 1-33, 2019.

Aiken, A. C., Decarlo, P. F., Kroll, J. H., Worsnop, D. R., Huffman, J. A., Docherty, K. S., Ulbrich, I. M., Mohr, C., Kimmel, J. R., and Sueper, D.: O/C and OM/OC ratios of primary, secondary, and ambient organic aerosols with high-resolution time-of-flight aerosol mass spectrometry, Environmental science & technology, 42, 4478-4485, 2008.

Alexander, D. T., Crozier, P. A., and Anderson, J. R.: Brown carbon spheres in East Asian outflow and their optical properties, Science, 321, 833-836, 2008.

Bai, Z., Zhang, L., Cheng, Y., Zhang, W., Mao, J., Chen, H., Li, L., Wang, L., and Chen, J.: Water/Methanol-Insoluble Brown Carbon Can Dominate Aerosol-Enhanced Light Absorption in Port Cities, Environmental Science & Technology, 54, 14889-14898, 2020.

Bond, T. C., and Bergstrom, R. W.: Light absorption by carbonaceous particles: An investigative review, Aerosol science and technology, 40, 27-67, 2006.

Brown, H., Liu, X., Feng, Y., Jiang, Y., Wu, M., Lu, Z., Wu, C., Murphy, S., and Pokhrel, R.: Radiative effect and climate impacts of brown carbon with the Community Atmosphere Model (CAM5), Lawrence Berkeley National Laboratory (LBNL), Berkeley, CA (United States …1680-7375, 2018.

Chakrabarty, R., Moosmuller, H., Chen, L.-W., Lewis, K., Arnott, W., Mazzoleni, C., Dubey, M., Wold, C., Hao, W., and Kreidenweis, S.: Brown carbon in tar balls from smoldering biomass combustion, Atmospheric Chemistry and Physics. 10: 6363-6370., 6363-6370, 2010.

Chen, Y., and Bond, T.: Light absorption by organic carbon from wood combustion, Atmospheric Chemistry and Physics, 10, 1773-1787, 2010.

Cheng, Y., He, K.-b., Du, Z.-y., Engling, G., Liu, J.-m., Ma, Y.-l., Zheng, M., and Weber, R. J.: The characteristics of brown carbon aerosol during winter in Beijing, Atmospheric Environment, 127, 355-364, 2016.

Cheng, Y., He, K.-b., Engling, G., Weber, R., Liu, J.-m., Du, Z.-y., and Dong, S.-p.: Brown and black carbon in Beijing aerosol: Implications for the effects of brown coating on light absorption by black carbon, Science of the Total Environment, 599, 1047-1055, 2017.

Cheng, Z., Atwi, K., Hajj, O. E., Ijeli, I., Fischer, D. A., Smith, G., and Saleh, R.: Discrepancies Between Brown Carbon Light-absorption Properties Retrieved from Online and Offline Measurements, Aerosol Science and Technology, 1-15, 2020.

Cheng, Z. Z., Atwi, K., Onyima, T., and Saleh, R.: Investigating the dependence of light-absorption properties of combustion carbonaceous aerosols on combustion conditions, Aerosol Science and Technology, 53, 419-434, 10.1080/02786826.2019.1566593, 2019.

Corbin, J. C., Czech, H., Massabò, D., de Mongeot, F. B., Jakobi, G., Liu, F., Lobo, P., Mennucci, C., Mensah, A. A., and Orasche, J.: Infrared-absorbing carbonaceous tar can dominate light absorption by marine-engine exhaust, npj Climate and Atmospheric Science, 2, 1-10, 2019.

Corbin, J. C., and Gysel-Beer, M.: Detection of tar brown carbon with a single particle soot photometer (SP2), Atmospheric Chemistry and Physics, 19, 15673-15690, 2019.

El-Zanan, H. S., Lowenthal, D. H., Zielinska, B., Chow, J. C., and Kumar, N.: Determination of the organic aerosol mass to organic carbon ratio in IMPROVE samples, Chemosphere, 60, 485-496, 2005.

Feng, Y., Ramanathan, V., and Kotamarthi, V. R.: Brown carbon: a significant atmospheric absorber of solar radiation?, Atmos. Chem. Phys., 13, 8607-8621, 10.5194/acp-13-8607-2013, 2013.

Fine, P. M., Cass, G. R., and Simoneit, B. R.: Chemical characterization of fine particle emissions from the fireplace combustion of woods grown in the southern United States, Environmental Science & Technology, 36, 1442-1451, 2002.

Huang, R.-J., Yang, L., Shen, J., Yuan, W., Gong, Y., Guo, J., Cao, W., Duan, J., Ni, H., and Zhu, C.: Water-Insoluble Organics Dominate Brown Carbon in Wintertime Urban Aerosol of China: Chemical Characteristics and Optical Properties, Environmental Science & Technology, 54, 7836-7847, 2020.

Khan, B., Hays, M. D., Geron, C., and Jetter, J.: Differences in the OC/EC ratios that characterize ambient and source aerosols due to thermal-optical analysis, Aerosol Science and Technology, 46, 127-137, 2012.

Kumar, N. K., Corbin, J. C., Bruns, E. A., Massabó, D., Slowik, J. G., Drinovec, L., Močnik, G., Prati, P., Vlachou, A., and Baltensperger, U.: Production of particulate brown carbon during atmospheric aging of residential wood-burning emissions, Atmospheric Chemistry & Physics, 18, 2018.

Lack, D. A., Langridge, J. M., Bahreini, R., Cappa, C. D., Middlebrook, A. M., and Schwarz, J. P.: Brown carbon and internal mixing in biomass burning particles, Proceedings of the National Academy of Sciences, 2012.

Lambe, A. T., Cappa, C. D., Massoli, P., Onasch, T. B., Forestieri, S. D., Martin, A. T., Cummings, M. J., Croasdale, D. R., Brune, W. H., and Worsnop, D. R.: Relationship between oxidation level and optical properties of secondary organic aerosol, Environmental science & technology, 47, 6349-6357, 2013.

Lei, Y., Shen, Z., Wang, Q., Zhang, T., Cao, J., Sun, J., Zhang, Q., Wang, L., Xu, H., and Tian, J.: Optical characteristics and source apportionment of brown carbon in winter PM2. 5 over Yulin in Northern China, Atmospheric Research, 213, 27-33, 2018.

Li, X., Chen, Y., and Bond, T. C.: Light absorption of organic aerosol from pyrolysis of corn stalk, Atmospheric Environment, 144, 249-256, 2016.

Lu, Z., Streets, D. G., Winijkul, E., Yan, F., Chen, Y., Bond, T. C., Feng, Y., Dubey, M. K., Liu, S., and Pinto, J. P.: Light absorption properties and radiative effects of primary organic aerosol emissions, Environmental Science & Technology, 49, 4868-4877, 2015.

McClure, C. D., Lim, C. Y., Hagan, D. H., Kroll, J. H., and Cappa, C. D.: Biomass-burning-derived particles from a wide variety of fuels–Part 1: Properties of primary particles, Atmospheric Chemistry & Physics, 20, 2020.

Pachauri, R. K., Allen, M. R., Barros, V. R., Broome, J., Cramer, W., Christ, R., Church, J. A., Clarke, L., Dahe, Q., and Dasgupta, P.: Climate change 2014: synthesis report. Contribution of Working Groups I, II and III to the fifth assessment report of the Intergovernmental Panel on Climate Change, Ipcc, 2014.

Phillips, S. M., and Smith, G. D.: Spectroscopic comparison of water-and methanol-soluble brown carbon particulate matter, Aerosol Science and Technology, 51, 1113-1121, 2017.

Saleh, R., Robinson, E. S., Tkacik, D. S., Ahern, A. T., Liu, S., Aiken, A. C., Sullivan, R. C., Presto, A. A., Dubey, M. K., and Yokelson, R. J.: Brownness of organics in aerosols from biomass burning linked to their black carbon content, Nature Geoscience, 7, 647, 2014.

Saleh, R., Cheng, Z., and Atwi, K.: The brown–black continuum of light-absorbing combustion aerosols, Environmental Science & Technology Letters, 5, 508-513, 2018.

Saleh, R.: From Measurements to Models: Toward Accurate Representation of Brown Carbon in Climate Calculations, Current Pollution Reports, 1-15, 2020.

Satish, R., and Rastogi, N.: On the use of brown carbon spectra as a tool to understand their broader composition and characteristics: a case study from crop-residue burning samples, ACS omega, 4, 1847-1853, 2019.

Sengupta, D., Samburova, V., Bhattarai, C., Kirillova, E., Mazzoleni, L., Iaukea-Lum, M., Watts, A., Moosmüller, H., and Khlystov, A.: Light absorption by polar and non-polar aerosol compounds from laboratory biomass combustion, Atmos. Chem. Phys., 18, 10849-10867, 10.5194/acp-18-10849-2018, 2018.

Shetty, N., Beeler, P., Paik, T., Brechtel, F. J., and Chakrabarty, R. K.: Bias in Quantification of Light Absorption Enhancement of Black Carbon Aerosol Coated with Low Volatility Brown Carbon, Aerosol Science and Technology, 1-16, 2021.

Shetty, N. J., Pandey, A., Baker, S., Hao, W. M., and Chakrabarty, R. K.: Measuring light absorption by freshly emitted organic aerosols: optical artifacts in traditional solvent-extraction-based methods, Atmos. Chem. Phys., 19, 8817-8830, 10.5194/acp-19-8817-2019, 2019.

Stevens, R., and Dastoor, A.: A review of the representation of aerosol mixing state in atmospheric models, Atmosphere, 10, 168, 2019.

Subramanian, R., Khlystov, A. Y., Cabada, J. C., and Robinson, A. L.: Positive and negative artifacts in particulate organic carbon measurements with denuded and undenuded sampler configurations special issue of aerosol science and technology on findings from the fine particulate matter supersites program, Aerosol Science and Technology, 38, 27-48, 2004.

Updyke, K. M., Nguyen, T. B., and Nizkorodov, S. A.: Formation of brown carbon via reactions of ammonia with secondary organic aerosols from biogenic and anthropogenic precursors, Atmospheric environment, 63, 22-31, 2012.

Wang, X., Heald, C., Ridley, D., Schwarz, J., Spackman, J., Perring, A., Coe, H., Liu, D., and Clarke, A.: Exploiting simultaneous observational constraints on mass and absorption to estimate the global direct radiative forcing of black carbon and brown carbon, 2014.

Wu, C., Huang, X., Ng, W. M., Griffith, S. M., and Yu, J. Z.: Inter-comparison of NIOSH and IMPROVE protocols for OC and EC determination: implications for inter-protocol data conversion, Atmospheric Measurement Techniques, 9, 4547-4560, 2016.

Xie, M., Shen, G., Holder, A. L., Hays, M. D., and Jetter, J. J.: Light absorption of organic carbon emitted from burning wood, charcoal, and kerosene in household cookstoves, Environmental pollution, 240, 60-67, 2018.

Yao, L., Yang, L., Chen, J., Wang, X., Xue, L., Li, W., Sui, X., Wen, L., Chi, J., and Zhu, Y.: Characteristics of carbonaceous aerosols: Impact of biomass burning and secondary formation in summertime in a rural area of the North China Plain, Science of the Total Environment, 557, 520-530, 2016.

Zhang, Y., Forrister, H., Liu, J., Dibb, J., Anderson, B., Schwarz, J. P., Perring, A. E., Jimenez, J. L., Campuzano-Jost, P., and Wang, Y.: Top-of-atmosphere radiative forcing affected by brown carbon in the upper troposphere, Nature Geoscience, 10, 486-489, 2017.

Zheng, M., Cass, G. R., Schauer, J. J., and Edgerton, E. S.: Source apportionment of PM2. 5 in the southeastern United States using solvent-extractable organic compounds as tracers, Environmental science & technology, 36, 2361-2371, 2002.

CHAPTER 3

PHYSICOCHEMICAL PROPERTIES AND CYTOTOXICITY OF BROWN CARBON PRODUCED UNDER DIFFERENT COMBUSTION CONDITIONS[2]

[2] Atwi, K., Mondal, A., Pant, J., Cheng, Z., El Hajj, O., Ijeli, I., . . . Saleh, R. (2021). *Atmospheric environment*, 244, 117881. doi:10.1016/j.atmosenv.2020.117881

Abstract

Light-absorbing organic particulate matter (PM), or brown carbon (BrC), may constitute an important fraction of combustion PM. Here, we investigate the effect of combustion conditions on the molecular sizes of BrC, their light-absorption properties, and their cytotoxicity. We used toluene in a combustion reactor with highly controlled conditions to produce two different types of BrC under two conditions corresponding to smoldering and near-flaming combustion, with temperatures of 670 °C and 1035 °C, respectively. We performed online measurements of the size distributions and light-absorption properties of the BrC. The BrC produced at 1035 °C was more light absorbing, with an imaginary component of the refractive index at 532 nm (k_{532}) an order of magnitude larger than that of the BrC produced at 670 °C. We also collected samples for offline chemical characterization using laser desorption ionization (LDI) mass spectrometry. The LDI mass spectra showed that the BrC produced at 1035 °C was composed of species with significantly larger molecular sizes than the BrC produced at 670 °C. Using human lung epithelial cells, we conducted *in vitro* cytotoxicity analysis on the two types of BrC with doses ranging from 3.5 to 136.0 μg of BrC/ml. After 24-h exposure, the viability of the cells was assessed using a WST-8 assay. The cytotoxicity analysis showed that, for both BrC samples, the cells exhibited a clear dose-dependent response with significant BrC cytotoxicity that plateaued at the higher doses. However, while the viability of cells exposed to the BrC produced at 1035 °C reached a minimum of around 65% at the highest dose, the BrC produced at 670 °C proved to be significantly more toxic, with the viability dropping asymptotically to 25%. The results presented here suggest that organic PM of smaller molecular sizes produced under lower temperature, smoldering combustion could be significantly more toxic than those of larger molecular sizes produced under

higher temperature, flaming conditions. The use of a single-molecule fuel in a highly controlled combustion setup distinguishes this work from experiments that rely on real-life sources and combustion setups, where different combustion conditions could be occurring simultaneously and clouding the conclusions.

3.1 Introduction

Primary combustion particulate matter (PM), emitted from various combustion sources, is associated with increased morbidity through cardiovascular and cardiopulmonary diseases (Pope III and Dockery, 2006;Donaldson et al., 2005). Primary combustion PM is ubiquitous, contributing one to two thirds of all carbonaceous PM over the continental United States (Park et al., 2003;Yu et al., 2004;Bond et al., 2004). There are numerous sources of combustion PM, including the combustion of fossil fuels and biofuels (transportation, power generation, industrial applications) and the combustion of solid biomass in domestic heating and cooking as well as agricultural burning and forest fires. Despite the prevalence of combustion PM, there are lingering gaps in our understanding of its health effects (Black et al., 2017). The composition of combustion PM is highly complex, with varying fractions of organic carbon (OC) and elemental carbon (EC), inorganics, metals, ions, and ash (Hays et al., 2005;Fine et al., 2002;Liu et al., 2017). While all of those species have been associated with toxicological and health impacts, their relative importance is unclear (Dilger et al., 2016;Kasurinen et al., 2017;Reisen et al., 2015). Importantly, the composition of combustion PM is dependent not only on the source, but also on combustion conditions (Saleh, 2020;McClure et al., 2020). Therefore, even for the same fuel, differences in combustion conditions have been found to induce differences in toxicity of the emitted PM (Kim et al., 2019;Bølling et al., 2012;Tapanainen et al., 2011;Leskinen et al., 2014). In this paper, we aim to shed light on the fundamental physicochemical properties of the organic fraction of combustion PM, their dependence on combustion conditions, and how that translates into different toxicological outcomes.

3.1.1 PM formation in combustion

First, it is instructive to discuss the current understanding of the formation pathways of combustion PM. The initial steps of combustion of hydrocarbon fuels involve fuel decomposition into smaller hydrocarbons or radicals (Frenklach, 2002;McEnally et al., 2006;Wang, 2011). When combustion is incomplete, those radicals react to form stable species, including aromatics such as benzene, which constitute the backbone for further molecular growth into various gaseous and particulate emissions – pollutants. The growth of small aromatics into larger, condensable polycyclic aromatic hydrocarbons (PAHs) is thought to describe the formation of carbonaceous combustion PM (or soot), where the extent of this growth describes what is known as soot maturity (Michelsen, 2017). Mature soot, mostly comprised of EC, is the final product of soot formation. Between the first produced condensable species, or incipient soot (Michelsen, 2017), and mature soot lie myriad intermediate organic species (Frenklach, 2002;Wang, 2011). Depending on combustion conditions, combustion PM can comprise soot of varying levels of maturity and, therefore, varying levels of EC and organics (Cheng et al., 2019;Saleh et al., 2018). For example, diesel engines and flaming forest fires feature combustion conditions (high temperatures) that are conducive for the formation of mature soot with little contribution from organics. On the other hand, the combustion conditions (low temperatures) in smoldering forest fires are not conducive for the completion of the soot-formation process and thus produce mostly organic PM.

Mature soot is a strong light absorber in the visible spectrum and, due to its black appearance, is classified as black carbon (BC) in the atmospheric sciences literature. In addition to its adverse health effects (Kim et al., 2018;Kelly and Fussell, 2012), BC absorbs solar radiation and is a strong

climate warmer (IPCC, 2014). The intermediate organic species also absorb light, though to a lesser extent than BC, and exhibit absorption spectra that are more skewed towards short-visible and ultraviolet wavelengths (Desgroux et al., 2013;Russo et al., 2013;Saleh et al., 2018), giving them a brownish appearance. In the atmospheric science literature, such light-absorbing organic PM is classified as brown carbon (BrC) (Andreae and Gelencsér, 2006;Laskin et al., 2015). BrC is also an important absorber of solar radiation, yet with a much more complex and uncertain effect on the climate system than BC (Saleh, 2020). We have previously shown that combustion BrC exhibits a continuum of molecular sizes and light-absorption properties (Saleh et al., 2018). In specific, the BrC molecules become larger and more light-absorbing as they approach the BC-formation threshold. Therefore, different combustion conditions of the same fuel can produce BC and/or BrC with varying physicochemical properties (Cheng et al., 2019), which is expected to translate into variability in health effects.

3.1.2 Dependence of combustion PM toxicity on combustion conditions

Several studies have attempted to compare the toxicological effects of emissions from fuels combusted under different regimes using setups such as biomass burners, residential heating equipment, stoves, and pellet boilers (Leskinen et al., 2014;Bølling et al., 2012;Kocbach et al., 2008;Kim et al., 2018;Kim et al., 2019;Happo et al., 2013). The results emerging from the different studies, however, point in different directions.

Bølling et al. (2012) found that PM emitted from the combustion of wood in a cast-iron wood stove at low temperatures (500-800 °C) caused a higher cytotoxic response and pro-inflammatory cytokine IL-6 release than PM emitted at high temperature (700-1000 °C). They also reported that the organic fraction of biomass combustion PM was better correlated with the heightened

toxicological response than were the insoluble “washed” pellets. Similar results were reported by Kocbach et al. (2008) for PM emitted from the combustion of wood in a conventional stove burning birch wood at 700-1000 °C. As described in Section 3.1.1, the organic fraction of combustion PM dominates in low-temperature combustion conditions, while the emissions of insoluble EC increase at higher temperatures. Thus, the results above support the finding that PM from lower temperature combustion is more toxic. Similarly, Jalava et al. (2010) found the emissions from the inefficient operation of a masonry heater (restricted air flow, fuel overload), which would lead to relatively lower combustion temperatures, caused more cell death than those from normal operation. Tapanainen et al. (2011) compared the toxicity of emissions from a conventional masonry heater and a pellet boiler and found that those emitted from the masonry heater, an example of a less efficient setup, caused more cell apoptosis and higher production of inflammatory cytokines TNF-α and MIP-2.

On the other hand, several studies reported that the PM from higher temperature combustion conditions were more toxic. Happo et al. (2013) found that particulate emissions from newer biomass heating appliances, which are typically more efficient technologies that achieve higher combustion temperatures than older technologies, induced higher inflammatory, cytotoxic, and genotoxic activities in a mice model per unit mass. Furthermore, the increased inflammatory response was better correlated with the ash component of emissions, more prevalent in newer technologies, than with PAH concentrations, emitted in higher concentrations in the older technologies. Uski et al. (2014) compared the toxicity of PM from smoldering and efficient combustion in heating appliances and found that, while the PM emitted under smoldering conditions caused greater DNA damage and cell death, those emitted from more efficient

combustion were more effective in decreasing metabolic activity and causing oxidative stress. Leskinen et al. (2014) reported that the PM emissions from more efficient wood combustion (higher temperatures) caused more cell death, which they attributed to the high concentrations of ash and metals. Kim et al. (2018) compared the toxicity induced in mice respiratory systems by PM from the combustion of different biomass fuels under smoldering and flaming conditions. They found that the latter had higher toxic and mutagenic potencies per unit mass of emitted PM. In a follow-up study in which the mice directly inhaled the biomass combustion emissions, they found that lung inflammation caused by peat and eucalyptus smoke under both flaming and smoldering conditions was not reproduced with oak smoke (Kim et al., 2019).

Clearly, the results from different studies have not converged to determine which combustion regime generates the most toxic PM. A possible explanation of this discrepancy is the difficulty of controlling conditions, particularly in the case of biomass combustion. Even though a combustion experiment is performed within a certain regime (e.g., smoldering or flaming), uncontrolled combustion still features wide spatial and temporal variability in temperatures and air-to-fuel ratios. This variability would lead to the release of a wide range of species that could extend from small-molecular-size organics of nascent soot (or BrC) to the EC in mature soot, possibly clouding the conclusions drawn from a comparison of induced toxic effects. To conduct a systematic comparison of the toxicity of PM from different combustion conditions, it is essential to ensure that the combustion conditions are spatially uniform and stable for the duration of the experiment.

3.1.3 Approach

In this paper, we investigate the effect of differences in combustion conditions on the cytotoxicity of the emitted organic PM, or BrC. We utilized a home-built reactor where the combustion temperature and air-to-fuel ratios can be accurately controlled over an extended period of time (Cheng et al., 2020;Cheng et al., 2019;Saleh et al., 2018), ensuring consistent PM production at each set condition. We generated BrC from the combustion of toluene controlled at two conditions representative of smoldering and near-flaming conditions. We performed light absorption measurements, thermal-optical measurements, and laser desorption ionization mass spectrometry to characterize the physicochemical differences between the two types of BrC. We assessed cytotoxicity using an *in-vitro* submersion setup with human lung epithelial cells. By using toluene instead of a complex biomass fuel, we ensure fuel homogeneity and thus restrict the study of the difference in cytotoxicity to the only variable, the combustion conditions. This also allows us to focus on the toxicity of BrC by eliminating the confounding toxic effects of other species present in combustion PM, such as metals and ash (Kelly and Fussell, 2012). We note that BrC emitted by toluene combustion exhibits resemblance to at least a fraction of that emitted from the combustion of complex fuels. Toluene is commonly found in gasoline and diesel fuels (Chin and Batterman, 2012). Further, as discussed in Section 3.1.1, intermediate aromatic species (such as toluene) constitute the building blocks for BrC formation in the combustion of any carbon-containing fuel. Finally, toluene is also commonly detected in the emissions of biomass fuels (Shen et al., 2012).

3.2 Methods

Using toluene as a fuel, we produced BrC under two different combustion conditions at temperatures of 670 °C and 1035 °C chosen to be representative of smoldering and flaming combustion, respectively (Akagi et al., 2011). We performed online measurements to characterize the particle size distributions and light-absorption properties at a 90 second resolution. Under each condition, we collected the BrC particles on Teflon filters for chemical analysis using laser desorption ionization (LDI) mass spectrometry and *in vitro* cytotoxicity assessment against lung epithelial cells. Experimental details are described in the subsequent sub-sections.

3.2.1 Combustion setup and control

Figure 3.1 shows a schematic of the combustion and filter collection setup. The setup has been described previously in more detail (Cheng et al., 2019;Saleh et al., 2018). In brief, combustion occurred in a flow-through quartz chamber enclosed in a ceramic heater. The heater controlled the temperature inside the chamber to within a degree, according to the combustion conditions desired. Toluene, which contains an aromatic ring, was used as the fuel. Aromatic rings are the critical building blocks of complex combustion products (see Section 3.1.1), for which we expect toluene combustion products to be representative of combustion products in general (Wang, 2011). Dry, clean air bubbled through a vessel containing toluene and carried the fuel into the combustion chamber, where it mixed with a controlled stream of air. In addition to the combustion temperature, the properties of the produced BrC are also dependent on the air-to-fuel ratio (Cheng et al., 2019). Thus, controlling that ratio at a set temperature would also modify the combustion conditions and produce BrC particles of different properties. The combustion

conditions are, in fact, highly sensitive to changes in the flow rates of air or fuel. To be able to finely tune the combustion conditions and maintain them once set, we used an additional flow of nitrogen acting as a passive diluent (Qiao et al., 2005;Tang et al., 2008). The addition of a nitrogen stream makes the combustion less complete and has a similar effect as making the combustion more fuel rich (Cheng et al., 2019;Saleh et al., 2018). The emissions from the combustion chamber were then mixed with a controlled stream of clean air in a dilution chamber in order to bring the concentrations down to within the measuring window of the online instruments.

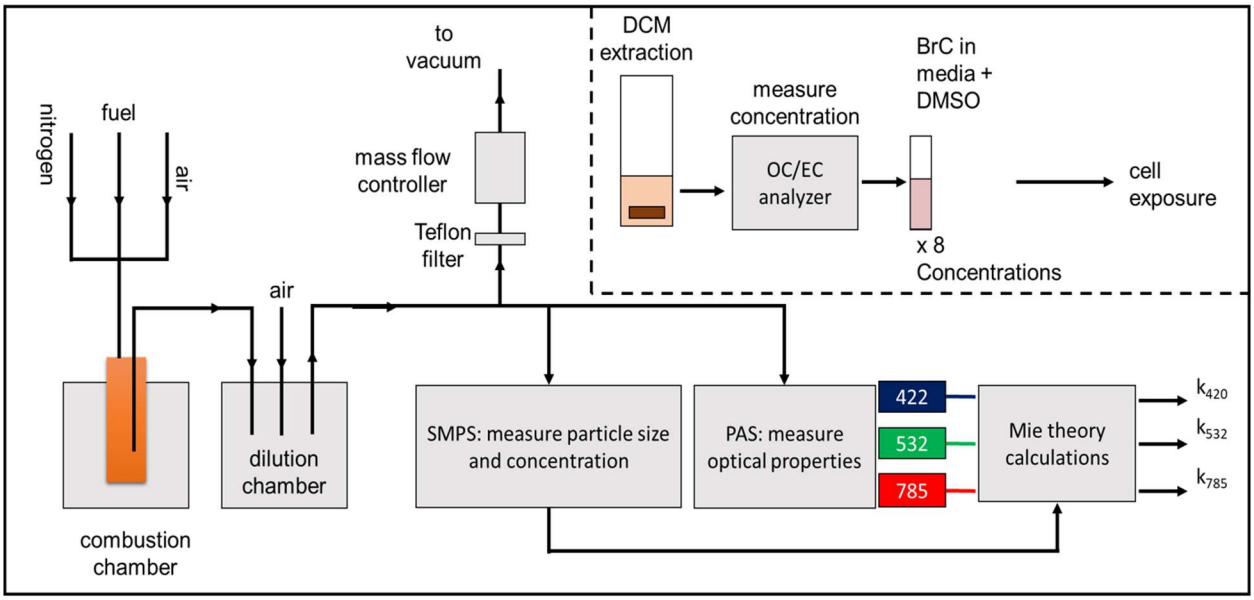

Figure 3.1. Schematic of the experimental setup. BrC was produced in a temperature-controlled combustion chamber. The BrC size distribution and light absorption properties were measured online using an SMPS and a PAS (Section 3.2.2). BrC particles were collected on Teflon filters and then extracted using dichloromethane to prepare for the chemical and cytotoxicity analyses (Section 3.2.3).

3.2.2 Particle size distributions and light absorption properties

We continuously measured the particle size distribution in the 10-500 nm range using a scanning mobility particle sizer (SMPS, TSI 3882). We also measured the real-time light absorption coefficients (b_{abs}, Mm^{-1}) of the particles at three wavelengths (422, 532, and 782 nm) using a photoacoustic spectrometer (PAS) (Fischer and Smith, 2018). The absorption coefficient, b_{abs}, is defined as the total absorption cross-section of the particles per unit volume of air (hence the inverse length dimension, Mm^{-1}). b_{abs} can be normalized by the total mass concentration of the particles, obtained by integrating the SMPS size distribution, to yield the mass absorption cross-section (MAC, m^2/g) at each wavelength. Furthermore, b_{abs} typically exhibits an inverse power-law dependence on wavelength, with the exponent of the power-law fit being the absorption Ångström exponent (AAE). MAC and AAE, while not true intensive properties since they depend on particle size, are often used as effective light-absorption properties of atmospheric PM. In particular, larger MAC and smaller AAE (i.e., a flatter absorption spectrum) indicate darker PM (Saleh, 2020). Since they can be readily calculated in real-time, we used MAC and AAE in this study to constrain the light-absorption properties of BrC when tuning the combustion conditions. In post processing, we retrieved the fundamental light-absorption properties of the generated BrC, i.e., the imaginary part of the refractive index (k). Unlike the absorption quantified by MAC, k is a material property and does not depend on particle size. To retrieve k, we used Mie theory calculations (Bohren and Huffman, 2008) and the measured particle size distributions to find k_λ (the wavelength-specific k at wavelength λ) that best reproduced the measured light absorption following the approach of optical closure (Saleh et al., 2013;Chakrabarty et al., 2010;Lack et al., 2012). As with MAC, k exhibits an inverse power law dependence on wavelength. The exponent

of the power-law fit to k vs λ (w) is related to AAE such that AAE ≈ w + 1 for particles much smaller than λ. Larger k and MAC values correspond to stronger light absorption and are coupled with smaller w and AAE values, such that BrC with a larger k appears darker than BrC with a smaller k (Saleh, 2020).

Implicit in the use of Mie theory calculations is the assumption of spherical particles, which we have previously confirmed for the BrC produced in our setup using scanning electron microscopy (Saleh et al., 2018). Mie calculations also require the knowledge of the real part of the refractive index, which we assumed to be 1.6 and wavelength independent (Saleh et al., 2014;Moise et al., 2015;Browne et al., 2019;Li et al., 2019).

3.2.3 Particle collection and extraction

For each combustion condition, BrC particles were collected on 47 mm Teflon filters (0.2 Micron, Whatman) at a flow rate of 10 lpm. We collected a total of approximately 1.2 mg on four separate filters (300 µg each) to avoid clogging, which happens at loadings larger than 350 µg. We ensured that the particle concentrations and light absorption properties were stable over the sampling period of approximately 1 hour (Section 3.3.1). We estimated the sampled BrC mass loading based on the sampling flow rate and the real-time mass concentrations obtained from integrating the SMPS volume distribution assuming a density of 1.3 g/cm^3 (Cheng et al., 2019). The filters collected for each condition were then extracted together to form one parent solution. For extraction, the filters were placed in a glass vial, immersed in 10 ml of dichloromethane (DCM), and then sonicated for 40 minutes. The solution was then filtered in a glass syringe with a metal luer lock tip through a 13 mm Teflon filter (0.2 Micron, Sterlitech) to remove suspended particles, since those could affect the measurements of concentration to follow and produce

nonuniformities in the exposure experiments (Verma et al., 2012;Dilger et al., 2016). We then used UV-Vis spectrophotometry to verify there were no suspended particles remaining (See Figure S1).

The concentration of BrC in the solutions was determined using an OC-EC analyzer (Sunset Laboratory Inc, model 4L) running the IMPROVE-A protocol (Karanasiou et al., 2015;Salako et al., 2012). We pipetted 100 µl of each parent solution onto a pre-baked 1.5 cm^2 punch of quartz filter and vaporized the DCM using a stream of clean, dry air, thus leaving the BrC for analysis. The OC-EC analyzer uses an oven to convert all the carbon in the sample into CO_2, the concentration of which is measured to return the total carbon concentration. Since the BrC in our setup is expected to be largely composed of hydrocarbons, and given that most of the mass of hydrocarbon species is contributed by the carbon atoms, the measured carbon concentration can provide a good estimate of the BrC concentration.

3.2.4 Chemical speciation

Laser desorption ionization mass spectrometry is a soft ionization method capable of detecting organic species of large molecular sizes in combustion PM with minimal fragmentation (Faccinetto et al., 2011;Faccinetto et al., 2015;Apicella et al., 2010;Saleh et al., 2018). We used LDI to chemically characterize our samples. We used a small fraction of the parent BrC in DCM solutions to prepare 2 solutions of 1 µg/µl concentration. We then spotted a 10 µl total of each solution onto an LDI plate, spotting 2 µl at a time and then letting the DCM dry off. We conducted the LDI analysis using a Bruker Autoflex TOF mass spectrometer operated in reflectron mode to increase the peak resolution of the spectra. The instrument uses a 337 nm nitrogen laser in

positive mode. The ion source voltage was set to 19 kV and the reflector voltage to 20 kV. For each sample, the resulting spectrum was an average produced from 200 laser shots.

LDI is a semi-quantitative technique, meaning that the peak intensity observed in a spectrum cannot be used to calculate the concentration of the analyte (Faccinetto et al., 2011). However, by operating the instrument under identical conditions, a comparison of the relative abundance of species between different samples is possible without a need for accurate quantification. Further, the decreasing ionization efficiency in LDI with increasing molecular size also means that larger species are detected less efficiently than smaller ones. In order to detect larger species more efficiently, we used two settings for laser power and detector sensitivity depending on the molecular size region under investigation. For m/z < 650 u, the laser was operated at 50%, whereas for m/z > 1500, the laser power was raised to 100% and the detector sensitivity increased. Those settings were identical for both BrC samples, allowing us to compare the spectra obtained within each molecular size region.

3.2.5 Cytotoxicity analysis

The parent solution of BrC in DCM from each combustion condition was divided into eight portions with progressively increasing volumes (i.e., with increasing BrC mass) in order to obtain different BrC doses for the cytotoxicity analysis. The DCM was left to evaporate overnight inside a fume hood at 20 °C, leaving the dried BrC (Bai et al., 2001;Lin et al., 2008). The BrC was subsequently resuspended in 2.9 ml of culture media (Lonza BEBM™) and dimethyl sulfoxide (DMSO, final concentration in wells was 0.3%), which increases the solubility of the particles in media (Bølling et al., 2012). The samples were then sonicated for 5 minutes to dissolve the BrC in the media + DMSO solution and set aside until exposure. The samples were prepared such that

the final concentrations of BrC at exposure were 3.5, 6.0, 10.0, 16.0, 27.0, 49.0, 82.0, and 136.0 µg BrC/ml media.

The cytotoxicity of BrC was assessed in vitro using a tetrazolium salt-based colorimetric assay (WSt-8) from Sigma Aldrich's Cell Counting Kit-8 (CCK-8, Sigma Aldrich) to quantify the live cells. Cell cultures were prepared by growing human lung epithelial cells in a cell culture grade T-flask with Bronchial Lung Epithelial Basal Cell medium with growth supplements and glutamine (Lonza BEBM™). The cell culture was kept at 37°C in a humidified atmosphere with 5% CO2. The medium was replaced every 2 days until a confluence of 70-80 % was reached, after which the cells were split enzymatically by a 5-minute incubation in 0.18% trypsin (and 5 mM EDTA) followed by centrifugation at 1100 rpm for 7 minutes. The supernatant was discarded, and fresh medium was added to the cell pellet. The cells were counted by trypan blue assay using an automated Cell Counter (Nano EnTek). The counted cells were diluted with the medium to seed 100 µl of 10,000 cells/ml in each well of a 96-well plate.

We added 10 µl of the BrC-containing solutions of different concentrations into each well, with 7 replicates per concentration. 10 µl of media + DMSO solution were also added to 14 control wells and 7 blanks (media without cells). The cells were then incubated for 24 hours. Before measuring the cell viability using the colorimetric assay, we used a plate reader (Cytation 5, Biotek, Winooski, VT) to ensure that there was no significant contribution to absorption from the added BrC, which would have biased the viability results. Afterwards, the WST-8 assay (2-(2-methoxy-4-nitrophenyl)-3-(4-nitrophenyl)-5-(2,4-disulfophenyl)-2H-tetrazolium, monosodium salt)) was introduced following the manufacturer's protocol. The absorbance of formazan,

proportional to viability, was then measured at 450 nm by light-absorption spectroscopy using the Citation-5 plate reader. Relative cell viability is reported relative to controls (see above).

After exposure, we conducted further analysis on the unused fractions of the samples to assess the resuspension efficiency of BrC in the media + DMSO solution. We discarded the remaining solutions, washed the vials with DI water to remove residual media and DMSO, and dried the vials using a stream of air, thus leaving only the BrC that was not extracted by the media + DMSO in the vials. We then added 200 µl of DCM to each vial to re-dissolve the BrC and measured its concentration using the same technique described in Section 3.2.3. The measured BrC mass, reflecting the amount of BrC that had not dissolved in the BrC + media solutions, was then subtracted from the designed concentrations of those solutions listed above to obtain a "corrected" concentration. Finally, since the media and DMSO are organic, any residual not washed out by the DI water would show as carbon in the OC-EC analyzer and would bias the residual BrC measurement. Using blank vials (i.e., vials with media +DMSO but no BrC), we estimated the bias due to residual media and DMSO, which ranged between 1% and 50% of the remaining BrC concentration for the samples with the highest (136.0 µg/ml) and lowest (3.5µg/ml) original BrC concentration, respectively.

For the cytotoxicity data analysis, we used MATLAB (R2020a, MathWorks Inc.) to conduct a two-way analysis of variance (ANOVA) followed by the Tukey Honest Significant Difference (HSD) post-hoc test to determine the differences in cell viability within each BrC sample relative to control and across the two BrC samples at each concentration. Significant differences are considered as $p < 0.05$. We fitted a Hill model to the viability data using the EPA's BMDS software (Davis et al.,

2011). The Hill model is commonly used to represent dose-response curves, as it captures the plateaus at the lower and higher concentration exposures.

3.3 Results and Discussion

3.3.1 Particle concentrations and size distributions

Time series of the mass median diameter (MMD) and total aerosol mass concentration ($C_{aerosol}$) of the BrC particles over 90 minutes of filter collection are shown in Figure 3.2a and Figure 3.2b, respectively, for the two combustion conditions at low-temperature (670 °C) and high-temperature (1035 °C). MMD and $C_{aerosol}$ are stable within 1% and 2.5%, respectively, under both combustion conditions. This highlights the stability of the combustion conditions during filter collection, a significant advantage of the controlled combustion setup used in this work. Figure 3.2c shows the particle mass size distributions averaged over the periods shown in Figures 3.2a and 3.2b. For both combustion conditions, the BrC mass is dominated by ultrafine (< 100 nm) particles, which is typical for organic combustion PM. The small size of ultrafine particles gives them a high penetration efficiency in the lungs, allowing them to efficiently realize their toxicological effects (Chen et al., 2016). We note that while particle size is an important factor in determining the lung penetration depth of inhaled particles, thus their possible toxicity, it is unlikely that such factors are relevant in the methods used in this work. Since the BrC particles are collected on a filter and then solvent-extracted and dissolved, the particle size statistics that describe their properties in the aerosol phase do not apply in the liquid solution.

3.3.2 Light-absorption properties

The time series of the imaginary part of the refractive indices at 422 nm (k_{422}) and 532 nm (k_{532}) over a 90-minute period of filter collection are shown in Figure 3.3a for the two combustion

conditions. k_{422} and k_{532} values are stable to within 6% and 5% for the BrC produced at 670 °C and 1035 °C, respectively, confirming the stability of the combustion conditions. As discussed in Section 3.1.1, the light absorption properties of BrC are indicative of their chemical composition and of the combustion conditions under which they were produced. As expected, the results in Figure 3.3a show that the BrC produced at a higher temperature exhibits stronger light absorption at both 422 and 532 nm, in agreement with our previous findings (Cheng et al., 2019;Saleh et al., 2018). As shown in Figure 3.3b, the larger *k* is associated with visibly darker BrC when collected on Teflon filters.

Figure 3.3c shows the *k* values over the wavelength range of 400-800 nm obtained from the optical closure analysis (Section 3.2.2). The darker BrC, produced at 1035 °C, has a k_{532} of 0.028, an order of magnitude higher than the BrC produced at 670 °C, with a k_{532} of 0.003. The k_{532} values of the BrC produced at the lower and higher combustion temperatures are similar to those of BrC produced from the smoldering (Chakrabarty et al., 2010;Browne et al., 2019) and near-flaming combustion of biomass fuels (Saleh et al., 2013;Kumar et al., 2018;Xie et al., 2018), respectively. Figure 3.3c also shows the difference in the wavelength dependence (*w*) of *k* for the two types of BrC. The *w* values calculated were 5.4 and 8.8 for the BrC produced at 1035 °C and 670 °C, respectively. The coupled *k* and *w* reported in this work agree with trends reported in our previous works (Cheng et al., 2020;Saleh et al., 2018). The two types of BrC generated in this study fall in the categories of weakly absorptive BrC (W-BrC, $10^{-3} < k_{550} < 10^{-2}$) and moderately absorptive BrC (M-BrC, $10^{-2} < k_{550} < 10^{-1}$) suggested by Saleh (2020). As discussed in Section 3.1.1, the strength of light absorption by combustion PM determines their effect on atmospheric radiation (climate effect). In the case of the BrC produced in this work, that generated at 1035 °C

has stronger light absorption and is thus expected to contribute more strongly to warming than the BrC produced at 670 °C.

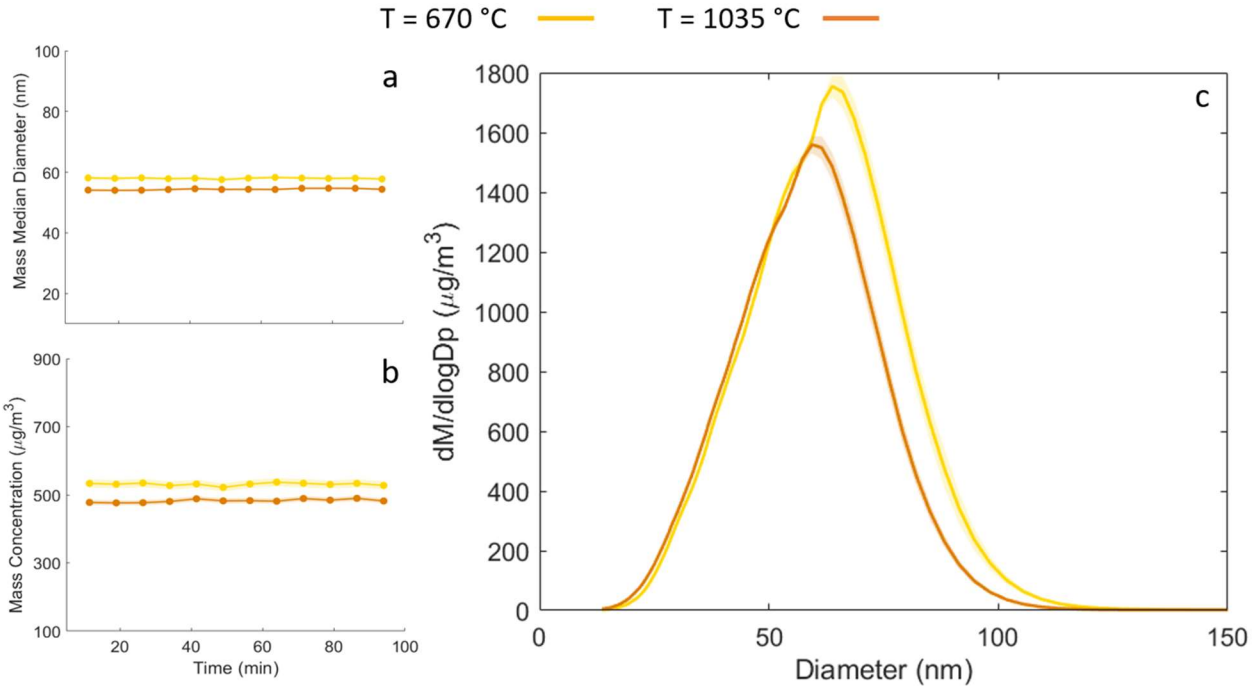

Figure 3.2. Particle size statistics over a filter collection period of 90 minutes for the two combustion conditions. The points shown are averages of 5 measured data points, with a data point retrieved every 90 seconds. The surrounding shaded areas represent the standard deviation throughout measurement. (a) Average particle mass median diameter. (b) Particle mass concentration. (c) Particle mass distributions averaged over the entire 90-minute collection period.

3.3.3 Molecular size distributions

The mass spectra obtained from LDI-MS for the BrC samples are shown in two m/z ranges in Figure 3.4. In Figure 3.4a, the spectra of the two samples are shown in relative intensity in the range of 150 to 650 m/z units. The spectrum of the sample collected at 670 °C is inverted for clarity. A comparison between the two spectra shows that the peaks from the 670 °C condition

are concentrated towards the smaller molecular sizes, with the most significant peaks falling below 250 m/z. For the 1035 °C condition, peaks are significantly more pronounced for all molecular sizes above 200 m/z. In Figure 3.4b, the spectra in the range of 1500 to 4500 m/z, in absolute intensity, show the disparity in signal between the two conditions. For the 670 °C combustion, peaks are almost nonapparent, while evenly spaced peaks remain apparent throughout for the 1035 °C condition. The spectrum of the combustion at 1035 °C also clearly shows an even spacing of molecules throughout the low and high molecular size regions. The spacings of 12 and 24 atomic mass units, seen in Figure 3.4a, reflect the BrC growth by the hydrogen abstraction acetylene addition (HACA) mechanism, the dominant PAH growth mechanism in combustion (Wang, 2011). 12 and 24 atomic mass unit-spacings have been previously reported by studies using LDI-MS to characterize soot in combustion emissions (Faccinetto et al., 2011;Michela et al., 2008).

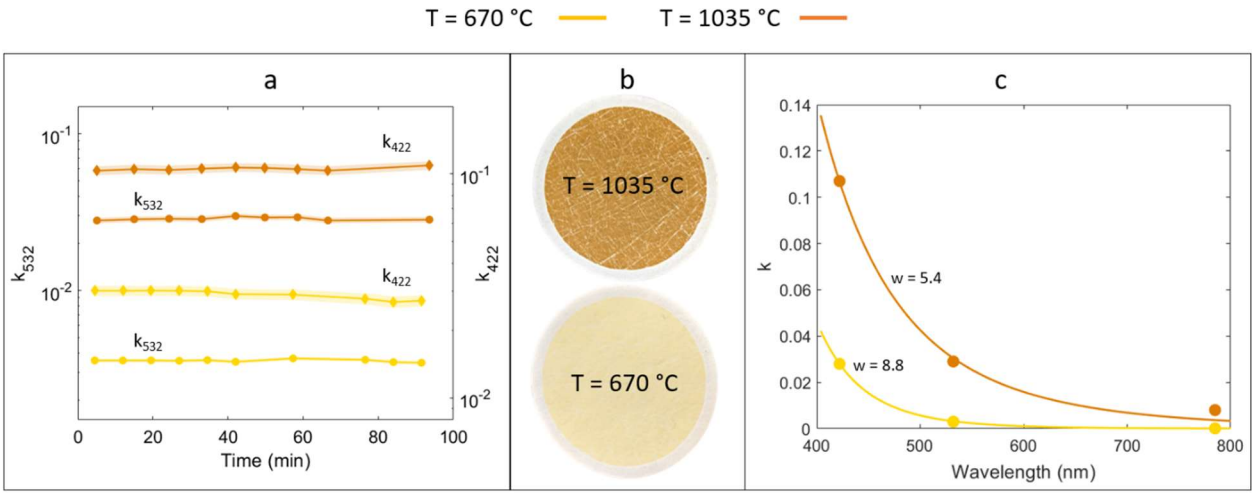

Figure 3.3. The light absorption properties of the two BrC samples show clear distinctions. (a) The imaginary part of the refractive indices at 532 nm (k_{532}) and 422 nm (k_{422}) of the two samples over a filter collection period of 90 minutes. (b) Pictures of the two BrC samples collected on

Teflon filters. (c) The imaginary part of the refractive index (k) as a function of wavelength for both samples averaged over the sampling period.

The LDI spectra confirm our previously reported findings showing that as the combustion conditions approach the BC-formation threshold, the species produced grow in molecular size and approach the large carbon structures that constitute BC (Saleh et al., 2018). As discussed in Section 3.1.1, the growth in molecular sizes is also accompanied by the stronger light absorption. Figures 3.3 and 3.4 show how the BrC produced at 1035 °C had significantly stronger absorption and was constituted of species of larger molecular sizes.

3.3.4 Cytotoxicity

Figure 3.5a depicts the dose-dependent viability of human lung epithelial cells exposed to BrC produced from the combustion of toluene at 670 °C and 1035 °C. The Hill model dose-response fits obtained using the EPA's BMDS software are also plotted (Davis et al., 2011). The response of cells to both samples of BrC shows a region of no response at the lower doses and a region of a plateauing response towards the higher doses, which is well captured by the Hill model. For the BrC sample produced at 670 °C, the cell viability was significantly different ($p < 0.05$) from control for all concentrations at and higher than 10.0 μg/ml, whereas viability was significantly different from control at all concentration at or higher than 16.0 μg/ml for the BrC produced at 1035 °C. The response of cells exposed to the higher concentrations of BrC produced at 670 °C appears to plateau at around 25%, while that of cells exposed to BrC produced at 1035 °C plateaus at around 65%. For all BrC exposure concentrations at and higher than 27.0 μg/ml, the viability of cells exposed to the BrC produced at 670 °C was significantly lower ($p < 0.05$) than that of cells exposed to the BrC produced at 1035 °C.

Figure 3.5b shows the dose-response data in Figure 3.5a along with the doses corrected for incomplete solubility based on the method explained in Sections 2.5. The OC-EC data and correction procedure are detailed in the SI. The BrC concentrations in this figure are all shifted towards lower values, indicating that the BrC did not completely dissolve in the media + DMSO solution. The trends in this figure reveal that using the design concentrations as is would result in an underestimation of the BrC toxicity in the response region of the curve, though not around the plateaus, where the viability is constant. The dose correction, however, does not affect the observed differences in response across samples, where the BrC produced at 670 °C remains significantly more toxic at the higher concentrations.

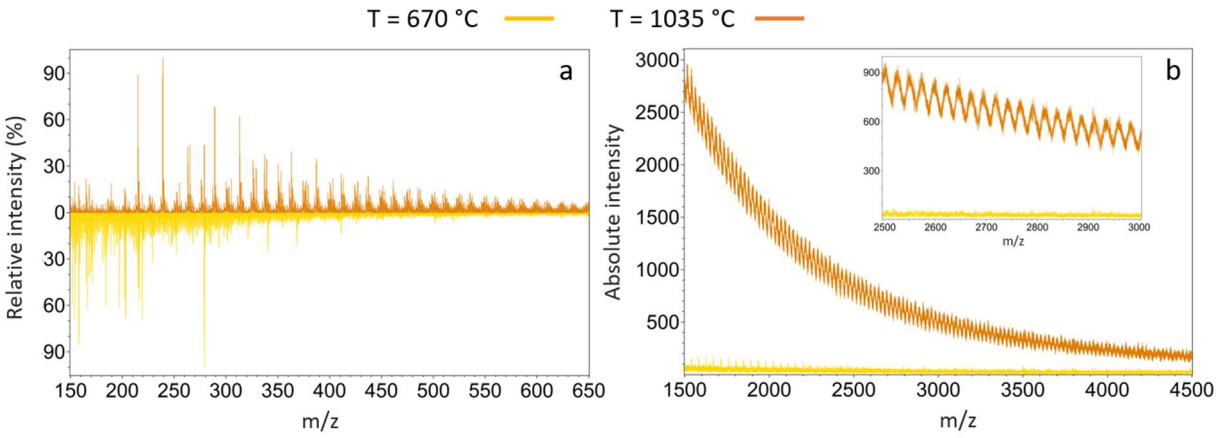

Figure 3.4. LDI-MS mass spectra of the two BrC samples produced at 670 °C and 1035 °C. (a) Mass spectra in the 150 to 650 m/z range, shown in intensity relative to the largest peak, with the laser operated at 50% power. (b) Mass spectra in the 1500 to 4500 m/z range, shown in absolute intensity, with the laser operated at 100% power and higher sensitivity. The inset in panel (b) shows a close up of the spectra in the 2500 to 3000 m/z range.

While both BrC samples are likely to be primarily composed of PAHs, the BrC produced at higher temperature underwent further development on the soot formation pathway, which is reflected

in a growth in molecular sizes. This molecular growth is likely to translate into lower bioavailability, a measure of a compound's ability to cross the cellular membrane (Semple et al., 2004), and thus lower toxicity (Kostal, 2016). The growth is also accompanied by a significant reduction in C/H ratios, as the combustion products become more carbonized (Michelsen, 2017). Those differences, caused by the change in combustion conditions, could be a critical factor causing the difference in cytotoxicity between the two samples.

Our findings are in qualitative agreement with those of several other studies that compared the cytotoxicity of particulate emissions from different modes of combustion (Bølling et al., 2009;Bølling et al., 2012;Jalava et al., 2010;Tapanainen et al., 2011). However, others found PM from more efficient combustion conditions (higher temperatures) to be more toxic (Happo et al., 2013;Leskinen et al., 2014;Kim et al., 2019;Kim et al., 2018). An explanation of the disagreement among different studies could be the difficulty in effectively controlling the combustion conditions in real-life sources. Except for Kim et al. (2018, 2019), the studies cited above performed their experiments using combustion regimes in which the conditions varied significantly within each regime (e.g., temperatures varied over a range of 300 °C in Bølling et al. (2012) and Kocbach et al. (2008) within each regime). The variability in combustion conditions within each regime, a consequence of the chaotic nature of real-life combustion, induces uncertainty that complicates the comparison between the two regimes. The systematic approach involving highly controlled combustion conditions in this study minimizes this uncertainty and enables isolating the effect of combustion conditions on the toxicity of combustion PM, which can help shed light on the design and data interpretation of real-life combustion studies.

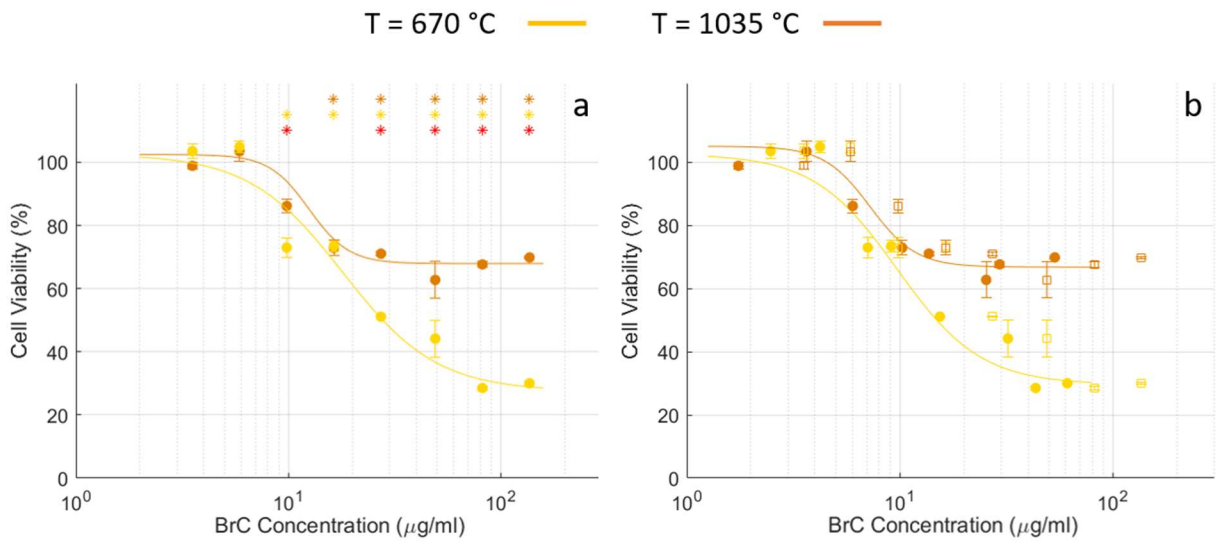

Figure 3.5. Viability of human lung epithelial cells compared to control after exposure to increasing doses of the two BrC samples produced at different combustion conditions. Bars represent standard error of the mean. Panel (a) shows the viability against the designed exposure dose. Significant differences ($p < 0.05$) relative to control are shown with a (*) matching the sample's legend color. Significant differences in viability ($p < 0.05$) between the two combustion conditions at a specific dose are marked with a red (*). Panel (b) shows the viability against the corrected doses (whole circles) and the design doses (empty squares). Numeric values of the corrected doses are shown in Table A2.1.

Kim et al. (2018, 2019) used a novel method of controlling combustion by surrounding a biomass fuel with a moving ring furnace that operated at 500 °C and 640 °C, for smoldering and flaming combustion, respectively. Both studies found that the emissions at higher temperature had a higher toxicity on a per-unit-mass basis. It should be noted, however, that the higher temperature in those studies (640 °C) is close to the lower temperature in our study (670 °C). Therefore, the findings of those studies are not necessarily inconsistent with ours. Furthermore, Kim et al. (2018) collected both vapor and PM emissions using a cryogenic trap and Kim et al.

(2019) exposed mice directly to the biomass combustion exhaust. Thus, both studies were not restricted to PM emissions, but accounted for the combined effects of PM and vapor emissions, while our study focuses solely on PM.

The observed biological responses can also depend on differences in certain physicochemical properties of the PM (e.g., size, shape, solubility), and the effects of these properties can manifest differently depending on the method of exposure, e.g., *in vivo* or *in vitro*. For example, *in vitro* exposure often relies on the collection of particulate matter on a filter, to then be extracted using a solvent. Under higher temperatures and more efficient conditions, insoluble PM (EC and ash) could remain unextracted, thus providing incorrect insight into the cytotoxicity of higher temperature combustion PM as a whole. If not fully soluble, those particles could also form agglomerates, reducing their effective dose in a submerged exposure setting (Paur et al., 2011). An advantage of our combustion setup is that we could control the emissions to produce only organics (BrC), leaving our results unaffected by the potential presence of EC or ash. It should be noted, however, that by limiting the study to those organics, our methods do not account for the cytotoxicity of EC or ash produced at higher temperatures. Further, by focusing on soluble species, we only address the toxicity activated through the chemical makeup of PM rather than its physical structure, which could also be of importance (BéruBé et al., 2007). In this and other submerged exposure studies, the uncertainties in estimating the actual exposure dose make it difficult to provide an accurate prediction of per gram toxicity. Clearance mechanisms in *in vivo* exposure could alter the effective exposure time, thus leading to different biological endpoints, as suggested by Happo et al. (2013).

3.4 Conclusions

The highly controlled combustion setup used in this study introduces a new method to isolate the effect of combustion conditions on the toxicity of the emitted PM. While it does not replace experiments using real-word, chaotic combustion to assess the toxicity of residential, traffic, or wildfire PM, it paves a way towards better understanding this toxicity by significantly reducing the complexity of the problem and focusing on specific components. Using this system, we have found that the brown carbon produced from less efficient combustion conditions at lower temperatures induced significantly more death in human lung epithelial cells than that produced under more efficient conditions at higher temperatures. Our findings indicate that the elevated cytotoxicity of brown carbon produced at lower temperatures could be due to the higher prevalence of species of smaller molecular sizes compared with the brown carbon produced at higher temperatures.

References

Akagi, S., Yokelson, R. J., Wiedinmyer, C., Alvarado, M., Reid, J., Karl, T., Crounse, J., and Wennberg, P.: Emission factors for open and domestic biomass burning for use in atmospheric models, Atmospheric Chemistry and Physics, 11, 4039-4072, 2011.

Andreae, M., and Gelencsér, A.: Black carbon or brown carbon? The nature of light-absorbing carbonaceous aerosols, Atmospheric Chemistry and Physics, 6, 3131-3148, 2006.

Apicella, B., Alfè, M., Amoresano, A., Galano, E., and Ciajolo, A.: Advantages and limitations of laser desorption/ionization mass spectrometric techniques in the chemical characterization of complex carbonaceous materials, International Journal of Mass Spectrometry, 295, 98-102, 2010.

Bai, Y., Suzuki, A. K., and Sagai, M.: The cytotoxic effects of diesel exhaust particles on human pulmonary artery endothelial cells in vitro: role of active oxygen species, Free Radical Biology and Medicine, 30, 555-562, 2001.

BéruBé, K., Balharry, D., Sexton, K., Koshy, L., and Jones, T.: Combustion-derived nanoparticles: Mechanisms of pulmonary toxicity, Clinical and Experimental Pharmacology and Physiology, 34, 1044-1050, 2007.

Black, C., Tesfaigzi, Y., Bassein, J. A., and Miller, L. A.: Wildfire smoke exposure and human health: Significant gaps in research for a growing public health issue, Environmental toxicology and pharmacology, 55, 186-195, 2017.

Bohren, C. F., and Huffman, D. R.: Absorption and scattering of light by small particles, John Wiley & Sons, 2008.

Bølling, A. K., Pagels, J., Yttri, K. E., Barregard, L., Sallsten, G., Schwarze, P. E., and Boman, C.: Health effects of residential wood smoke particles: the importance of combustion conditions and physicochemical particle properties, Particle and fibre toxicology, 6, 29, 2009.

Bølling, A. K., Totlandsdal, A. I., Sallsten, G., Braun, A., Westerholm, R., Bergvall, C., Boman, J., Dahlman, H. J., Sehlstedt, M., and Cassee, F.: Wood smoke particles from different combustion phases induce similar pro-inflammatory effects in a co-culture of monocyte and pneumocyte cell lines, Particle and fibre toxicology, 9, 45, 2012.

Bond, T. C., Streets, D. G., Yarber, K. F., Nelson, S. M., Woo, J. H., and Klimont, Z.: A technology-based global inventory of black and organic carbon emissions from combustion, Journal of Geophysical Research: Atmospheres, 109, 2004.

Browne, E. C., Zhang, X., Franklin, J. P., Ridley, K. J., Kirchstetter, T. W., Wilson, K. R., Cappa, C. D., and Kroll, J. H.: Effect of heterogeneous oxidative aging on light absorption by biomass burning organic aerosol, Aerosol Science and Technology, 53, 663-674, 2019.

Chakrabarty, R., Moosmuller, H., Chen, L.-W., Lewis, K., Arnott, W., Mazzoleni, C., Dubey, M., Wold, C., Hao, W., and Kreidenweis, S.: Brown carbon in tar balls from smoldering biomass combustion, Atmospheric Chemistry and Physics. 10: 6363-6370., 6363-6370, 2010.

Chen, R., Hu, B., Liu, Y., Xu, J., Yang, G., Xu, D., and Chen, C.: Beyond PM2. 5: the role of ultrafine particles on adverse health effects of air pollution, Biochimica et Biophysica Acta (BBA)-General Subjects, 1860, 2844-2855, 2016.

Cheng, Z., Atwi, K. M., Yu, Z., Avery, A., Fortner, E. C., Williams, L., Majluf, F., Krechmer, J. E., Lambe, A. T., and Saleh, R.: Evolution of the light-absorption properties of combustion brown

carbon aerosols following reaction with nitrate radicals, Aerosol Science and Technology, 1-15, 2020.

Cheng, Z. Z., Atwi, K., Onyima, T., and Saleh, R.: Investigating the dependence of light-absorption properties of combustion carbonaceous aerosols on combustion conditions, Aerosol Science and Technology, 53, 419-434, 10.1080/02786826.2019.1566593, 2019.

Chin, J.-Y., and Batterman, S. A.: VOC composition of current motor vehicle fuels and vapors, and collinearity analyses for receptor modeling, Chemosphere, 86, 951-958, 2012.

Davis, J. A., Gift, J. S., and Zhao, Q. J.: Introduction to benchmark dose methods and US EPA's benchmark dose software (BMDS) version 2.1. 1, Toxicology and applied pharmacology, 254, 181-191, 2011.

Desgroux, P., Mercier, X., and Thomson, K. A.: Study of the formation of soot and its precursors in flames using optical diagnostics, Proceedings of the Combustion Institute, 34, 1713-1738, 2013.

Dilger, M., Orasche, J., Zimmermann, R., Paur, H.-R., Diabaté, S., and Weiss, C.: Toxicity of wood smoke particles in human A549 lung epithelial cells: the role of PAHs, soot and zinc, Archives of toxicology, 90, 3029-3044, 2016.

Donaldson, K., Tran, L., Jimenez, L. A., Duffin, R., Newby, D. E., Mills, N., MacNee, W., and Stone, V.: Combustion-derived nanoparticles: a review of their toxicology following inhalation exposure, Particle and fibre toxicology, 2, 10, 2005.

Faccinetto, A., Desgroux, P., Ziskind, M., Therssen, E., and Focsa, C.: High-sensitivity detection of polycyclic aromatic hydrocarbons adsorbed onto soot particles using laser

desorption/laser ionization/time-of-flight mass spectrometry: An approach to studying the soot inception process in low-pressure flames, Combustion and Flame, 158, 227-239, 2011.

Faccinetto, A., Focsa, C., Desgroux, P., and Ziskind, M.: Progress toward the quantitative analysis of PAHs adsorbed on soot by laser desorption/laser ionization/time-of-flight mass spectrometry, Environmental science & technology, 49, 10510-10520, 2015.

Fine, P. M., Cass, G. R., and Simoneit, B. R.: Chemical characterization of fine particle emissions from the fireplace combustion of woods grown in the southern United States, Environmental Science & Technology, 36, 1442-1451, 2002.

Fischer, D. A., and Smith, G. D.: A portable, four-wavelength, single-cell photoacoustic spectrometer for ambient aerosol absorption, Aerosol Science and Technology, 52, 393-406, 2018.

Frenklach, M.: Reaction mechanism of soot formation in flames, Physical chemistry chemical Physics, 4, 2028-2037, 2002.

Happo, M. S., Uski, O., Jalava, P. I., Kelz, J., Brunner, T., Hakulinen, P., Mäki-Paakkanen, J., Kosma, V.-M., Jokiniemi, J., and Obernberger, I.: Pulmonary inflammation and tissue damage in the mouse lung after exposure to PM samples from biomass heating appliances of old and modern technologies, Science of the total environment, 443, 256-266, 2013.

Hays, M. D., Fine, P. M., Geron, C. D., Kleeman, M. J., and Gullett, B. K.: Open burning of agricultural biomass: physical and chemical properties of particle-phase emissions, Atmospheric environment, 39, 6747-6764, 2005.

Jalava, P. I., Salonen, R. O., Nuutinen, K., Pennanen, A. S., Happo, M. S., Tissari, J., Frey, A., Hillamo, R., Jokiniemi, J., and Hirvonen, M.-R.: Effect of combustion condition on cytotoxic and

inflammatory activity of residential wood combustion particles, Atmospheric Environment, 44, 1691-1698, 2010.

Karanasiou, A., Minguillón, M. C., Viana, M., Alastuey, A., Putaud, J.-P., Maenhaut, W., Panteliadis, P., Močnik, G., Favez, O., and Kuhlbusch, T. A.: Thermal-optical analysis for the measurement of elemental carbon (EC) and organic carbon (OC) in ambient air a literature review, 2015.

Kasurinen, S., Jalava, P. I., Happo, M. S., Sippula, O., Uski, O., Koponen, H., Orasche, J., Zimmermann, R., Jokiniemi, J., and Hirvonen, M. R.: Particulate emissions from the combustion of birch, beech, and spruce logs cause different cytotoxic responses in A549 cells, Environmental toxicology, 32, 1487-1499, 2017.

Kelly, F. J., and Fussell, J. C.: Size, source and chemical composition as determinants of toxicity attributable to ambient particulate matter, Atmospheric environment, 60, 504-526, 2012.

Kim, Y. H., Warren, S. H., Krantz, Q. T., King, C., Jaskot, R., Preston, W. T., George, B. J., Hays, M. D., Landis, M. S., and Higuchi, M.: Mutagenicity and lung toxicity of smoldering vs. flaming emissions from various biomass fuels: implications for health effects from wildland fires, Environmental health perspectives, 126, 017011, 2018.

Kim, Y. H., King, C., Krantz, T., Hargrove, M. M., George, I. J., McGee, J., Copeland, L., Hays, M. D., Landis, M. S., and Higuchi, M.: The role of fuel type and combustion phase on the toxicity of biomass smoke following inhalation exposure in mice, Archives of toxicology, 1-13, 2019.

Kocbach, A., Herseth, J. I., Låg, M., Refsnes, M., and Schwarze, P. E.: Particles from wood smoke and traffic induce differential pro-inflammatory response patterns in co-cultures, Toxicology and applied pharmacology, 232, 317-326, 2008.

Kostal, J.: Computational Chemistry in Predictive Toxicology: status quo et quo vadis?, in: Advances in Molecular Toxicology, Elsevier, 139-186, 2016.

Kumar, N. K., Corbin, J. C., Bruns, E. A., Massabó, D., Slowik, J. G., Drinovec, L., Močnik, G., Prati, P., Vlachou, A., and Baltensperger, U.: Production of particulate brown carbon during atmospheric aging of residential wood-burning emissions, Atmospheric Chemistry & Physics, 18, 2018.

Lack, D. A., Langridge, J. M., Bahreini, R., Cappa, C. D., Middlebrook, A. M., and Schwarz, J. P.: Brown carbon and internal mixing in biomass burning particles, Proceedings of the National Academy of Sciences, 2012.

Laskin, A., Laskin, J., and Nizkorodov, S. A.: Chemistry of atmospheric brown carbon, Chemical reviews, 115, 4335-4382, 2015.

Leskinen, J., Tissari, J., Uski, O., Virén, A., Torvela, T., Kaivosoja, T., Lamberg, H., Nuutinen, I., Kettunen, T., and Joutsensaari, J.: Fine particle emissions in three different combustion conditions of a wood chip-fired appliance–Particulate physico-chemical properties and induced cell death, Atmospheric environment, 86, 129-139, 2014.

Li, C., He, Q., Hettiyadura, A. P. S., Käfer, U., Shmul, G., Meidan, D., Zimmermann, R., Brown, S. S., George, C., and Laskin, A.: Formation of secondary brown carbon in biomass burning aerosol proxies through NO3 radical reactions, Environmental Science & Technology, 54, 1395-1405, 2019.

Lin, C.-C., Chen, S.-J., Huang, K.-L., Lee, W.-J., Lin, W.-Y., Tsai, J.-H., and Chaung, H.-C.: PAHs, PAH-induced carcinogenic potency, and particle-extract-induced cytotoxicity of traffic-related nano/ultrafine particles, Environmental science & technology, 42, 4229-4235, 2008.

Liu, L., Kong, S., Zhang, Y., Wang, Y., Xu, L., Yan, Q., Lingaswamy, A., Shi, Z., Lv, S., and Niu, H.: Morphology, composition, and mixing state of primary particles from combustion sources—crop residue, wood, and solid waste, Scientific reports, 7, 1-15, 2017.

McClure, C. D., Lim, C. Y., Hagan, D. H., Kroll, J. H., and Cappa, C. D.: Biomass-burning-derived particles from a wide variety of fuels–Part 1: Properties of primary particles, Atmospheric Chemistry & Physics, 20, 2020.

McEnally, C. S., Pfefferle, L. D., Atakan, B., and Kohse-Höinghaus, K.: Studies of aromatic hydrocarbon formation mechanisms in flames: Progress towards closing the fuel gap, Progress in Energy and Combustion Science, 32, 247-294, 2006.

Michela, A., Barbara, A., Antonio, T., and Anna, C.: Identification of large polycyclic aromatic hydrocarbons in carbon particulates formed in a fuel-rich premixed ethylene flame, Carbon, 46, 2059-2066, 2008.

Michelsen, H.: Probing soot formation, chemical and physical evolution, and oxidation: A review of in situ diagnostic techniques and needs, Proceedings of the Combustion Institute, 36, 717-735, 2017.

Moise, T., Flores, J. M., and Rudich, Y.: Optical properties of secondary organic aerosols and their changes by chemical processes, Chemical reviews, 115, 4400-4439, 2015.

Pachauri, R. K., Allen, M. R., Barros, V. R., Broome, J., Cramer, W., Christ, R., Church, J. A., Clarke, L., Dahe, Q., and Dasgupta, P.: Climate change 2014: synthesis report. Contribution of

Working Groups I, II and III to the fifth assessment report of the Intergovernmental Panel on Climate Change, Ipcc, 2014.

Park, R. J., Jacob, D. J., Chin, M., and Martin, R. V.: Sources of carbonaceous aerosols over the United States and implications for natural visibility, Journal of Geophysical Research: Atmospheres, 108, 2003.

Paur, H.-R., Cassee, F. R., Teeguarden, J., Fissan, H., Diabate, S., Aufderheide, M., Kreyling, W. G., Hänninen, O., Kasper, G., and Riediker, M.: In-vitro cell exposure studies for the assessment of nanoparticle toxicity in the lung—A dialog between aerosol science and biology, Journal of Aerosol Science, 42, 668-692, 2011.

Pope III, C. A., and Dockery, D. W.: Health effects of fine particulate air pollution: lines that connect, Journal of the air & waste management association, 56, 709-742, 2006.

Qiao, L., Kim, C., and Faeth, G.: Suppression effects of diluents on laminar premixed hydrogen/oxygen/nitrogen flames, Combustion and Flame, 143, 79-96, 2005.

Reisen, F., Duran, S. M., Flannigan, M., Elliott, C., and Rideout, K.: Wildfire smoke and public health risk, International Journal of Wildland Fire, 24, 1029-1044, 2015.

Russo, C., Stanzione, F., Ciajolo, A., and Tregrossi, A.: Study on the contribution of different molecular weight species to the absorption UV–Visible spectra of flame-formed carbon species, Proceedings of the Combustion Institute, 34, 3661-3668, 2013.

Salako, G. O., Hopke, P. K., Cohen, D. D., Begum, B. A., Biswas, S. K., Pandit, G. G., Chung, Y.-S., Rahman, S. A., Hamzah, M. S., and Davy, P.: Exploring the variation between EC and BC in a variety of locations, Aerosol and Air Quality Research, 12, 1-7, 2012.

Saleh, R., Hennigan, C., McMeeking, G., Chuang, W., Robinson, E., Coe, H., Donahue, N., and Robinson, A.: Absorptivity of brown carbon in fresh and photo-chemically aged biomass-burning emissions, Atmospheric Chemistry and Physics, 13, 7683-7693, 2013.

Saleh, R., Robinson, E. S., Tkacik, D. S., Ahern, A. T., Liu, S., Aiken, A. C., Sullivan, R. C., Presto, A. A., Dubey, M. K., and Yokelson, R. J.: Brownness of organics in aerosols from biomass burning linked to their black carbon content, Nature Geoscience, 7, 647, 2014.

Saleh, R., Cheng, Z., and Atwi, K.: The brown–black continuum of light-absorbing combustion aerosols, Environmental Science & Technology Letters, 5, 508-513, 2018.

Saleh, R.: From Measurements to Models: Toward Accurate Representation of Brown Carbon in Climate Calculations, Current Pollution Reports, 1-15, 2020.

Semple, K. T., Doick, K. J., Jones, K. C., Burauel, P., Craven, A., and Harms, H.: Peer reviewed: defining bioavailability and bioaccessibility of contaminated soil and sediment is complicated. ACS Publications, 2004.

Shen, G., Tao, S., Wei, S., Zhang, Y., Wang, R., Wang, B., Li, W., Shen, H., Huang, Y., and Chen, Y.: Emissions of parent, nitro, and oxygenated polycyclic aromatic hydrocarbons from residential wood combustion in rural China, Environmental science & technology, 46, 8123-8130, 2012.

Tang, C., Huang, Z., He, J., Jin, C., Wang, X., and Miao, H.: Effects of N2 dilution on laminar burning characteristics of propane− air premixed flames, Energy & Fuels, 23, 151-156, 2008.

Tapanainen, M., Jalava, P. I., Mäki-Paakkanen, J., Hakulinen, P., Happo, M. S., Lamberg, H., Ruusunen, J., Tissari, J., Nuutinen, K., and Yli-Pirilä, P.: In vitro immunotoxic and genotoxic

activities of particles emitted from two different small-scale wood combustion appliances, Atmospheric Environment, 45, 7546-7554, 2011.

Uski, O., Jalava, P., Happo, M., Leskinen, J., Sippula, O., Tissari, J., Mäki-Paakkanen, J., Jokiniemi, J., and Hirvonen, M.-R.: Different toxic mechanisms are activated by emission PM depending on combustion efficiency, Atmospheric Environment, 89, 623-632, 2014.

Verma, V., Rico-Martinez, R., Kotra, N., King, L., Liu, J., Snell, T. W., and Weber, R. J.: Contribution of water-soluble and insoluble components and their hydrophobic/hydrophilic subfractions to the reactive oxygen species-generating potential of fine ambient aerosols, Environmental science & technology, 46, 11384-11392, 2012.

Wang, H.: Formation of nascent soot and other condensed-phase materials in flames, Proceedings of the Combustion Institute, 33, 41-67, 2011.

Xie, M., Shen, G., Holder, A. L., Hays, M. D., and Jetter, J. J.: Light absorption of organic carbon emitted from burning wood, charcoal, and kerosene in household cookstoves, Environmental pollution, 240, 60-67, 2018.

Yu, S., Dennis, R. L., Bhave, P. V., and Eder, B. K.: Primary and secondary organic aerosols over the United States: estimates on the basis of observed organic carbon (OC) and elemental carbon (EC), and air quality modeled primary OC/EC ratios, Atmospheric Environment, 38, 5257-5268, 2004.

CHAPTER 4

CHEMICAL COMPOSITION AND CYTOTOXICITY OF FRESH AND PHOTOCHEMICALLY AGED BIOMASS BURNING ORGANIC AEROSOLS[3]

[3] Atwi, K., Edenfield, R., El Hajj, O., Mondal, A., Perri, C., Wilson, S.N., Easley, C.A., Handa, H., Saleh, R. To be submitted to *Environmental Science and Technology*, August 1, 2021

Abstract

The combustion of biomass fuels in wildland fires is a significant source of atmospheric pollutants with negative health impacts for millions of people. In the atmosphere, biomass combustion emissions undergo myriad processes that lead to the continuous evolution of the chemical composition of the biomass burning organic aerosol (BBOA). While BBOA in general has been repeatedly shown to have negative health impacts, studies that have investigated the impact of atmospheric evolution (or aging) on the toxicity of BBOA are scarce. In this work, we conducted laboratory experiments producing BBOA from the combustion of different biomass fuels: dead oak foliage, hickory twigs, and pine needles. We used UV radiation to initiate photochemical aging of emissions, leading to the production of secondary organic aerosol (SOA). We collected fresh and photochemically aged BBOA and compared their toxicity *in vitro* to human bronchial epithelial cells using a cell viability (WST-8) assay. Using ultra-high resolution electrospray ionization mass spectrometry (ESI-MS), we found that the aging of the BBOA samples led to significant changes in their chemical makeup. Using induction-coupled plasma mass spectrometry (ICP-MS), we detected trace concentrations of known toxic heavy metals such as arsenic, selenium, manganese, and others. In the cell viability assays, we found that the fresh hickory BBOA was the most toxic, followed by the pine and oak BBOA. For all fuels, the fresh BBOA particles was slightly more toxic than the aged BBOA at the highest exposure doses. However, at intermediate doses, there was a marked difference in the onset of toxicity, with the fresh BBOA more toxic at lower doses. The differences in toxicity are likely caused by a combination of factors, including the availability and concentrations of toxic metals in the different samples as well as chemical changes following oxidation. In general, our findings

indicate that both fresh and aged BBOA are significantly toxic. However, we detected differences in toxicity at intermediate doses that warrant further investigation.

4.1 Introduction

Wildland fires are a major source of air pollution globally, with significant impacts on health (Jaffe et al., 2020;Larsen et al., 2018) and climate (Sokolik et al., 2019). In the United States, it is estimated that in 2011, nearly 212 million people lived in counties that were affected by wildfire smoke (Knowlton, 2013). Further, between 2008 and 2012, more than 10 million people lived in counties that had unhealthy air quality for over 10 days a year due to wildfire smoke, with particular implications for vulnerable communities (Rappold et al., 2017). Wildfire emissions have been repeatedly associated with increased morbidity, increased hospitalization, and negative cardiovascular and respiratory effects (Fann et al., 2018;Cascio, 2018;Dennekamp et al., 2015). On the other hand, prescribed wildland fires play an essential role in maintaining the health of natural ecosystems and mitigating uncontrolled wildfires (Hiers et al., 2020;O'Brien et al., 2018). As the response vis-a-vis air pollution and climate change gears towards lower anthropogenic emissions, and as climate change drives wildland fires to increase in frequency and intensity (Flannigan et al., 2009;Goss et al., 2020), emissions from both prescribed and wildfires will become the dominant health risk for millions of people (Aguilera et al., 2021;Navarro et al., 2018). However, the physicochemical properties and toxicological effects of biomass combustion emissions are still poorly characterized (Jaffe et al., 2020;Black et al., 2017;Sokolik et al., 2019).

A large fraction of biomass combustion emissions is contributed by organic species in both the particle (Lanz et al., 2010;Nicolae et al., 2013) and gas (Akherati et al., 2020;Ahern et al., 2019) phases. Immediately after they are emitted, organic combustion emissions undergo processes that change their chemical identity and alter their phase state (Garofalo et al., 2019;Cappa et al., 2020;Hodshire et al., 2019). Downstream of the combustion source, primary organic aerosols

(POA), i.e., those that are emitted in the particle phase at the source, react with atmospheric oxidants such as ozone and hydroxyl radicals, becoming more oxidized, with higher O:C ratios (Cappa et al., 2020;Hodshire et al., 2019). POA could also undergo further changes due to photolytic aging (Wong et al., 2017). In addition, species emitted in the vapor phase can undergo photooxidation reactions, decreasing their volatility and leading to their condensation into the particle phase, thus forming secondary organic aerosols (SOA) (Ahern et al., 2019;Akherati et al., 2020). In a competing mechanism, the dilution of combustion plumes as they move away from the source leads to the evaporation of the more volatile components of the POA. These processes lead to fundamentally different biomass burning organic aerosol (BBOA) compositions as combustion emissions evolve in the atmosphere and reach human populations, with possible implications for their effect on human health.

While there have been numerous studies documenting the toxicological effects of BBOA using *in vitro* or *in vivo* biological models (Naeher et al., 2007;Black et al., 2017), there are no studies that have looked systematically at the impact of atmospheric aging on the toxicity of BBOA using biological models. We have found two studies that compared the oxidative potential (OP) of fresh and aged BBOA using the dithiothreitol (DTT) chemical assay (Wong et al., 2019;Jiang and Jang, 2018). Wong et al. (2019) used field and laboratory data to compare the effect of atmospheric transport time (field) and different aging mechanisms (laboratory) on the BBOA's OP. They reported a 50% increase in the OP of field BBOA after only a few hours of atmospheric transport, with relatively stable OP after that. In their laboratory experiments, however, they found that the aging of BBOA by photolysis increased their OP initially only to cause a decline after some time, while aqueous OH oxidation rapidly led to a significant decline in OP. They also examined

the effects of dilution and found that the reduction of water-soluble organic content, as the more volatile species evaporated, led to a large increase in OP. Jiang and Jang (2018) measured the DTT activity of wood smoke particles over a period of several hours of photooxidation. They found that the photochemical aging of the particles led to a significant decrease in their OP, which they attributed to the decomposition of oxidizers. In all, those studies showed that atmospheric processes can have a significant effect on the OP of BBOA.

In field data that further confirms an effect of aging on the OP of organic aerosols (OA), Verma et al. (2015) used an aerosol mass spectrometer to group ambient OA collected at different locations in the southeastern United States according to identity/source. Using the DTT assay, they found that BBOA had the highest OP per mol, followed by cooking-OA. Other aerosol fractions, such as oxygenated OA and hydrocarbon-like OA had lower intrinsic OP per mol. In previous work, Verma et al. (2014) found the BBOA and SOA dominated the OP of ambient aerosol in the southeastern United States, with strong seasonal dependence (BBOA in the winter, SOA in the summer). Although these studies highlight the importance of BBOA as hazardous pollutants, it is not possible to draw a clear distinction between primary BBOA and BBOA-derived oxygenated OA, which hinders a conclusion as to how atmospheric aging affects the toxicity of BBOA.

In this study, we produced BBOA from the combustion of different biomass fuels inside an environmental chamber. We simulated photochemical atmospheric aging using UV lights, initiating photooxidation reactions that led to the condensation of new species into the particle phase as well as possible heterogeneous processing of existing particulate species. We collected fresh BBOA (before aging under UV lights) and aged BBOA (after aging under UV lights) on Teflon

filters. We analyzed the collected particles using ultra-high resolution electrospray ionization mass spectrometry to study their chemical composition and induction-coupled plasma mass spectrometry to determine their metal content. We treated immortalized human bronchial epithelial cells with different concentrations of the fresh and aged BBOA samples from each combustion experiment and compared their cytotoxicity toward the cells using a cell viability assay.

4.2 Methods

4.2.1 Biomass combustion experiments

We burnt dead oak foliage, hickory twigs, and pine needles, fuels commonly consumed in wildland fires in the Southeastern United States (Zheng et al., 2002;Fine et al., 2002), inside a 7.5 m^3 environmental chamber. The environmental chamber was lined with 44 UV lamps (GE Blacklight F40BL) on the bottom. Before each experiment, the chamber was conditioned to a relative of around 50% to promote OH radical production when the UV lights were turned on. After each experiment, the chamber was flushed with clean, dry air with the UV-lights on until the next experiment.

The fuels were either collected from the University of Georgia campus (hickory and oak) or purchased from a supply store (pine needles). We dried the fuels inside an oven for 24 hours at 60 °C to reduce their moisture content. For combustion, we burnt 25-50 grams of each fuel inside the environmental chamber, restricting the combustion to the smoldering phase. By focusing the experiments on the smoldering stage of combustion, we ensured that there were minimal concentrations of black carbon and that the particles inside the chamber were largely soluble in

methanol (Li et al., 2016;Chen and Bond, 2010), the importance of which is further discussed below.

We measured the particle size distribution inside the chamber throughout the experiment using a scanning mobility particle sizer (SMPS, TSI 3882), covering particles in the range of 10-500 nm. The total aerosol concentration (C_{OA}) in the chamber was calculated by integrating the SMPS size distribution, with an assumed particle density of 1.2 g/cm^3 (Sumlin et al., 2018;Cross et al., 2007). After the UV lights were turned on, C_{OA} increased due to the production of SOA from the photooxidation and subsequent condensation of vapor species. We estimated the concentration of SOA produced by subtracting the fresh BBOA concentration (i.e., C_{OA} before the lights were turned on) from the particle concentration after the lights were turned on. To do that successfully, we had to account for particle losses to the chamber walls. In particular, particles are known to be lost to chamber walls due to diffusion, convection, and electrostatic or gravitational forces (Wang et al., 2018). Thus, while C_{OA} grows due to the added SOA, underlying wall-losses simultaneously cause a decrease in particle concentration. To correct for wall losses, we fit an exponential curve to C_{OA} vs time (t) before the UV lights were turned on (t = 0) and estimated $C_{OA,Fresh}$ (C_{OA} of the fresh BBOA at t > 0) accordingly. The concentration of SOA could then be calculated using $C_{SOA} = C_{OA(t)} - C_{OA,Fresh(t)}$. The fold increase in C_{OA}, referred to as OA enhancement, is calculated as $C_{OA,Aged}/ C_{OA,Fresh}$.

We collected fresh and aged BBOA particles on 47 mm Teflon filters (0.2 microns, Sterlitech Corporation, PTU024750), collecting on 4 filters at a time with a flow rate of 5 SLPM through each. After collecting the fresh particles, we turned the UV lights on and waited for two hours, monitoring the particle concentration throughout. After two hours, we started collecting the

aged BBOA, leaving the lights on. Under each condition, we collected a total of 8 Teflon filters, with approximately 300 μg of BBOA on each filter, estimated using C_{OA} and the air flowrate through the filters. We extracted 7 of the 8 filters collected under each condition in 10 ml of methanol inside a glass vial, sonicating the vial for 10 minutes. We then removed the Teflon filters and filtered the solution in a glass syringe with a metal luer lock tip through a 13 mm Teflon filter (0.2 microns, Sterlitech Corporation, PTU021350) to remove suspended particles, since those could create nonuniformities in the exposure tests (Verma et al., 2012;Dilger et al., 2016). As mentioned earlier, restricting the combustion experiments to the smoldering phase reduces the amount of methanol-insoluble particles, such as black carbon, that would be filtered out in this process. Thus, the species extracted in methanol were largely representative of the particles in the chamber. At the end of this process, we had 6 vials representing parent solutions for each of the conditions under study (3 biomass fuels, fresh and aged BBOA from each).

We determined the carbon concentration in the solutions using an OCEC analyzer (Sunset Laboratory Inc, model 4L) running the NIOSH-870 protocol (Karanasiou et al., 2015). The OCEC analyzer measures the total amount of carbon on a quartz punch by heating the sample at different temperature stages and then measuring the carbon species, as CO_2, using a non-dispersive infrared sensor. To measure the concentration of carbon in the solutions, we pipetted 200 μL of each solution onto a pre-baked 1.5 cm^2 punch in 50 μL steps. After each step, we allowed the methanol to evaporate under a stream of clean, dry air. To estimate the concentration of the parent solutions, we divided the total OC measured by the OCEC analyzer by the volume pipetted onto the Quartz filter punch (200 μL). The further preparation of BBOA samples for cell exposure is described in Section 2.4.

4.2.2 Chemical Analysis

4.2.2.1 Ultra-high resolution electrospray ionization mass spectrometry

We used ultra-high resolution electrospray ionization mass spectrometry (ESI-MS) to chemically characterize the BBOA samples. To do so, we extracted one half of a Teflon filter collected from each combustion experiment in 2 ml of HPLC grade methanol (Sigma Aldrich, >99.9% methanol). We then filtered the extract as before in a glass syringe using a 0.2-micron, 13 mm Teflon filter. We also prepared a background sample consisting of a fresh Teflon filter extracted and filtered in the same procedure as the combustion samples. The mass spectra of the samples were obtained using a Bruker SolariX XR 12T. The ESI source was operated in positive ion mode with a 6000 V capillary voltage. Peaks were picked using open-source software mmass (mmass.org) with a signal-to-noise ratio of 3. Background peaks (i.e., those appearing for a blank Teflon filter extracted in methanol) were excluded from the sample peaks with a tolerance of 1 ppm. We used Formularity, an automated formula assignment software, (https://omics.pnl.gov/software/formularity) to identify probable molecular formulae (Tolić et al., 2017;Kujawinski and Behn, 2006).

4.2.2.2 Metal analysis

Metals are common components in biomass combustion particulate emissions, and their toxicity in trace concentrations has been repeatedly demonstrated (Hieu and Lee, 2010;Massey et al., 2013;Yuan et al., 2019). We analyzed the BBOA samples for metal content using induction-coupled plasma mass spectrometry (ICP-MS). One half of a Teflon filter corresponding to the fresh BBOA samples from each combustion experiment was transferred into a Teflon digestion vessel and treated with 5ml of trace metals-grade nitric acid. The vessel was then subjected to

microwave digestion, following EPA protocols (USEPA, 1996). After cooling to room temperature, the vessels were opened, treated with 20 ml of water, and shaken thoroughly. 1 ml from each vessel was then diluted to 10 ml with 1% nitric acid and analyzed using the ICP-MS (Perkin Elmer Elan 9000) according to EPA method 200.8 protocol (Creed et al., 1994).

4.2.3 Toxicity analysis

4.2.3.1 BBOA sample preparation

We exposed cells to different doses of the BBOA particles by preparing solutions of 5 concentrations for each combustion sample. To do so, we first added different volumes from the parent BBOA solutions (prepared as described in Section 2.1) into vials. Knowing the concentration of the parent BBOA solution from the OCEC analyzer, as explained in Section 2.1, this corresponded to adding specific masses of BBOA into each vial. We allowed the methanol to evaporate overnight, leaving behind dry BBOA particles. We then added equal volumes of a solution of dimethyl sulfoxide (DMSO) in deionized water (1% DMSO in DI water, resulting in a 0.1% final DMSO concentration at exposure) into each vial. We finally sonicated the vials to resuspend the particles in the DI water + DMSO solution, producing solutions of equal volume and varying BBOA concentrations.

4.2.3.2 Cell Preparation

Cell cultures were prepared by growing immortalized human bronchial epithelial cells (cell line 16HBE14o) in a cell culture grade T-flask with Bronchial Lung Epithelial Basal Cell medium with growth supplements and glutamine (Lonza BEBM™). The cell culture was kept at 37°C in a humidified environment with 5% CO_2. The medium was replaced every 2 days until a confluence of 70-80 % was reached, after which the cells were split enzymatically by a 5-minute incubation

in 0.18% trypsin (and 5 mM EDTA) followed by centrifugation at 1100 rpm for 7 minutes. The supernatant was discarded, and fresh medium was added to the cell pellet. The cells were counted by trypan blue assay using an automated Cell Counter (Nano EnTek).

4.2.3.3 Cytotoxicity evaluation

The cytotoxicity of the BBOA samples was assessed in vitro in 96-well plates using a tetrazolium salt-based colorimetric WST-8 assay (2-(2-methoxy-4-nitrophenyl)-3-(4-nitrophenyl)-5-(2,4-disulfophenyl)-2H-tetrazolium, monosodium salt)) from Sigma Aldrich's Cell Counting Kit-8 (CCK-8, Sigma Aldrich). The cleavage of the salt by viable cells leads to the formation of formazan, the concentration of which can then be measured optically due to its absorbance of light at 450 nm. Thus, higher absorption at 450 nm corresponds to higher cell viability.

We evaluated the cytotoxicity of the 6 different BBOA samples at 5 doses each. At each dose, we conducted the exposure in quintuplets, and the experiments were repeated 2 times. In 96-well plates, each well contained 90 µL of cells in media, at a concentration 1000 cells/well. We added 10 µL of the BBOA in water + DMSO solutions into each well and 10 µL of water + DMSO into the control and blank wells. The final concentrations of the BBOA at exposure were 2, 20, 55, 90, and 215 µg BBOA/mL. After adding the BBOA samples, we used a plate reader (Cytation 5, Biotek, Winooski, VT) to measure the background absorption of the cells + BBOA at 450 and 650 nm prior to adding the WST-8 assay. Since the BBOA samples are light absorbing, their absorption can be confounded with the absorption by formazan, biasing the cell viability estimates. After 24-hour incubation, we added the WST-8 assay according to the manufacturer's specifications. We then used the Cytation-5 plate reader to measure the absorption at 450 and 650 nm, corresponding

to the formazan and formazan-free absorption, respectively. We calculated the viability in each well as:

$$Viability\ (\%) = 100 \times \frac{\left(sample_{450} - sample_{bkg,450}\right) - \left(sample_{650} - sample_{bkg,650}\right)}{\left(control_{450} - control_{bkg,450}\right) - \left(control_{650} - control_{bkg,650}\right)}$$

Here, the $sample_{\lambda}$ corresponds to the absorption at wavelength λ nm after the addition of WST-8, whereas $sample_{bkg,\lambda}$ corresponds to the absorption measured prior to the addition of WST-8. The same applies to $control_{\lambda}$ and $control_{bkg,\lambda}$.

4.2.4 Statistical Analysis

We conducted analysis of variance (ANOVA) followed by the Bonferroni post-hoc test to determine significant differences in cell viability within each sample relative to control, across fresh and aged samples from each fuel combustion experiment, and across the fresh and aged samples from different fuels. Significant differences are reported as $p < 0.05$. We further fit the cytotoxicity data to a 5th degree exponential function using EPA's BMDS 3.2 tool (https://www.epa.gov/bmds) and determined the benchmark dose (BMD) that caused a 50% reduction in cell viability.

4.3 Results and discussion

4.3.1 Photochemical aging and SOA formation

Figure 4.1 shows a time series of the total particle concentration (C_{OA}) in the chamber produced from the combustion of hickory twigs. The C_{OA} time series for the combustion of oak foliage and pine needles are shown in Figures A3.1. At t <0, C_{OA} decays due to wall loss in the chamber. At t = 0, when the UV lights were turned on, a reversal in the decay of C_{OA} is observed due to the production of SOA. In order to estimate the amount of SOA produced, we fit C_{OA} vs t at t<0 to an exponential decay function. We then used this fit to determine what the particle mass would be

without the additional SOA (i.e., $C_{OA,Fresh}$ in Section 2.1). The fit is shown in dashed lines in Figure 4.1. We estimated the mass of SOA produced as the maximum difference between C_{OA} and $C_{OA,Fresh}$ at t>0, as shown in the figure. The OA enhancement, or the fold increase in OA concentration due to the mass contributed by the newly formed SOA, was approximately 1.42 for the oak BBOA, 1.46 for the hickory BBOA, and 1.21 for the pine BBOA. It is important to note that the aging of the BBOA is not restricted to the production of SOA from the photooxidation of volatile species. Heterogenous oxidation reactions can also alter the chemical composition of species in the particle phase.

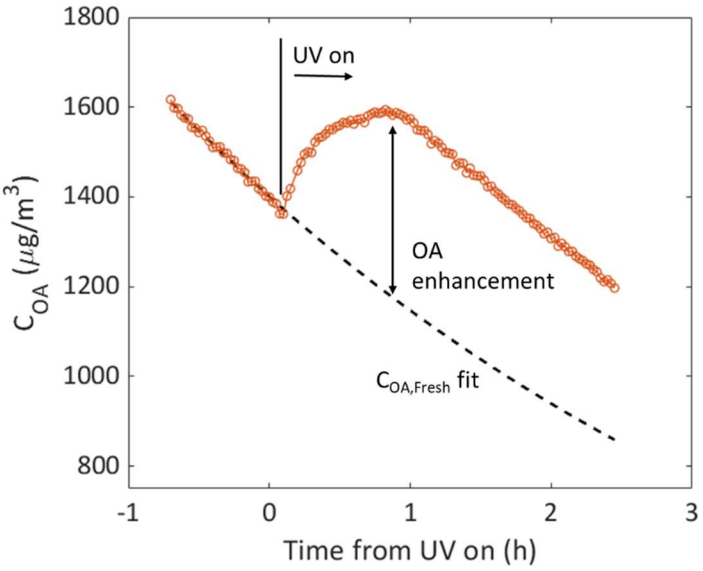

Figure 4.1. The evolution of particle mass concentration in the chamber (C_{OA}) for the hickory twigs combustion experiment. At t = 0, the UV lights were turned on and the photochemical aging of the emissions began, evident by a spike in C_{OA} due to the formation of SOA. The figure also shows the exponential fit to the fresh BBOA, used to estimate the OA enhancement due to SOA formation.

4.3.2 Chemical speciation

The mass spectra of the different fresh and aged combustion samples, retrieved using ultra-high resolution ESI-MS, are shown in Figure 4.2. Several thousand formula assignments were completed for each sample, with a number of such assignments displayed in the figure. The compounds depicted in Figure 4.2 include species that are common markers for or have been identified in biomass combustion emissions along with species that have been previously identified as secondary organic compounds. Those include levoglucosan ($C_6H_{10}O_5$) (Fraser and Lakshmanan, 2000;Robinson et al., 2006), fructose ($C_6H_{12}O_6$) (Medeiros et al., 2006;Kourtchev et al., 2008), diethyl phthalate ($C_{12}H_{14}O_4$) (Straka and Havelcova, 2012;Smith et al., 2009), dibutyl phthalate ($C_{16}H_{22}O_4$) (Smith et al., 2009;Straka and Havelcova, 2012) as the biomass combustion emission markers. We also identified some compounds that were only present in the aged BBOA samples such as $C_{10}H_{14}O$, $C_8H_{12}O_8$, $C_{16}H_{30}O_5$ (Kourtchev et al., 2015), $C_{10}H_{16}O_6$, $C_{10}H_{18}O_5$ (Pereira et al., 2014), and others. There are evident qualitative differences between the spectra of the different combustion samples shown in Figure 4.2. Quantitatively, those differences were also apparent as thousands of compounds that were distinct between the fresh and aged BBOA samples or across the BBOA samples from different fuels.

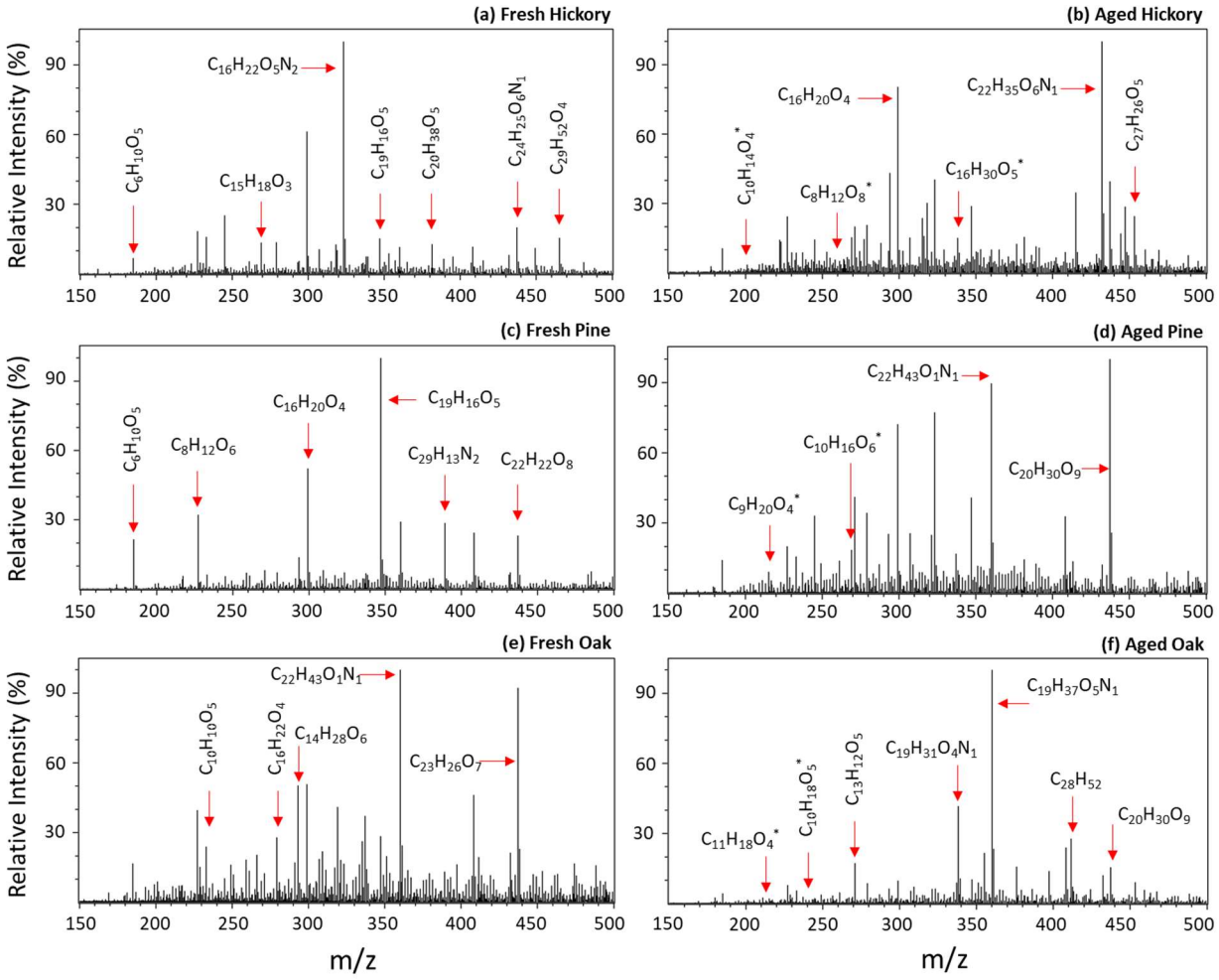

Figure 4.2. The mass spectra in the range of 100-500 m/z of the different BBOA samples, retrieved using ultra-high resolution ESI-MS. Prominent peaks are labeled with chemical formulae retrieved using Formularity. Compounds identified in the aged but not in the fresh BBOA are labeled with an asterisk. Note that the mass to charge ratio includes the mass of the charge carrier, H^+ or Na^+.

In Figure 4.3, those differences are summarized as the fractions of each sample contributed by species of different elemental compositions. The procedure for calculating those fractions is included in the appendix A3.2. Both similarities and differences between the elemental compositions of the different samples can be observed. For all of the samples, the identified

species were composed predominantly of compounds with a CHO or CHON elemental composition, in agreement with previous studies (Lanz et al., 2010;Nicolae et al., 2013). However, the hickory combustion sample had more sulfur containing species than the oak and pine samples, in which the fraction by mass of the sulfur-containing species did not exceed 5% (not shown). The differences between the fresh and aged samples can also be discerned. For example, for the hickory and oak samples, oxidation led to an increase in the fraction of CHON species, which could be explained by the condensation of nitrogen-containing species that have been previously detected in aged BBOA (Hatch et al., 2015;Warneke et al., 2011;Laskin et al., 2009).

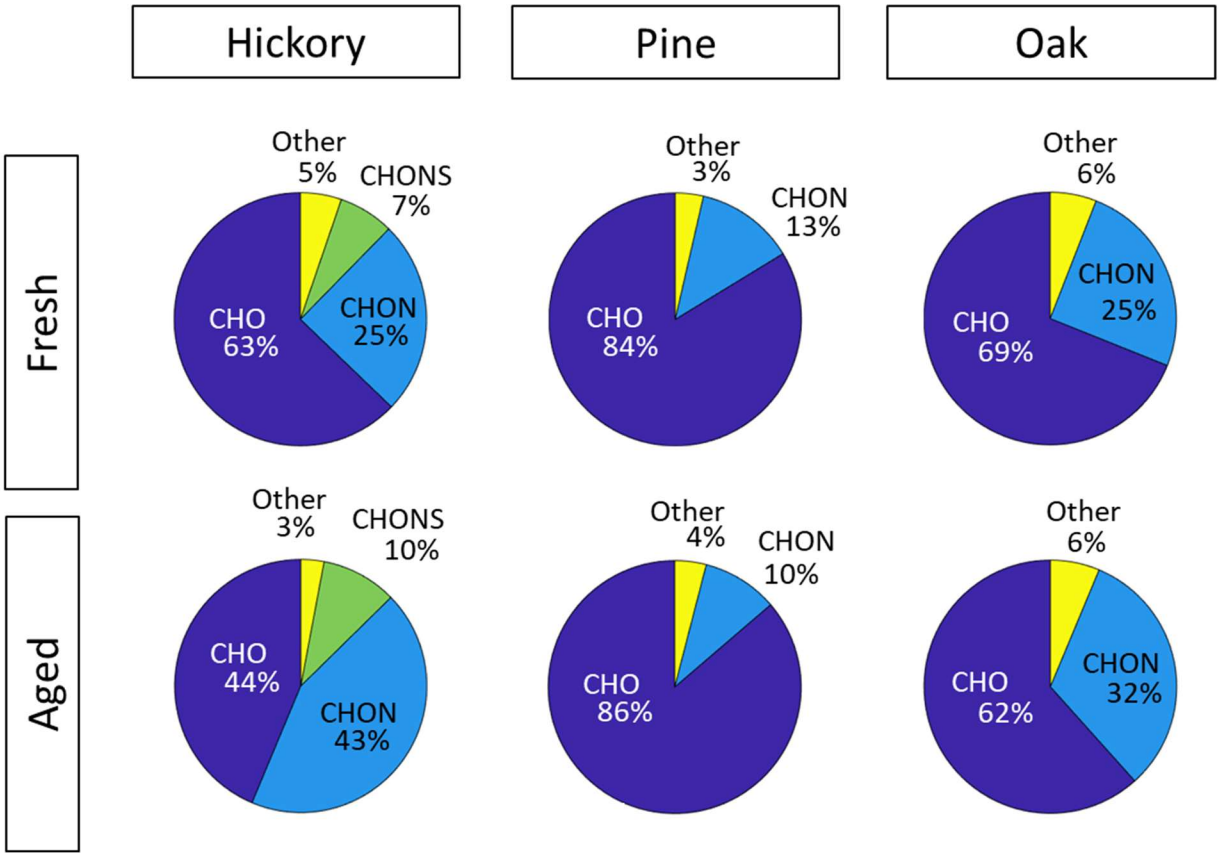

Figure 4.3. Mass fractions of species with distinct elemental compositions in the different BBOA samples.

The effect of photo-oxidation is most apparent in Figure 4.4a, which shows the ratio of organic matter (OM) to organic carbon (OC), OM:OC, plotted against their O:C ratio. In Figure 4.4b, we also show the O:C vs N:C ratios of the fresh and aged particles. As mentioned earlier, the oxidation of organic compounds leads to an increase in their O:C ratios (Cappa et al., 2020;Hodshire et al., 2019). In agreement with the trends of OA enhancement (as seen in Figure 4.1), the largest change in O:C upon oxidation was for the hickory sample (OA enhancement = 1.46), which increased from 0.28 to 0.33. The O:C ratio for the oak sample (OA enhancement = 1.42) increased from 0.25 to 0.27 upon oxidation, whereas the that of the pine sample (OA enhancement = 1.21) increased from 0.37 to 0.38. It is also worth noting the natively higher O:C ratio of the pine sample. The O:C ratios reported here and their change upon oxidation are consistent with those reported in other studies (Ahern et al., 2019). In concurrence with the O:C ratio, the OM:OC ratio also increased with oxidation for all fuels, with a trend correlating with OA enhancement and in agreement with previous reports of OM:OC (Aiken et al., 2008). In Figure 4.4b, a slight increase in the N:C ratio with aging can be observed for the oak and hickory BBOA, which, as explained earlier, can be explained by the condensation of nitrogen-containing volatile organics found in BBOA (Hatch et al., 2015;Warneke et al., 2011;Laskin et al., 2009).

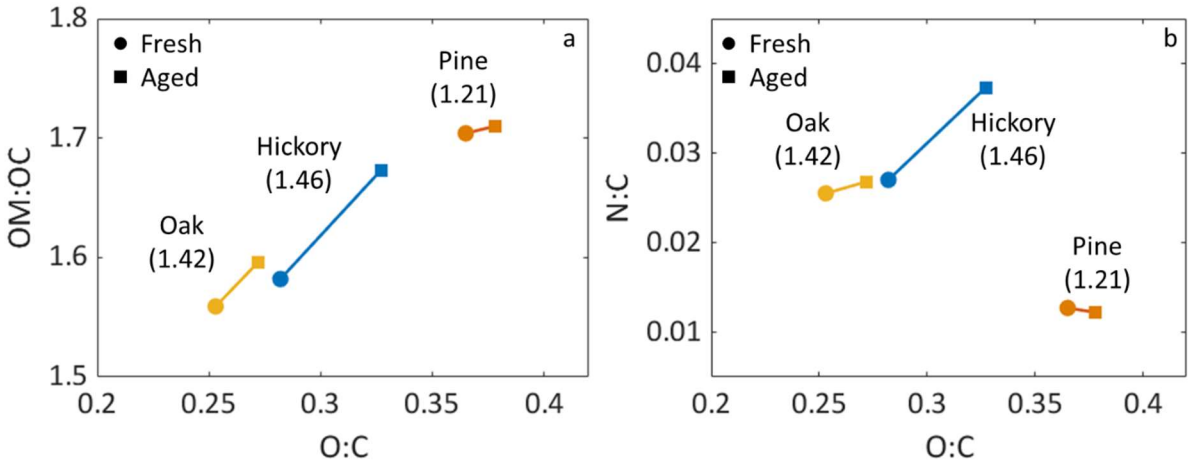

Figure 4.4. The changes in (a) OC:OM vs O:C and (b) N:C vs O:C ratios upon aging calculated for the different combustion samples.

4.3.3 Heavy metals

Table 1 shows the concentrations of different toxic heavy metals detected in the fresh BBOA combustion samples, retrieved using ICP-MS. The concentration of the metals in the aged BBOA, calculated using the OA enhancement as described in Section 2.2.2, is also shown. The detected metals are known to be correlated with increased toxicity and OP of PM samples (De Kok et al., 2006;Mirowsky et al., 2015;Steenhof et al., 2011). Cobalt (Cb), with established toxicity (Leyssens et al., 2017), was among the most abundant metals detected in the BBOA from the different fuels. Cadmium (Cd) (Bernhoft, 2013;Zwolak, 2020;Genchi et al., 2020;Satarug et al., 2017) was also detected in trance concentrations in all samples. Toxic metals such as chromium (Cr) (Costa and Klein, 2006;Shekhawat et al., 2015;Gad, 1989;Pavesi and Moreira, 2020), manganese (Mn) (O'Neal and Zheng, 2015), and nickel (Ni) (Buxton et al., 2019;Fu and Xi, 2020) were detected in the pine and oak BBOA but not in the hickory BBOA. Other toxic metals such arsenic (As) (Jomova et al., 2011;Bjørklund et al., 2018;Sodhi et al., 2019), Antimony (Sb) (Winship, 1987;Cooper and

Harrison, 2009), Selenium (Sun et al., 2014;MacFarquhar et al., 2010;Nuttall, 2006), and Thallium (Tl) (Cvjetko et al., 2010;Osorio-Rico et al., 2017) were detected in hickory but not in pine or oak. Given the established role of metals in the toxicity of particulate matter, those differences could cause different toxicological endpoints, as further discussed in Section 3.4.

Table 4.1. The concentrations of different metals found in the fresh BBOA from the combustion of the different fuels. Concentrations are shown as ng of metal in μg of BBOA.

	Hickory	Pine	Oak
Metal	**Metal concentration (ng/μg)**		
As	0.56	ND	ND
Ba	0.10	0.06	0.34
Cd	0.03	0.01	0.01
Co	1.07	1.59	1.59
Cr	ND	0.48	0.38
Mn	ND	0.88	1.02
Ni	ND	0.96	0.08
Sb	0.27	ND	ND
Se	1.27	ND	ND
Tl	2.39	ND	ND

4.3.4 Cytotoxicity

We evaluated the cytotoxicity of the different combustion samples at 5 different exposure concentrations by measuring the cell viability using the WST-8 assay. In Figure 4.5, the cell viability w.r.t control is shown after 24-hour exposure to each of the fresh and aged BBOA from the 3 different fuels. The dashed lines represent the 5^{th} degree exponential fits calculated using BMDS 3.2. All samples exhibited typical dose-response profiles, with a significant decrease in cell viability at all exposure doses equal to or higher than 20 μg BBOA/ml. The results in Figure 4.5 reflect dependence of cell viability (i.e. toxicity) on both fuel type and photochemical age. These trends can be conveniently summarized using the BMD required to reach 50% cell viability, where

a smaller BMD indicates higher toxicity. The retrieved BMD values are shown in Figure 4.5 for each sample over its corresponding panel along with its 95% confidence interval. Comparing BMD values of the fresh BBOA, our results indicate significant differences in toxicity between the three fuels, with fresh BBOA from hickory combustion being the most toxic, followed by pine, and oak. For all fuels, the BMD for the fresh BBOA was significantly lower than the BMD of the aged BBOA, thus indicating a decrease in toxicity with photochemical aging. The variation in BMD of the aged BBOA samples across fuels was smaller than for the fresh BBOA, with aged BBOA from hickory combustion being more toxic than pine and oak, which had similar toxicities.

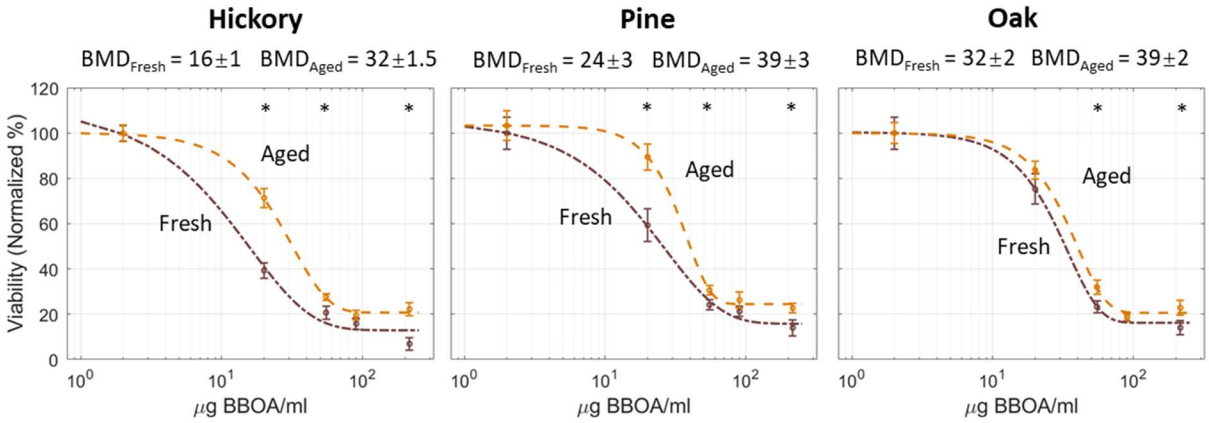

Figure 4.5. The normalized cell viability of human bronchial epithelial cells exposed to fresh and aged BBOA particles from the combustion of (a) hickory twigs, (b) dead pine needles, and (c) dead oak foliage. The dashed lines represent 5th degree exponential fits and asterisks indicate significant differences cell viability between the fresh and aged BBOA. Above the panel for each fuel is the BMD for 50% reduction in cell viability.

Given the relatively small number of samples in this study, it is not straightforward to establish clear linkages between the observed differences in the toxicity of BBOA from different fuels and their chemical composition. As shown in Figure 4.3, all BBOA samples were predominantly

composed of oxygenated and nitrated hydrocarbons (CHOs and CHONs), which are known to exhibit high OP (Misaki et al., 2016;McCarrick et al., 2019;Chlebowski et al., 2017). Therefore, one might expect OP, and potentially toxicity, to correlate with O:C and N:C (Chowdhury et al., 2018;Tuet et al., 2017). However, the variations in O:C and N:C (Figure 4.4b) and in BMD (Figure 4.5) do not allow for deriving any conclusions beyond stating that both could have an effect on toxicity. For example, among the fresh BBOA samples, pine BBOA has the highest O:C, the lowest N:C, and a BMD in between that of the other two fresh samples.

Our results indicate that the aged BBOA was significantly less toxic than the fresh BBOA for all fuels, which is in-line with the findings of Jiang and Jang (2018), who found that atmospheric aging decreased the OP of BBOA due to the decomposition of oxidizing species. However, Wong et al. (2019) presented a more complicated picture in which the OP of lab-aged BBOA decreased over time while that of field-collected BBOA increased. However, their findings also uncovered an important role for dilution, whereby diluted samples had significantly higher OP per unit mass. A role for heavy metals, as discussed next, would help explain this increased OP.

Though existing in trace amounts, it is plausible that heavy metals play an important role in the observed variation in toxicity among the BBOA samples. As shown in Table 1, there is a significant variation in the concentrations in heavy metals across samples. There are no definitive comparative studies on the relative toxicity of these metals. However, arsenic (As) is considered one of the most highly toxic heavy metals in atmospheric particles (alongside lead and mercury)) (Jomova et al., 2011;Bjørklund et al., 2018;Sodhi et al., 2019). The fact that it was only detected in the hickory BBOA samples might explain why hickory BBOA exhibited the highest toxicity compared to the other samples. Furthermore, the toxicity being driven by heavy metals would

explain the observed decrease in BBOA toxicity upon photochemical aging. While we did not measure the concentrations of heavy metals in the aged samples, OA enhancement due to SOA formation is expected to dilute the heavy metals in the particles, thus reducing their concentrations in the aged BBOA doses. This would agree with finding by Wong et al. (2019) that BBOA dilution, which would have the opposite effect of concentrating the heavy metals in the particles, led to a significant increase in OP per unit mass.

4.4 Conclusions

We produced BBOA from the combustion of dead oak foliage, hickory twigs, and pine needles inside an environmental chamber. We then simulated the effects of atmospheric photochemical aging using UV lights installed in the chamber. Using a WST-8 cell viability assay, we found that the BBOA from the combustion of hickory twigs was the most toxic to cells. Further, for all fuels, we found that the fresh BBOA was significantly more toxic than the aged BBOA. Although we identified significant differences in the chemical compositions of the fresh and aged BBOA, we could not conclusively attribute the differences in toxicity to one factor or another. However, the differences in toxic metal content between the fresh and aged samples as well as between the different fuels likely play an important role. In all, we recommend that further studies are conducted to isolate the impact of the multiple factors at play.

References

Aguilera, R., Corringham, T., Gershunov, A., and Benmarhnia, T.: Wildfire smoke impacts respiratory health more than fine particles from other sources: observational evidence from Southern California, Nature communications, 12, 1-8, 2021.

Ahern, A., Robinson, E., Tkacik, D., Saleh, R., Hatch, L., Barsanti, K., Stockwell, C., Yokelson, R., Presto, A., and Robinson, A.: Production of secondary organic aerosol during aging of biomass burning smoke from fresh fuels and its relationship to VOC precursors, Journal of Geophysical Research: Atmospheres, 124, 3583-3606, 2019.

Aiken, A. C., Decarlo, P. F., Kroll, J. H., Worsnop, D. R., Huffman, J. A., Docherty, K. S., Ulbrich, I. M., Mohr, C., Kimmel, J. R., and Sueper, D.: O/C and OM/OC ratios of primary, secondary, and ambient organic aerosols with high-resolution time-of-flight aerosol mass spectrometry, Environmental science & technology, 42, 4478-4485, 2008.

Akherati, A., He, Y., Coggon, M. M., Koss, A. R., Hodshire, A. L., Sekimoto, K., Warneke, C., de Gouw, J., Yee, L., and Seinfeld, J. H.: Oxygenated aromatic compounds are important precursors of secondary organic aerosol in biomass-burning emissions, Environmental Science & Technology, 54, 8568-8579, 2020.

Bernhoft, R. A.: Cadmium toxicity and treatment, The Scientific World Journal, 2013, 2013.

Bjørklund, G., Aaseth, J., Chirumbolo, S., Urbina, M. A., and Uddin, R.: Effects of arsenic toxicity beyond epigenetic modifications, Environmental geochemistry and health, 40, 955-965, 2018.

Black, C., Tesfaigzi, Y., Bassein, J. A., and Miller, L. A.: Wildfire smoke exposure and human health: Significant gaps in research for a growing public health issue, Environmental toxicology and pharmacology, 55, 186-195, 2017.

Buxton, S., Garman, E., Heim, K. E., Lyons-Darden, T., Schlekat, C. E., Taylor, M. D., and Oller, A. R.: Concise review of nickel human health toxicology and ecotoxicology, Inorganics, 7, 89, 2019.

Cappa, C. D., Lim, C. Y., Hagan, D. H., Coggon, M., Koss, A., Sekimoto, K., Gouw, J. d., Onasch, T. B., Warneke, C., and Kroll, J. H.: Biomass-burning-derived particles from a wide variety of fuels–part 2: effects of photochemical aging on particle optical and chemical properties, Atmospheric Chemistry and Physics, 20, 8511-8532, 2020.

Cascio, W. E.: Wildland fire smoke and human health, Science of the total environment, 624, 586-595, 2018.

Chen, Y., and Bond, T.: Light absorption by organic carbon from wood combustion, Atmospheric Chemistry and Physics, 10, 1773-1787, 2010.

Chlebowski, A. C., Garcia, G. R., La Du, J. K., Bisson, W. H., Truong, L., Massey Simonich, S. L., and Tanguay, R. L.: Mechanistic investigations into the developmental toxicity of nitrated and heterocyclic PAHs, Toxicological Sciences, 157, 246-259, 2017.

Chowdhury, P. H., He, Q., Lasitza Male, T., Brune, W. H., Rudich, Y., and Pardo, M.: Exposure of lung epithelial cells to photochemically aged secondary organic aerosol shows increased toxic effects, Environmental Science & Technology Letters, 5, 424-430, 2018.

Cooper, R. G., and Harrison, A. P.: The exposure to and health effects of antimony, Indian journal of occupational and environmental medicine, 13, 3, 2009.

Costa, M., and Klein, C. B.: Toxicity and carcinogenicity of chromium compounds in humans, Critical reviews in toxicology, 36, 155-163, 2006.

Creed, J., Brockhoff, C., and Martin, T.: EPA Method 200.8: Determination of Trace Elements in Waters and Wastes by Inductively Coupled Plasma-Mass Spectrometry (Revision 5.4). Cincinnati, OH: United States Environmental Protection Agency (USEPA), 1994.

Cross, E. S., Slowik, J. G., Davidovits, P., Allan, J. D., Worsnop, D. R., Jayne, J. T., Lewis, D. K., Canagaratna, M., and Onasch, T. B.: Laboratory and ambient particle density determinations using light scattering in conjunction with aerosol mass spectrometry, Aerosol Science and Technology, 41, 343-359, 2007.

Cvjetko, P., Cvjetko, I., and Pavlica, M.: Thallium toxicity in humans, Arhiv za higijenu rada i toksikologiju, 61, 111-118, 2010.

De Kok, T. M., Driece, H. A., Hogervorst, J. G., and Briedé, J. J.: Toxicological assessment of ambient and traffic-related particulate matter: a review of recent studies, Mutation Research/Reviews in Mutation Research, 613, 103-122, 2006.

Dennekamp, M., Straney, L. D., Erbas, B., Abramson, M. J., Keywood, M., Smith, K., Sim, M. R., Glass, D. C., Del Monaco, A., and Haikerwal, A.: Forest fire smoke exposures and out-of-hospital cardiac arrests in Melbourne, Australia: a case-crossover study, Environmental health perspectives, 123, 959-964, 2015.

Dilger, M., Orasche, J., Zimmermann, R., Paur, H.-R., Diabaté, S., and Weiss, C.: Toxicity of wood smoke particles in human A549 lung epithelial cells: the role of PAHs, soot and zinc, Archives of toxicology, 90, 3029-3044, 2016.

Fann, N., Alman, B., Broome, R. A., Morgan, G. G., Johnston, F. H., Pouliot, G., and Rappold, A. G.: The health impacts and economic value of wildland fire episodes in the US: 2008–2012, Science of the total environment, 610, 802-809, 2018.

Fine, P. M., Cass, G. R., and Simoneit, B. R.: Chemical characterization of fine particle emissions from the fireplace combustion of woods grown in the southern United States, Environmental Science & Technology, 36, 1442-1451, 2002.

Flannigan, M. D., Krawchuk, M. A., de Groot, W. J., Wotton, B. M., and Gowman, L. M.: Implications of changing climate for global wildland fire, International journal of wildland fire, 18, 483-507, 2009.

Fraser, M. P., and Lakshmanan, K.: Using levoglucosan as a molecular marker for the long-range transport of biomass combustion aerosols, Environmental Science & Technology, 34, 4560-4564, 2000.

Fu, Z., and Xi, S.: The effects of heavy metals on human metabolism, Toxicology mechanisms and methods, 30, 167-176, 2020.

Gad, S. C.: Acute and chronic systemic chromium toxicity, Science of the Total Environment, 86, 149-157, 1989.

Garofalo, L. A., Pothier, M. A., Levin, E. J., Campos, T., Kreidenweis, S. M., and Farmer, D. K.: Emission and evolution of submicron organic aerosol in smoke from wildfires in the western United States, ACS Earth and Space Chemistry, 3, 1237-1247, 2019.

Genchi, G., Sinicropi, M. S., Lauria, G., Carocci, A., and Catalano, A.: The effects of cadmium toxicity, International journal of environmental research and public health, 17, 3782, 2020.

Goss, M., Swain, D. L., Abatzoglou, J. T., Sarhadi, A., Kolden, C. A., Williams, A. P., and Diffenbaugh, N. S.: Climate change is increasing the likelihood of extreme autumn wildfire conditions across California, Environmental Research Letters, 15, 094016, 2020.

Hatch, L. E., Luo, W., Pankow, J. F., Yokelson, R. J., Stockwell, C. E., and Barsanti, K.: Identification and quantification of gaseous organic compounds emitted from biomass burning using two-dimensional gas chromatography–time-of-flight mass spectrometry, Atmospheric Chemistry and Physics, 15, 1865-1899, 2015.

Hiers, J. K., O'Brien, J. J., Varner, J. M., Butler, B. W., Dickinson, M., Furman, J., Gallagher, M., Godwin, D., Goodrick, S. L., and Hood, S. M.: Prescribed fire science: the case for a refined research agenda, Fire Ecology, 16, 1-15, 2020.

Hieu, N. T., and Lee, B.-K.: Characteristics of particulate matter and metals in the ambient air from a residential area in the largest industrial city in Korea, Atmospheric Research, 98, 526-537, 2010.

Hodshire, A. L., Akherati, A., Alvarado, M. J., Brown-Steiner, B., Jathar, S. H., Jimenez, J. L., Kreidenweis, S. M., Lonsdale, C. R., Onasch, T. B., and Ortega, A. M.: Aging effects on biomass burning aerosol mass and composition: A critical review of field and laboratory studies, Environmental science & technology, 53, 10007-10022, 2019.

Jaffe, D. A., O'Neill, S. M., Larkin, N. K., Holder, A. L., Peterson, D. L., Halofsky, J. E., and Rappold, A. G.: Wildfire and prescribed burning impacts on air quality in the United States, Journal of the Air & Waste Management Association, 70, 583-615, 2020.

Jiang, H., and Jang, M.: Dynamic oxidative potential of atmospheric organic aerosol under ambient sunlight, Environmental science & technology, 52, 7496-7504, 2018.

Jomova, K., Jenisova, Z., Feszterova, M., Baros, S., Liska, J., Hudecova, D., Rhodes, C., and Valko, M.: Arsenic: toxicity, oxidative stress and human disease, Journal of Applied Toxicology, 31, 95-107, 2011.

Karanasiou, A., Minguillón, M. C., Viana, M., Alastuey, A., Putaud, J.-P., Maenhaut, W., Panteliadis, P., Močnik, G., Favez, O., and Kuhlbusch, T. A.: Thermal-optical analysis for the measurement of elemental carbon (EC) and organic carbon (OC) in ambient air a literature review, 2015.

Knowlton, K.: Where there's fire, there's smoke: wildfire smoke affects communities distant from deadly flames, NRDC Issue Brief, 2013.

Kourtchev, I., Warnke, J., Maenhaut, W., Hoffmann, T., and Claeys, M.: Polar organic marker compounds in PM2. 5 aerosol from a mixed forest site in western Germany, Chemosphere, 73, 1308-1314, 2008.

Kourtchev, I., Doussin, J.-F., Giorio, C., Mahon, B., Wilson, E. M., Maurin, N., Pangui, E., Venables, D. S., Wenger, J. C., and Kalberer, M.: Molecular composition of fresh and aged secondary organic aerosol from a mixture of biogenic volatile compounds: a high-resolution mass spectrometry study, Atmospheric Chemistry and Physics, 15, 5683-5695, 2015.

Kujawinski, E. B., and Behn, M. D.: Automated analysis of electrospray ionization Fourier transform ion cyclotron resonance mass spectra of natural organic matter, Analytical chemistry, 78, 4363-4373, 2006.

Lanz, V., Prévôt, A., Alfarra, M., Weimer, S., Mohr, C., DeCarlo, P., Gianini, M., Hueglin, C., Schneider, J., and Favez, O.: Characterization of aerosol chemical composition with aerosol mass

spectrometry in Central Europe: an overview, Atmospheric Chemistry and Physics, 10, 10453-10471, 2010.

Larsen, A. E., Reich, B. J., Ruminski, M., and Rappold, A. G.: Impacts of fire smoke plumes on regional air quality, 2006–2013, Journal of exposure science & environmental epidemiology, 28, 319-327, 2018.

Laskin, A., Smith, J. S., and Laskin, J.: Molecular characterization of nitrogen-containing organic compounds in biomass burning aerosols using high-resolution mass spectrometry, Environmental science & technology, 43, 3764-3771, 2009.

Leyssens, L., Vinck, B., Van Der Straeten, C., Wuyts, F., and Maes, L.: Cobalt toxicity in humans—A review of the potential sources and systemic health effects, Toxicology, 387, 43-56, 2017.

Li, X., Chen, Y., and Bond, T. C.: Light absorption of organic aerosol from pyrolysis of corn stalk, Atmospheric Environment, 144, 249-256, 2016.

MacFarquhar, J. K., Broussard, D. L., Melstrom, P., Hutchinson, R., Wolkin, A., Martin, C., Burk, R. F., Dunn, J. R., Green, A. L., and Hammond, R.: Acute selenium toxicity associated with a dietary supplement, Archives of internal medicine, 170, 256-261, 2010.

Massey, D. D., Kulshrestha, A., and Taneja, A.: Particulate matter concentrations and their related metal toxicity in rural residential environment of semi-arid region of India, Atmospheric Environment, 67, 278-286, 2013.

McCarrick, S., Cunha, V., Zapletal, O., Vondráček, J., and Dreij, K.: In vitro and in vivo genotoxicity of oxygenated polycyclic aromatic hydrocarbons, Environmental Pollution, 246, 678-687, 2019.

Medeiros, P. M., Conte, M. H., Weber, J. C., and Simoneit, B. R.: Sugars as source indicators of biogenic organic carbon in aerosols collected above the Howland Experimental Forest, Maine, Atmospheric Environment, 40, 1694-1705, 2006.

Mirowsky, J. E., Jin, L., Thurston, G., Lighthall, D., Tyner, T., Horton, L., Galdanes, K., Chillrud, S., Ross, J., and Pinkerton, K. E.: In vitro and in vivo toxicity of urban and rural particulate matter from California, Atmospheric Environment, 103, 256-262, 2015.

Misaki, K., Takamura-Enya, T., Ogawa, H., Takamori, K., and Yanagida, M.: Tumour-promoting activity of polycyclic aromatic hydrocarbons and their oxygenated or nitrated derivatives, Mutagenesis, 31, 205-213, 2016.

Naeher, L. P., Brauer, M., Lipsett, M., Zelikoff, J. T., Simpson, C. D., Koenig, J. Q., and Smith, K. R.: Woodsmoke health effects: a review, Inhalation toxicology, 19, 67-106, 2007.

Navarro, K. M., Schweizer, D., Balmes, J. R., and Cisneros, R.: A review of community smoke exposure from wildfire compared to prescribed fire in the United States, Atmosphere, 9, 185, 2018.

Nicolae, D., Nemuc, A., Müller, D., Talianu, C., Vasilescu, J., Belegante, L., and Kolgotin, A.: Characterization of fresh and aged biomass burning events using multiwavelength Raman lidar and mass spectrometry, Journal of Geophysical Research: Atmospheres, 118, 2956-2965, 2013.

Nuttall, K. L.: Evaluating selenium poisoning, Annals of Clinical & Laboratory Science, 36, 409-420, 2006.

O'Brien, J., Hiers, J., Varner, J., Hoffman, C., Dickinson, M., Michaletz, S., Loudermilk, E., and Butler, B.: Advances in mechanistic approaches to quantifying biophysical fire effects, Current Forestry Reports, 4, 161-177, 2018.

O'Neal, S. L., and Zheng, W.: Manganese toxicity upon overexposure: a decade in review, Current environmental health reports, 2, 315-328, 2015.

Osorio-Rico, L., Santamaria, A., and Galván-Arzate, S.: Thallium toxicity: general issues, neurological symptoms, and neurotoxic mechanisms, Neurotoxicity of Metals, 345-353, 2017.

Pavesi, T., and Moreira, J. C.: Mechanisms and individuality in chromium toxicity in humans, Journal of Applied Toxicology, 40, 1183-1197, 2020.

Pereira, K., Hamilton, J., Rickard, A., Bloss, W., Alam, M., Camredon, M., Muñoz, A., Vázquez, M., Borrás, E., and Ródenas, M.: Secondary organic aerosol formation and composition from the photo-oxidation of methyl chavicol (estragole), Atmospheric Chemistry and Physics, 14, 5349-5368, 2014.

Rappold, A. G., Reyes, J., Pouliot, G., Cascio, W. E., and Diaz-Sanchez, D.: Community vulnerability to health impacts of wildland fire smoke exposure, Environmental Science & Technology, 51, 6674-6682, 2017.

Robinson, A. L., Subramanian, R., Donahue, N. M., Bernardo-Bricker, A., and Rogge, W. F.: Source apportionment of molecular markers and organic aerosol. 2. Biomass smoke, Environmental science & technology, 40, 7811-7819, 2006.

Satarug, S., Vesey, D. A., and Gobe, G. C.: Kidney cadmium toxicity, diabetes and high blood pressure: the perfect storm, The Tohoku journal of experimental medicine, 241, 65-87, 2017.

Shekhawat, K., Chatterjee, S., and Joshi, B.: Chromium toxicity and its health hazards, International Journal of Advanced Research, 3, 167-172, 2015.

Smith, J. S., Laskin, A., and Laskin, J.: Molecular characterization of biomass burning aerosols using high-resolution mass spectrometry, Analytical chemistry, 81, 1512-1521, 2009.

Sodhi, K. K., Kumar, M., Agrawal, P. K., and Singh, D. K.: Perspectives on arsenic toxicity, carcinogenicity and its systemic remediation strategies, Environmental Technology & Innovation, 16, 100462, 2019.

Sokolik, I., Soja, A., DeMott, P., and Winker, D.: Progress and challenges in quantifying wildfire smoke emissions, their properties, transport, and atmospheric impacts, Journal of Geophysical Research: Atmospheres, 124, 13005-13025, 2019.

Steenhof, M., Gosens, I., Strak, M., Godri, K. J., Hoek, G., Cassee, F. R., Mudway, I. S., Kelly, F. J., Harrison, R. M., and Lebret, E.: In vitro toxicity of particulate matter (PM) collected at different sites in the Netherlands is associated with PM composition, size fraction and oxidative potential-the RAPTES project, Particle and fibre toxicology, 8, 26, 2011.

Straka, P., and Havelcova, M.: Polycyclic aromatic hydrocarbons and other organic compounds in ashes from biomass combustion, Acta Geodyn. Geomater, 9, 481-490, 2012.

Sumlin, B. J., Oxford, C. R., Seo, B., Pattison, R. R., Williams, B. J., and Chakrabarty, R. K.: Density and homogeneous internal composition of primary brown carbon aerosol, Environmental science & technology, 52, 3982-3989, 2018.

Sun, H.-J., Rathinasabapathi, B., Wu, B., Luo, J., Pu, L.-P., and Ma, L. Q.: Arsenic and selenium toxicity and their interactive effects in humans, Environment international, 69, 148-158, 2014.

Tolić, N., Liu, Y., Liyu, A., Shen, Y., Tfaily, M. M., Kujawinski, E. B., Longnecker, K., Kuo, L.-J., Robinson, E. W., and Paša-Tolić, L.: Formularity: software for automated formula assignment

of natural and other organic matter from ultrahigh-resolution mass spectra, Analytical chemistry, 89, 12659-12665, 2017.

Tuet, W. Y., Chen, Y., Fok, S., Gao, D., Weber, R. J., Champion, J. A., and Ng, N. L.: Chemical and cellular oxidant production induced by naphthalene secondary organic aerosol (SOA): effect of redox-active metals and photochemical aging, Scientific reports, 7, 1-10, 2017.

USEPA, E.: Method 3052: Microwave assisted acid digestion of siliceous and organically based matrices, United States Environmental Protection Agency, Washington, DC USA, 1996.

Verma, V., Rico-Martinez, R., Kotra, N., King, L., Liu, J., Snell, T. W., and Weber, R. J.: Contribution of water-soluble and insoluble components and their hydrophobic/hydrophilic subfractions to the reactive oxygen species-generating potential of fine ambient aerosols, Environmental science & technology, 46, 11384-11392, 2012.

Verma, V., Fang, T., Guo, H., King, L., Bates, J., Peltier, R., Edgerton, E., Russell, A., and Weber, R.: Reactive oxygen species associated with water-soluble PM 2.5 in the southeastern United States: spatiotemporal trends and source apportionment, Atmospheric Chemistry and Physics, 14, 12915-12930, 2014.

Verma, V., Fang, T., Xu, L., Peltier, R. E., Russell, A. G., Ng, N. L., and Weber, R. J.: Organic aerosols associated with the generation of reactive oxygen species (ROS) by water-soluble PM2. 5, Environmental science & technology, 49, 4646-4656, 2015.

Wang, N., Jorga, S. D., Pierce, J. R., Donahue, N. M., and Pandis, S. N.: Particle wall-loss correction methods in smog chamber experiments, Atmospheric Measurement Techniques, 11, 6577-6588, 2018.

Warneke, C., Roberts, J., Veres, P., Gilman, J., Kuster, W., Burling, I., Yokelson, R., and De Gouw, J.: VOC identification and inter-comparison from laboratory biomass burning using PTR-MS and PIT-MS, International Journal of Mass Spectrometry, 303, 6-14, 2011.

Winship, K.: Toxicity of antimony and its compounds, Adverse drug reactions and acute poisoning reviews, 6, 67-90, 1987.

Wong, J. P., Nenes, A., and Weber, R. J.: Changes in light absorptivity of molecular weight separated brown carbon due to photolytic aging, Environmental science & technology, 51, 8414-8421, 2017.

Wong, J. P., Tsagkaraki, M., Tsiodra, I., Mihalopoulos, N., Violaki, K., Kanakidou, M., Sciare, J., Nenes, A., and Weber, R. J.: Effects of atmospheric processing on the oxidative potential of biomass burning organic aerosols, Environmental science & technology, 53, 6747-6756, 2019.

Yuan, Y., Wu, Y., Ge, X., Nie, D., Wang, M., Zhou, H., and Chen, M.: In vitro toxicity evaluation of heavy metals in urban air particulate matter on human lung epithelial cells, Science of The Total Environment, 678, 301-308, 2019.

Zheng, M., Cass, G. R., Schauer, J. J., and Edgerton, E. S.: Source apportionment of PM2. 5 in the southeastern United States using solvent-extractable organic compounds as tracers, Environmental science & technology, 36, 2361-2371, 2002.

Zwolak, I.: The role of selenium in arsenic and cadmium toxicity: an updated review of scientific literature, Biological trace element research, 193, 44-63, 2020.

CHAPTER 5

CONCLUSION

In this dissertation, we aimed to expand the state of the knowledge on biomass combustion emissions in general and BrC in particular. This was accomplished in multiple aspects. On the first front, we contributed to the growing understanding of the physicochemical properties of BrC by characterizing its strongly absorbing, methanol-insoluble fraction. On another, we examined the effect of combustion conditions on the toxicity of BrC. Finally, we also investigated the effect of aging on the toxicity of biomass combustions emissions.

In Chapter 2, we reported the existence of a methanol-insoluble BrC fraction produced in biomass combustion that is significantly more light-absorbing than the methanol-soluble BrC fraction. Those findings contribute to the growing body of literature on the association between solubility and its light-absorption properties of BrC. In agreement with previous studies, we found that methanol was efficient at extracting organic matter produced in our biomass-burning experiments, retrieving 90% ± 5% of the total carbonaceous species. However, we also showed the remaining methanol-insoluble fraction was critical in dictating the light-absorption properties of the BRC. Thus, our results showed that relying on methanol extraction to constrain the light-absorption properties of biomass-burning BrC results in a severe misrepresentation of these properties, leading to an order-of-magnitude underestimation of BrC light absorption at mid-visible wavelengths.

In Chapter 3, we used a highly controlled combustion setup to isolate the effect of combustion conditions on the toxicity of the emitted PM. Using this system, we introduced a new way to better understand the toxicity of combustion PM by significantly reducing the complexity of the problem and focusing on specific components. We found that the BrC produced from less efficient combustion conditions at lower temperatures induced significantly more death in human lung epithelial cells than that produced under more efficient conditions at higher temperatures. Coupled with chemical speciation we conducted, our findings indicate that the elevated cytotoxicity of BrC produced at lower temperatures could be due to the higher prevalence of species of smaller molecular sizes compared with the BrC produced at higher temperatures.

In Chapter 4, we produced biomass burning organic aerosols from the combustion of different biomass fuels inside an environmental chamber. We then used UV lights installed in the chamber to simulate the effect of photochemical atmospheric aging, producing significant amounts of secondary organic aerosols. We collected the fresh and aged particles on Teflon filters and analyzed their molecular composition using ultra-high resolution electrospray ionization mass spectrometry. We also used induction coupled plasma mass spectrometry to detect trace concentrations of toxic metals in the particles. In order to examine the effect of aging on the toxicity of the particles, we used the WST-8 cell viability assay. We found that both fresh and aged particles were very toxic to cells at high exposure concentrations. However, fresh particles were significantly more toxic at lower concentrations. Among the different fuels we studied, we found that hickory, which uniquely contained some toxic metals such as arsenic and selenium, was the most toxic. The difference in toxic metal content between the fresh and aged samples

as well as between the different fuels is likely a contributing factor for their different toxicological outcomes. However, our findings suggest that further studies are needed to isolate the impact of the multiple factors at play.

APPENDIX 1

SUPPLEMENTAL INFORMATION FOR CHAPTER 2

A DOMINANT CONTRIBUTION TO LIGHT ABSORPTION BY METHANOL-INSOLUBLE BROWN CARBON PRODUCED IN THE COMBUSTION OF BIOMASS FUELS

A1.1. Uncertainty Analysis:

A1.1.1. $TM = TM_{Q,unextracted} - TM_{QBT}$

$$\sigma_{TM}^2 = \sigma_{TM_{Q,unextracted}}^2 + \sigma_{TM_{QBT}}^2$$

A1.1.2. $OM_{MSBrC} = \left(TM_{Q,unextracted} - TM_{QBT}\right) - TM_{extracted}$

$$\sigma_{OM_{MSBrC}}^2 = \sigma_{TM_{Q,unextracted}}^2 + \sigma_{TM_{QBT}}^2 + \sigma_{TM_{extracted}}^2$$

Where $\sigma_{TM_{Q,unextracted}}$, $\sigma_{TM_{QBT}}$, and $\sigma_{TM_{extracted}}$ are retrieved from the OCEC analyzer.

A1.1.3. $f_{MSBrC} = \frac{OM_{MSBrC}}{TM}$; $f_{MIBrC} = \frac{OM_{MIBrC}}{TM}$; $f_{EC} = \frac{EC}{TM}$

$$\sigma_{f_{MSBrC}}^2 = \sigma_{OM_{MSBrC}}^2 \left(1/_{TM}\right)^2 + \sigma_{TM}^2 \left(OM_{MSBrC}/_{TM^2}\right)^2$$

$$\sigma_{f_{MIBrC}}^2 = \sigma_{OM_{MIBrC}}^2 \left(1/_{TM}\right)^2 + \sigma_{TM}^2 \left(OM_{MIBrC}/_{TM^2}\right)^2$$

$$\sigma_{f_{EC}}^2 = \sigma_{EC}^2 \left(1/_{TM}\right)^2 + \sigma_{TM}^2 \left(EC/_{TM^2}\right)^2$$

A1.1.4. $k_{MSBrC,\lambda} = \frac{A(\lambda)}{C_{MSBrC}} \times \frac{ln10\rho\lambda}{4\pi L}$

$$\sigma_{k_{MSBrC,\lambda}}^2 = \left(\frac{ln10\rho\lambda}{4\pi L}\right)^2 \times \left(\sigma_{A(\lambda)}^2 \left(1/_{C_{MSBrC}}\right)^2 + \sigma_{C_{MSBrC}}^2 \left(A(\lambda)/_{C_{MSBrC}{}^2}\right)^2\right)$$

Where C_{MSBrC} is the concentration of the MSBrC solution and $\sigma_{C_{MSBrC}}$ is retrieved from the OCEC analyzer. $\sigma_{A(\lambda)}$is 1% of $A(\lambda)$, per manufacturer's specifications.

A1.1.5. $w = \frac{\log(k_{422}/k_{532})}{\log(532/422)}$

$$\sigma_w^2 = \left(\frac{1}{\ln\left(532/422\right)}\right)^2 \times \left(\sigma_{k_{422}}^2 \left(1/_{k_{422}}\right)^2 + \sigma_{k_{532}}^2 \left(1/_{k_{532}}\right)^2\right)$$

In the cases where the equation above corresponds to aerosol measurements, $\sigma_{k_\lambda}$is the standard deviation of the k_λ values calculated from Mie theory calculations. For MSBrC and MIBrC, $\sigma_{k_\lambda}$is calculated as described below.

A1.1.6. $$k_{550} = k_{532}\left({}^{550}/_{532}\right)^{-w}$$

$$\sigma_{k_{550}}^2 = \sigma_{k_{532}}^2\left({}^{550}/_{532}\right)^{-w} + \sigma_w^2\left(k_{532} \times ln\left({}^{550}/_{532}\right) \times \left({}^{550}/_{532}\right)^{-w}\right)^2$$

A1.1.7. $$k_{MIBrC,\lambda} = \left(k_{BrC,aerosol,\lambda} - k_{MSBrC,\lambda}\frac{f_{MSBrC}}{f_{MSBrC}+f_{MIBrC}}\right)\frac{f_{MSBrC}+f_{MIBrC}}{f_{MIBrC}}$$

$$\sigma_{k_{MIBrC,\lambda}}^2 = \sigma_{BrC,aerosol,\lambda}^2\left(\frac{f_{MSBrC}+f_{MIBrC}}{f_{MIBrC}}\right)^2 + \sigma_{k_{MSBrC,\lambda}}^2\left(\frac{f_{MSBrC}}{f_{MIBrC}}\right)^2 + \sigma_{f_{MSBrC}}^2\left(\frac{k_{BrC,aerosol,\lambda}-k_{MSBrC,\lambda}}{f_{MIBrC}}\right)^2 + \sigma_{f_{MIBrC}}^2\left(\frac{k_{BrC,aerosol,\lambda}\times f_{MSBrC}-k_{MSBrC,\lambda}\times f_{MSBrC}}{f_{MIBrC}^{\ 2}}\right)^2$$

Where $\sigma_{BrC,aerosol,\lambda}$ is the standard deviation of the k_λ values calculated from Mie theory calculations.

A1.1.8. $$X_{abs,EC,\lambda} = \frac{b_{abs,EC}}{b_{abs}}$$

$$\sigma_{X_{abs,EC}}^2 = \sigma_{b_{abs,EC}}^2\left({}^{1}/_{b_{abs}}\right)^2 + \sigma_{b_{abs}}^2\left({}^{b_{abs,EC}}/_{b_{abs}^{\ 2}}\right)^2$$

Where $\sigma_{b_{abs}}$ is the standard deviation of the absorption measured from multi-PAS III and $\sigma_{b_{abs,EC}}$ is the standard deviation of the absorption attributed to EC.

A1.1.9. $$X_{abs,MSBrC,\lambda} = \left(1 - X_{abs,EC,\lambda}\right)\frac{\left(k_{MSBrC,\lambda}\times f_{MSBrC}/(f_{MSBrC}+f_{MIBrC})\right)}{k_{BrC,\lambda}}$$

$$\sigma^2_{X_{abs,MSBrC,\lambda}} = \sigma^2_{X_{abs,EC,\lambda}}\left(\frac{\left(k_{MSBrC,\lambda} \times f_{MSBrC}/(f_{MSBrC}+f_{MIBrC})\right)}{k_{BrC,\lambda}}\right)^2 + \sigma^2_{k_{MSBrC,\lambda}}\left(\frac{\left(1-X_{abs,EC,\lambda}\right)f_{MSBrC}/(f_{MSBrC}+f_{MIBrC})}{k_{BrC,\lambda}}\right)^2 + \sigma^2_{f_{MSBrC}}\left(\frac{\left(1-X_{abs,EC,\lambda}\right)k_{MSBrC,\lambda}}{k_{BrC,\lambda}} \times \frac{f_{MIBrC}}{(f_{MSBrC}+f_{MIBrC})^2}\right)^2 + \sigma^2_{f_{MIBrC}}\left(\frac{\left(1-X_{abs,EC,\lambda}\right)k_{MSBrC,\lambda} \times f_{MSBrC}}{k_{BrC,\lambda} \times (f_{MSBrC}+f_{MIBrC})^2}\right)^2 + \sigma^2_{k_{BrC,\lambda}}\left(\left(1-X_{abs,EC,\lambda}\right)\frac{\left(k_{MSBrC,\lambda} \times f_{MSBrC}/(f_{MSBrC}+f_{MIBrC})\right)}{{k_{BrC,\lambda}}^2}\right)^2$$

A1.1.10. $X_{abs,MIBrC,\lambda} = \left(1-X_{abs,EC,\lambda}\right)\frac{\left(k_{MIBrC,\lambda} \times f_{MIBrC}/(f_{MSBrC}+f_{MIBrC})\right)}{k_{BrC,\lambda}}$

$$\sigma^2_{X_{abs,MIBrC,\lambda}} = \sigma^2_{X_{abs,EC,\lambda}}\left(\frac{\left(k_{MIBrC,\lambda} \times f_{MIBrC}/(f_{MSBrC}+f_{MIBrC})\right)}{k_{BrC,\lambda}}\right)^2 + \sigma^2_{k_{MIBrC,\lambda}}\left(\frac{\left(1-X_{abs,EC,\lambda}\right)f_{MIBrC}/(f_{MSBrC}+f_{MIBrC})}{k_{BrC,\lambda}}\right)^2 + \sigma^2_{f_{MIBrC}}\left(\frac{\left(1-X_{abs,EC,\lambda}\right)k_{MIBrC,\lambda}}{k_{BrC,\lambda}} \times \frac{f_{MIBrC}}{(f_{MSBrC}+f_{MIBrC})^2}\right)^2 + \sigma^2_{f_{MSBrC}}\left(\frac{\left(1-X_{abs,EC,\lambda}\right)k_{MIBrC,\lambda} \times f_{MIBrC}}{k_{BrC,\lambda} \times (f_{MSBrC}+f_{MIBrC})^2}\right)^2 + \sigma^2_{k_{BrC,\lambda}}\left(\left(1-X_{abs,EC,\lambda}\right)\frac{\left(k_{MIBrC,\lambda} \times f_{MIBrC}/(f_{MSBrC}+f_{MIBrC})\right)}{{k_{BrC,\lambda}}^2}\right)^2$$

A1.2. Light absorption by the EC fraction

We employed alternative methods of estimating the contribution of the EC fraction to light absorption. In the main text, we assumed that the EC fraction was externally mixed with the BrC

and constituted a fraction of the number distribution equal to f_{EC}. We then used Mie Theory calculations to calculate the absorption by the EC fraction of the distribution.

Here, we use the Rayleigh-Debye-Gans (RDG) approximation to estimate the absorption by the EC fraction. In RDG, we assumed a diameter of 50 nm for the EC spherules, as an intermediate estimate between previously used values (Adler et al., 2010). The total number of EC spherules in a distribution can then be estimated by dividing the EC mass concentration in the distribution (i.e., C_{OA} x f_{EC}) by the mass of a single spherule, assuming an EC (black carbon) density of 1.8 g/cm^3 (Bond et al., 2013).

We used RDG to estimate $X_{abs,EC}$ and then retrieve $k_{MIBrC,\lambda}$, as in the main text. The results of $k_{MIBrC,\lambda}$ are shown in Figure A1.1 using the alternative calculation methods. On average, the difference between $k_{MIBrC,\lambda,Mie}$and $k_{MIBrC,\lambda,RDG}$ was around 3%, with one maximum value of 10%.

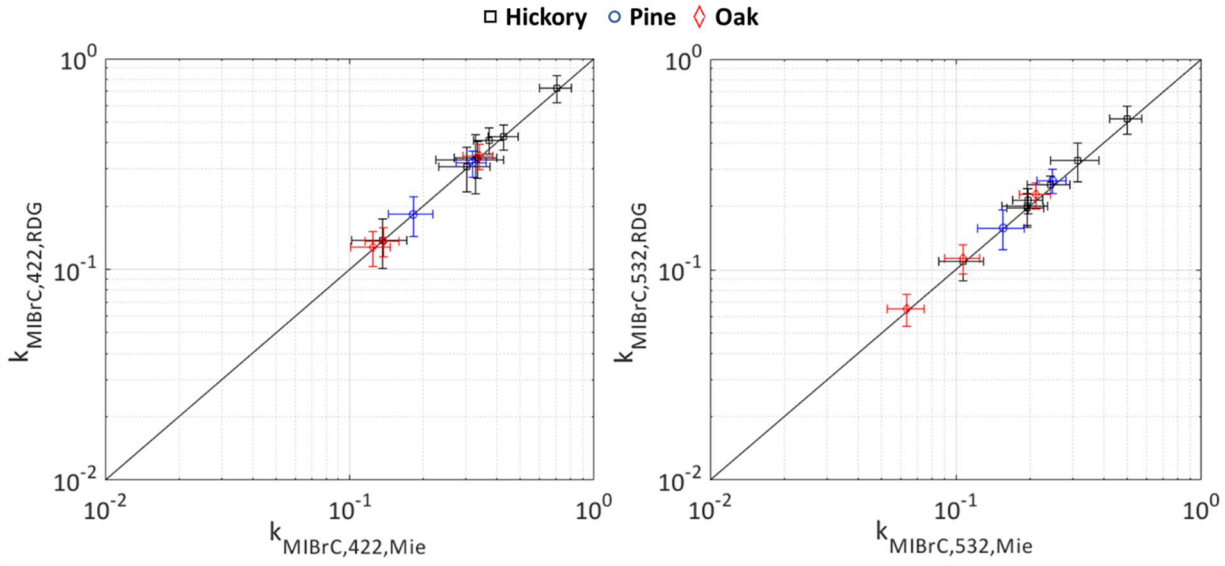

Figure A1.1. k_{422} and k_{422} calculated for the MIBrC using the assumptions of spherical elemental carbon particles and using the Rayleigh-Debye-Gans (RDG) approximation. At both wavelengths,

there was little difference between the two methods due to the small fraction of elemental carbon in our samples.

References

Adler, G., Riziq, A. A., Erlick, C., and Rudich, Y.: Effect of intrinsic organic carbon on the optical properties of fresh diesel soot, Proceedings of the National Academy of Sciences, 107, 6699-6704, 2010.

Bond, T. C., Doherty, S. J., Fahey, D., Forster, P., Berntsen, T., DeAngelo, B., Flanner, M., Ghan, S., Kärcher, B., and Koch, D.: Bounding the role of black carbon in the climate system: A scientific assessment, Journal of Geophysical Research: Atmospheres, 118, 5380-5552, 2013.

APPENDIX 2

SUPPLEMENTAL INFORMATION FOR CHAPTER 3

PHYSICOCHEMICAL PROPERTIES AND CYTOTOXICITY OF BROWN CARBON PRODUCED UNDER DIFFERENT COMBUSTION CONDITIONS

A2.1. UV-vis measurements of brown carbon extracts

We measured the UV-Vis absorbance in the range of 400-800 nm at a 1 nm resolution using a UV-Vis spectrophotometer (Agilent, Cary 60). We then retrieved the imaginary component of the refractive index *k* from the measured absorbance following the method of

The UV-vis absorbance of the BrC extracts was measured in the range 200 nm to 800 nm at a 1 nm resolution using a UV-vis Spectrophotometer (Agilent, Cary 60). We retrieved the wavelength-dependent imaginary part of the refractive index of the extracts ($k_{extracts}$) from the measured absorbance following the method of (Sun et al., 2007), such that *k* is related to the absorption coefficient of the BrC extracts as follows (α, cm^{-1}):

$$k(\lambda) = \frac{\lambda}{4\pi}\alpha(\lambda)$$

α is obtained from absorbance measurements as:

$$\alpha(\lambda) = ln10\ \frac{A(\lambda)\rho}{C_{\mathrm{BrC}}\ L}$$

Where *L* is the optical path length (1 cm), C_{BrC} is the concentration of BrC extract, retrieved using the OC-EC (Section 3.2.3), and ρ is the density of the extracted BrC, assumed to be 1.3 g cm^{-3} (Cheng et al., 2019).

Using the UV-Vis measurements of the extracts, we could verify that there were no suspended particles in the solution. Absorption by light absorbing molecules can be fitted using a power law function. However, since suspended particles cause extinction by both scattering and absorption,

a single power law function fit would be insufficient to reproduce the measured extinction using a UV-Vis (Phillips and Smith, 2017). In the case of the extracts in this work, a single power law function returned an R^2 of 0.996 and 0.999 for the BrC produced at 670 °C and at 1035 °C, respectively.

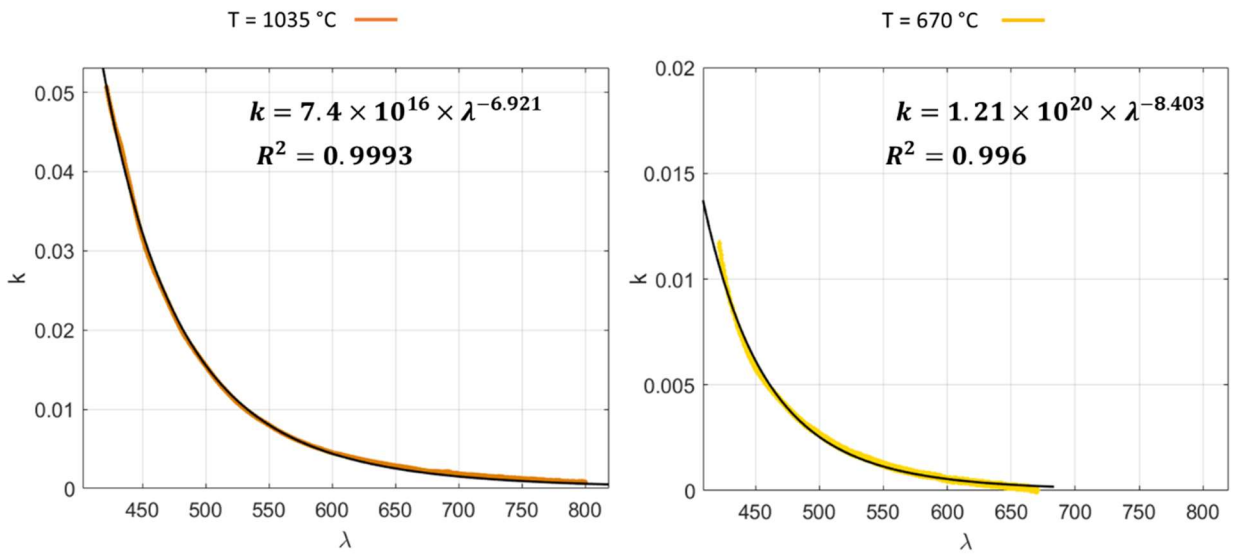

Figure A2.1. *k* vs λ retrieved from UV-Vis measurements of the BrC extracts fitted to a single power law function. (a) *k* vs λ of the BrC produced at 1035 °C in the range of 420 to 800 nm. (b) *k* vs λ of the BrC produced at 670 °C in the range of 420 to 670 nm. The very weak absorption by this BrC at wavelengths greater than 670 nm results in some negative values caused by baseline drift, which would hinder a power law fit.

A2.2. Correction of Exposure Doses

As detailed in Section 3.2.5, we resuspended the BrC remaining in the vials in 200 µl of DCM and measured the concentration of the solution using the OC-EC. Using the OC-EC measurements, we corrected the exposure dose by subtracting the remaining unextracted mass from the mass present in the BrC + media solutions, resulting in new, corrected concentrations, such that:

$$C_{Corrected} = m_{corrected} \times V_{sol} = \left(m_{design} - m_{unextracted}\right) \times V_{sol}$$

Where $C_{corrected}$ and $m_{corrected}$ are the corrected concentration and mass of BrC in the BrC + media solutions, V_{sol} is the volume of the solution, and $m_{unextracted}$ is the mass of the unextracted BrC, retrieved using the total carbon (TC) from the OC-EC measurements. The OC-EC data and resulting corrections and shown in Table A2.1.

Table A2.1. Data from the OC-EC analyzer to estimate the fraction of BrC unextracted in media. In all cases, 100 µl of the 200 µl BrC solution was pipetted onto a 1.5 cm^2 quartz punch, dried, and analyzed.

Sample	Exposure Dose (µg/ml)	Corrected Exposure Dose (µg/ml)	TC (µg/ cm^2)
670 °C	136.0	61.1	105.03 ± 5.45
670 °C	82.0	43.4	54.66 ± 2.93
670 °C	49.0	32.2	25.20 ± 1.46
670 °C	27.0	15.4	18.24 ± 1.11
670 °C	16.0	9.1	11.94 ± 0.80
670 °C	10.0	7.1	5.76 ± 0.49
670 °C	6.0	4.2	4.29 ± 0.41
670 °C	3.5	2.5	3.46 ± 0.37
1035 °C	136.0	53.3	115.68 ± 6.18
1035 °C	82.0	29.4	73.80 ± 3.89
1035 °C	49.0	25.4	34.41 ± 1.92
1035 °C	27.0	13.7	20.61 ± 1.23
1035 °C	16.0	10.2	10.38 ± 0.72
1035 °C	10.0	6.0	7.22 ± 0.56
1035 °C	6.0	3.6	5.08 ± 0.45
1035 °C	3.5	1.8	4.45 ± 0.42

References

Cheng, Z. Z., Atwi, K., Onyima, T., and Saleh, R.: Investigating the dependence of light-absorption properties of combustion carbonaceous aerosols on combustion conditions, Aerosol Science and Technology, 53, 419-434, 10.1080/02786826.2019.1566593, 2019.

Phillips, S. M., and Smith, G. D.: Spectroscopic comparison of water-and methanol-soluble brown carbon particulate matter, Aerosol Science and Technology, 51, 1113-1121, 2017.

Sun, H., Biedermann, L., and Bond, T. C.: Color of brown carbon: A model for ultraviolet and visible light absorption by organic carbon aerosol, Geophysical Research Letters, 34, 2007.

APPENDIX 3

SUPPLEMENTAL INFORMATION FOR CHAPTER 4

CHEMICAL COMPOSITION AND CYTOTOXICITY PROPERTIES OF FRESH AND PHOTOCHEMICALLY AGED BIOMASS BURNING ORGANIC AEROSOLS

A3.1 OA enhancement for the oak and pine BBOA.

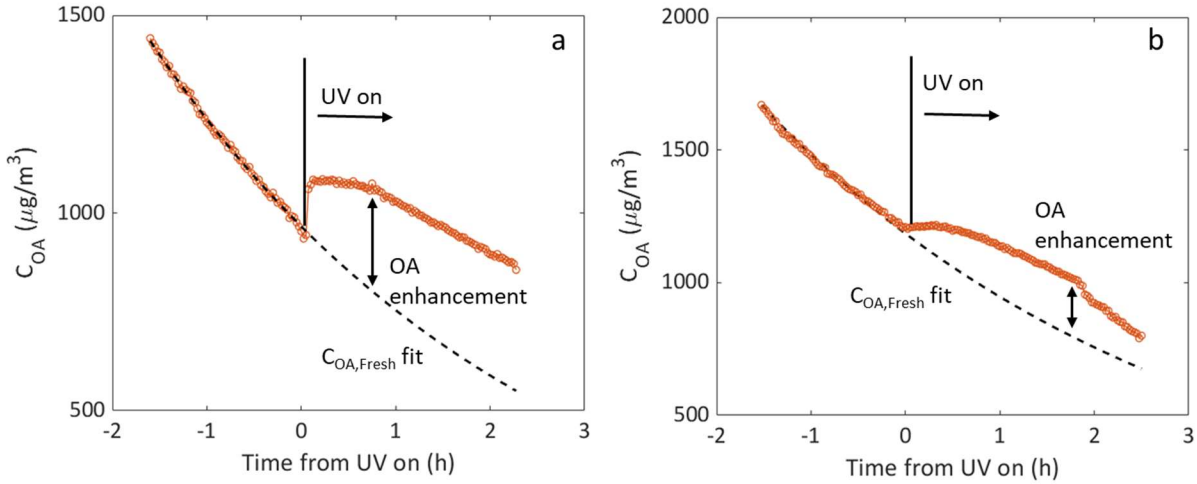

Figure A3.1. The OA enhancement for the (a) oak and (b) pine BBOA after photooxidation.

A3.2 Calculation of the mass fractions in the BBOA samples of species with different elemental compositions.

In order to estimate the mass fractions of species with different elemental compositions, we weighted the neutral mass of each identified compound by its detected intensity. We then divided the sum of those weights for each group of species by the sum for all identified compounds. For example, for CHO species,

$$x_{CHO} = \frac{\sum_i^{CHO} m_i \times \text{intensity}}{\sum_i^{all} m_i \times \text{intensity}}$$

where x_{CHO} is the mass fraction of compounds with an elemental composition of CHO and m_i is the neutral mass of each compound.